Experimental and modelling studies on HVO-methanol mixtures separation for superyachts applications

Ernesto La Colla

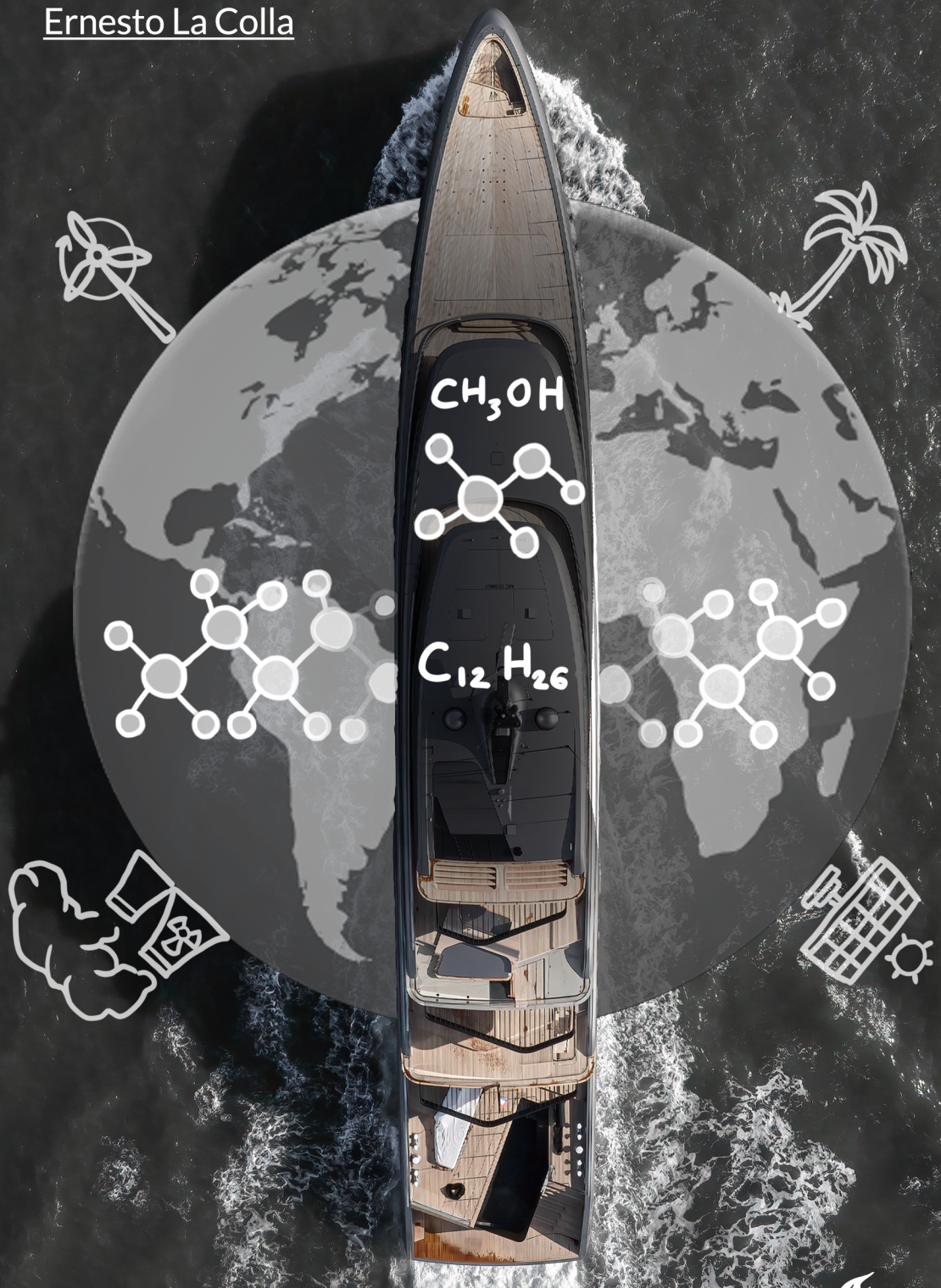

FEADSHIP
ROYAL DUTCH SHIPYARDS

TU Delft

Figure on titlepage: photo of *Obsidian*, adapted from [1]

Experimental and modelling studies on HVO-methanol mixtures separation for superyachts applications

MT54035: MT MSc Thesis

by

Ernesto La Colla

Performed at

Feadship, De Voogt Naval Architects B.V.

To obtain the degree of Master of Science in Marine Technology,
in the specialisations of Marine Engineering and Ship Design
at the Delft University of Technology

To be defended publicly on Tuesday September 26, 2023 at 9:00 AM

Student number:	5499348	
Report number:	MT.23/24.048.M	
Project duration:	January 9, 2023 - September 26, 2023	
Thesis committee:	Dr. ir. L. van Biert	TU Delft, daily supervisor
	Dr. ir. J.T. Padding	TU Delft
	B. Grenko MSc	TU Delft
	Ing. G. Loeff	De Voogt Naval Architects, daily supervisor

An electronic version of this thesis is available at https://repository.tudelft.nl.

TU Delft Delft University of Technology

FEADSHIP ROYAL DUTCH SHIPYARDS

In the loving memory of Carmine, Ernesto and Giuseppina

"We will move to a low-carbon world because nature will force us, or because policy will guide us. If we wait until nature forces us, the cost will be astronomical."
- Karen Christiana Figueres Olsen, 2014

Preface

The completion of the work that follows was marked by wonderful people, each of whom has played a significant role in shaping its development.

I am grateful to my daily supervisors, Ing. Giedo Loeff and Dr. ir. Lindert van Biert for giving me the chance to work on a project contributing to the decarbonisation of the shipping sector. A topic that resonates deeply with us and which fostered both in-depth technical and broader societal level discussions several times. Your ideas and feedback helped me shape this research into its current state. I would like to extend my gratitude to Bojan Grenko for his feedback and recommendations. Moreover, I thank Dr. ir. Johan Padding for agreeing to be on my committee. I happily remember his motivation when I explained to him the project for the first time. I thank Dr. Miguel Cabrera and Dr. Luis Portela for the time spent brainstorming with me on the fuels separation modelling. Furthermore, I thank Prof. Dr. ir. Robert van de Ketterij for his support and suggestions provided before, during and after the experiments. I am thankful to Sebastiaan Rampen, Gerard Boots, Elda Panoto and all the workers of the *Scheikundig Laboratorium Defensie* for offering me guidance, equipment and access to their facility. Thanks to *GoodFuels* for providing the tested fuels.

During the past year, a great amount of my time was spent in the office at *De Voogt*. There, before my thesis, I worked on another project aimed at contributing to more sustainable yachts. I believe that the two projects are interconnected, as a continuum within the decarbonisation timeline of the yachting sector. They both made me a better engineer and more conscious of the upcoming practical and societal challenges within the shipping industry. I am grateful to all my colleagues for the lessons learnt. Aaron Alkemade, thank you for your time spent answering my questions and discussing the further steps in the thesis project development. On the same note, I show my appreciation to Bram, Martijn, Beatrice, Lisa and Shrey for the shared ideas. I cannot forget to thank Engel-Jan on behalf of *Lloyd's Register*, for the stimulating discussions on the alternative fuels utilisation onboard yachts.

I am thankful to Jorge, Arjav, Iñaki, Tommaso, Matteo, Francesco, Lorenza, Felicia and all my Italian, Greek and Spanish friends, for the amusing moments and for always being there for each other. Words cannot express my gratitude to Daniëlle for being my unwavering source of strength and encouragement. Thank you for everything. Additionally, I am genuinely grateful to the person I considered to be my *zia*, mentor and friend. Maria, thank you for your vivid support. Your counsel and viewpoints have consistently offered a valuable and unique outlook on my career journey.

Last but certainly not least, my deepest gratitude to my family for their unconditional love and support. Writing these lines gives me goosebumps. There is so much I wish to express, far beyond the confines of this page. Perhaps the most significant message is that your silent pride in me has always been my driving force. This project on its own cannot fully repay the sacrifices you have been making, but I hope it adds to your happiness and sense of pride. This would have not been possible without your unwavering support. A heartfelt shout out to my brother, for his guidance and constructive big brotherly critiques that only he can provide.

Ernesto La Colla
Delft, September 2023

Summary

In the Feadship roadmap towards decarbonisation by 2030, the usage of multiple fuels provides built-in flexibility to ocean-crossing superyachts in a scenario where alternative fuels become progressively available worldwide. Paraffinic diesel - more specifically hydrotreated vegetable oil (HVO) - and methanol (MeOH) are selected among all possible sustainable fuels. The desired flexibility can be achieved with a multi-fuel system, which can have different designs. In this study, to make optimal use of the tanks' capacity, it was chosen to bunker HVO and methanol alternately in all tanks. Due to this mutual fuels contamination is expected. The lack of standards and research on accepted fuels impurity makes full fuels separation relevant to be explored to avoid performance degradation of dual-fuel (DF) engines. Among the investigated methods, gravity settling tanks and disc stack centrifuges appear to be suitable technologies for separating the mixed fuels. This work investigates whether complete HVO-methanol separation can be achieved via gravity settling tanks or disc stack centrifuges prior to their usage in DF engines.

In this work, shake tests were conducted on HVO-MeOH mixtures to quantify the separation time and relative volume concentration ratios to obtain a complete separation. The fuels were poured into a beaker with methanol at 1, 5, 10-70 % v/v. The mixture was stirred and samples were extracted at different time intervals. MeOH traces in HVO were identified through visual observations and the usage of a microscope. The tests revealed that full separation was not achieved in the 1 hour-3 days observation time. This phenomenon can be attributed to the low-density difference between the fuels. Hence, as the experimental outcomes evidenced incomplete HVO-methanol separation, centrifuges were studied to achieve this goal.

A mathematical model was developed for disc stack centrifuges to assess the separator performance and the separation time. The equations of motion of the denser droplets were derived within a successive discs' section. Considerations on the heavy-light phase interface position were done. A model of the multi-fuel system was built based on the mass conservation principle for defined operational profiles. The model provides the separator working conditions and identifies the system schematic change with varying the operating engine mode. The mathematical centrifuge model and the multi-fuel system model were integrated to size the centrifuge and assess its performance.

The centrifugal separator and multi-fuel system models were integrated following an iterative approach. Complete separation is theoretically possible with a separator larger than the existing disc-bowl type designs. This result is attributed to the low-density difference between methanol and HVO. The maximum separation time is in the range of 5-10 minutes for MeOH droplets with a diameter of 12-16 μm. Droplets with a diameter outside this range coalesce quasi-instantaneously. Lastly, results were derived relative to the impact of HVO-MeOH separation on the fuel system schematic. The experiments carried out on HVO-MeOH phase separation did not quantify the residual presence of one fuel within the other. Consequently, in the fuel system model, the fuels ratio was set as constant in the storage tanks. A fixed ratio was also hypothesised in the mixture at the separator inlet section. To adhere to these conditions, HVO and MeOH buffer tanks are needed onboard, respectively with about 1/3 and 1/20 of the storage tanks' capacity.

Contents

List of Figures

List of Tables

Nomenclature

Abbreviations

Abbreviation	Definition
ASTM	American Society for Testing and Materials
BECCS	Bio-Energy with Carbon Capture Storage
CapEx	CAPital EXpenditure
CEN	Comité Européen de Normalisation
CFD	Computational Fluid Dynamics
CLP	Chemical classification, Labelling & Packaging
COP	Conference Of Parties
DAC	Direct Air Capture
DF	Dual-Fuel
DME	DiMethyl Ether
DMFC	Direct Methanol Fuel Cell
DNV GL	Det Norske Veritas Germanischer Lloyd
DSR	Diesel Substitution Ratio
EN 15940	Paraffinic diesel
FAME	Fatty Acid Methyl Ester
FC	Fuel Cell
FT	Fischer Tropsch
GHG	GreenHouse Gas
GTL	Gas-To-Liquid
HDRD	Hydrogeneation-Derived Renewable Diesel
HVO	Hydrotreated Vegetable Oil
ICE	Internal Combustion Engine
IMO	International Maritime Organization
IMPCA	International Methanol Producers & Consumers Association
IRENA	International Renewable Energy Agency
ISO	International Organization for Standardization
IUPAC	International Union of Pure and Applied Chemistry
LHV	Lower Heating Value
LLE	Liquid-Liquid Extraction
LNG	Liquefied Natural Gas
LPG	Liquefied Petroleum Gas
MCR	Maximum continuous rating
MDO	Marine Diesel Oil
MENENS	Methanol als Energiestap Naar Emissieloze Nederlandse Scheepvaart
MeOH	Methanol

Abbreviation	Definition
MEPC	Marine Environment Protection Committee
MGO	Marine Gas Oil
NECA	Nitrogen Emission Control Area
OME	polyOxy-Methylene dimethyl Ether
OpEx	OPerating EXpenditure
PEM-FC	Proton Exchange Membrane Fuel Cell
PFI DF	Port Fuel Injection Dual Fuel
RR	Replacement Ratio
SAF	Sustainable Aviation Fuel
SF	Single Fuel
SMD	Sauter Mean Diameter
SOLAS	Safety Of Life At Sea
SOFC	Solid Oxid Fuel Cell
TRL	Technology Readiness Level
TTW	Tank-To-Wake
WTW	Well-To-Wake

Chemical formulations

Abbreviation	Definition
CO_2	Carbon Dioxide
CH_3OH	Methanol
CH_4	Methane
NO_x	Nitrogen Oxides
N_2O	Nitrous Oxide
-OH-	Hydroxy group
SO_x	Sulphur Oxides

Symbols

Symbol	Definition	Unit
B	Beam	[m]
C	Tanks capacity	[m^3]
C_D	Drag coefficient	[-]
D	Heavy fuel droplet diameter	[m]
d	Outlet channel diameter	[m]
d_{min}	Mixture inlet channel diameter	[m]
d_{range}	Range distance	[nm]
E	Eötvös number	[-]
F_S	Separation force	[N]
F_b	Buoyancy	[N]
F_{cor}	Coriolis force	[N]
F_D	Drag force	[N]

Symbol	Definition	Unit
F_L	Lift force	[N]
F_ω	Centrifugal force	[N]
g	Gravitational acceleration	[m/s^2]
G_S	Shear rate	[s^{-1}]
H	Discs section height	[m]
h_{crit}	Dispersed droplets critical distance	[m]
L	Discs length	[m]
LC_{50}	Median Lethal Concentration	[mg/l]
LD_{50}	Median Lethal Dose	[mg/kg$_{bw}$]
m_d	Heavy fuel droplet mass	[kg]
m/m	Mass percentage	[%]
Mo	Morton number	[-]
n	Discs number	[-]
$P_{aux,m}$	Mean auxiliary load	[kW]
P_b	Break power	[kW]
P_e	Electrical power	[kW]
P_S	Shaft power	[kW]
ppmV	parts per million	[mg/m^3]
Q	Volume flow	[m^3/s]
R_1	Inner radius	[m]
Re	Reynolds number	[-]
R_{int}	Interface position	[m]
R_T	Outer radius	[m]
R_{TOT}	Separator total radius	[m]
sfc	Specific fuel consumption	[g/kWh]
S	Outlet cross section	[m^2]
T	Draught	[m]
$t_{contact}$	Dispersed droplets contact time	[s]
$t_{drainage}$	Film drainage time	[s]
V_d	Heavy fuel droplet velocity	[m/s]
V_F	Mixture flow velocity	[m/s]
v_{max}	Maximum speed	[kn]
v_{range}	Range speed	[kn]
v_t	Terminal settling velocity	[m/s]
v/v	Volume percentage	[%]
wt	Weight percentage	[%]
Δ	Displacement	[t]
$\Delta\rho$	Density difference	[kg/m^3]
η_{TRM}	Transmission efficiency	[%]
μ	Dynamic viscosity	[kg/ms = 10^3 cP]
ν	Kinematic viscosity	[m^2/s = 10^6 cSt]
ρ	Density	[kg/m^3]
σ	Surface tension	[N/m = 10^3 dyn/cm]
φ	Discs inclination angle	[deg]
ω	Rotational speed	[rad/s]

Subscripts

Term	Definition
h	Heavy phase
l	Light phase

Superscripts

Term	Definition
$\dot{}$	First-order time derivative
$\ddot{}$	Second-order time derivative
$\vec{}$	Vector
$\hat{}$	Versor

1 Introduction

1.1. Background

The environmental footprint of fossil fuels deployment is evident. The concentration of CO_2 in the atmosphere stemming from human activities by dependency on fossil fuels is growing exponentially at levels higher than the pre-industrial era [2]. The CO_2 concentration in the troposphere has raised the average global temperature due to the greenhouse effect. Predictions show ceaseless mean temperature increase over the 21st century if greenhouse gas (GHG) emissions continue unabated. Measures need to be undertaken to mitigate catastrophic effects, namely global ocean warming, precipitation increase and Arctic sea ice shrinkage which impact the ecosystem and human species [3].

Initial efforts were put in place by the international community to alleviate the climate change effects. In December 2015, at the 21st United Nations Climate Change Conference of Parties (COP), the so-called Paris Agreement was achieved among the United Nations members. All involved countries are committed to limiting the mean temperature rise to 1.5°C [4].

The maritime sector plays an important role in the emitted pollutants. International shipping is a source of GHG emissions, speaking for 1076 million tonnes of CO_2 emitted in 2018. They represent roughly the 3% of the global GHG emissions [5], while superyachts have a global warming potential of approximately 5 Mt of CO_2 equivalent ($CO_2 - e$) nowadays [6].

The recent integration of the maritime transport in the EU Emissions Trading System within the European Green Deal issued in July 2021, is urging stakeholders to undertake actions to not undermine the objectives of the Paris Agreement [5]. The International Maritime Organisation (IMO) set the objective to cut released CO_2 from the shipping sector by 40% by 2030 compared to 2008 and reach near-zero GHG emissions by 2050 [7]. In this framework, the IMO within its Maritime Environment Protection Committee (MEPC) identified alternative fuels as a solution for harmful emissions release prevention [8].

In the yachting sector, as figure 1.1 (a) illustrates, in the well-to-wake (WTW) scenario, the GWP rises up as the yacht's length increases, in terms of equivalent CO_2 emitted both in auxiliary and sailing modes [6]. For an average Feadship's yacht of 80m in length, this means that these ships have a larger impact on the environment than smaller designs. Furthermore, as it can be noticed in figure 1.1 (b) same system and fuel utilisation undermines the IMO GHG reduction targets. Thus, efforts need to be put in place to phase out harmful emissions in the superyacht industry.

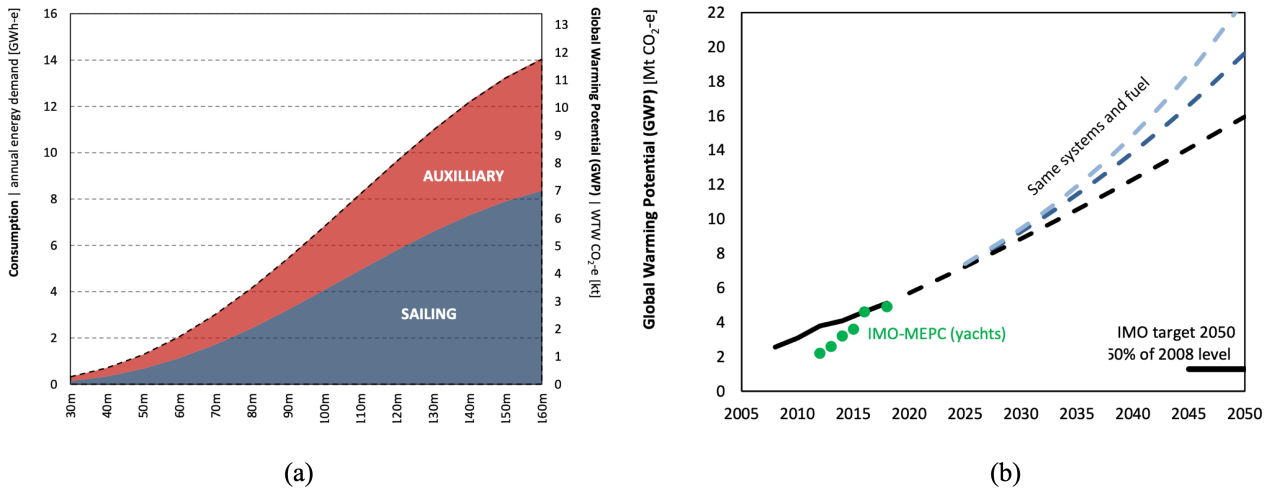

(a) (b)

Figure 1.1: (a): Global warming potential of yachts by length. (b): Global warming potential [*source: De Voogt Naval Architects*]

1.1.1. Alternative fuels for yachts

To phase out the yachts' emissions, the deployment of alternative fuels has been largely investigated. This because, within the operational phase of the yacht's life cycle, the yacht's footprint is dominated by the emissions mainly caused by the energy generation on board [9]. Within Feadship, main studies relate to the impact of hydrogen storage and fuel cells on the yacht's design [10, 11]. The follow-up of these studies is reflected in the recent announcement of the first Feadship hydrogen-propelled superyacht construction [12]. Other projects relate to hydrotreated vegetable oil (HVO) [13], methanol [6] and hybrid propulsion [14] [1]. Despite the highlighted positive features of these fuels their large-scale availability is a concern in the near term. For instance, methanol is nowadays available in only more than 100 ports [16]. Although this represents a good aspect from a large-scale perspective, this scenario still poses some limitations in alternative fuels availability when compared to conventional diesel. Uncertainties of alternative fuels availability can constrain the operations of ocean-crossing superyachts.

1.1.2. Built-in flexibility

To overcome the limited availability of alternative fuels on a large scale in the near term, Feadship has identified a strategy developing the concept of *built-in flexibility*. The delineated Feadship's roadmap [17] towards carbon neutrality highlights the importance of both non-fossil paraffinic fuels (eg. HVO e-diesel) and alcoholic fuels (eg. bio- and e-methanol or ethanol) in a near-term strategy. This means that by 2030 the yachts need to be able to store both non-fossil paraffinic fuels, namely HVO, and alcoholic fuels at full capacity. This allows refuelling an alternative fuel where in-harbour stations make it possible today, with diesel still representing a viable option while alternative fuels become increasingly available. Within the literature research, HVO and methanol were prioritised as alternative fuels based on a criteria-driven selection for their utilisation by 2030. Furthermore, in scenarios where HVO and methanol are unavailable, EN 590 diesel remains a viable bunkering option to ensure the yacht's operations.

The desired flexibility can be achieved with a multi-fuel system, which can have different designs. In

[1] Feadship is also part of the *Green Maritime Methanol* project [15], a consortium of 30 partners investigating the feasibility of application of methanol as a marine fuel. Furthermore, Feadship is a partner of *Water Revolution Foundation*, a Dutch public benefit organization aiming at driving sustainability in the superyacht industry through collaboration and innovation.

this study, to make optimal use of the tanks' capacity, it was chosen to bunker HVO and methanol alternately in all tanks. To guarantee this, integration with various power conversion systems was evaluated. Dual-fuel (DF) engines were selected among other technologies, as they enable a multi-fuel certified system, minimisation of required storage space on board, and fuels switchover. A dual-fuel system of this type warrants built-in flexibility in operations. Apart from limited fuel availability, bunker restrictions can be encountered in some areas due to high fuel taxation. A multi-fuel system can overcome this challenge. Furthermore, a system of this type allows the yachts to switch their operations from diesel to the more sustainable fuel in areas where severe restrictions on pollutant emissions are in place, such as in the Nitrogen Emissions Control Areas (NECAs) [18]. Moreover, flexibility in fuel selection permits ocean-crossing yachts to fulfill the maximum required range.

1.2. Problem statement

When storing multiple fuels in the same tank alternatively, the bunkered fuel's composition may vary due to the residual fuel left in the tank prior to bunkering. This leads to contamination of one of either two fuels to be deployed in DF engines, subsequently yielding potential engine performance deviation from its desired state or malfunction. The lack of standards and research on accepted fuels impurity, anti-wear additives and corrosion inhibitors makes full HVO-methanol separation relevant to be explored. The selection of the separation systems depends on the nature of the mixture formed in the storage tanks. However, research is limited regarding HVO-methanol mutual miscibility. Preliminary conclusions could be drawn knowing the compounds' properties, yielding the usage of gravity settling tanks or centrifuges for fuels separation. Investigation on gravity settling tanks and centrifugal separator also benefits from their usage onboard existing vessels [19, 20]. More specifically, disk-bowl type centrifuges are chosen among the latter within the literature research. Nevertheless, uncertainties remain relative to the separation efficacy and the required time for the separation. The latter aspect is fundamental to ensure that the cleaned fuel is ready to be supplied to the engines when required. Lastly, when switching from one fuel to another, HVO/methanol can remain partially or completely unused onboard. Hence, questions arise regarding the management of the unused fuel relative to its allocation within the multi-fuel system which can influence the schematic of the latter.

1.3. Thesis objectives

As mentioned in the previous section, considering the selected engine's state-of-art, full HVO-methanol separation is necessary. Thus, the main research question to be answered throughout this report is:

How can HVO and methanol be fully separated prior to their usage in DF engines?

Sub-questions are formulated to help answer the main research question. These are based on the thesis objectives stemming from the problem statement. In the previous section, it was mentioned that gravity settling tanks and centrifugal separators are identified as separation systems. It is an objective of this study to investigate the efficacy of these technologies. With either systems, researching the time required to achieve full separation is another goal of this study. Alongside this, understanding the centrifugal separation principles is fundamental in case gravity separation does not lead to full separation within a defined time. A centrifugal separator model is needed to assess its performance. Additionally, the boundary conditions shall be defined to constrain the problem. Furthermore, with the selected separation technology, it remains fundamental to ascertain the multi-fuel system schematic alterations to offer insights into the fuels handling. The multi-fuel system schematic would

also define the separation system working conditions. Consequently, to help answering the main research question, sub-questions are identified to be answered at the end of this study. These are presented as follows:

1. What is the time required by HVO-methanol mixtures to fully separate by gravity?
2. How can a centrifugal separator be modelled and what are the problem boundary conditions?
3. How does the fuels separation impact the multi-fuel system schematic?
4. How can complete methanol/HVO removal from HVO/methanol be achieved via centrifugal separation?
5. What is the time required by the centrifugal separator to achieve full separation?

1.4. Thesis outline

Following the introduction of the problem, the thesis layout is given:

- **Chapter 2 - Literature review:** it presents the summary of the main literature research findings. First, potential issues from HVO and/or methanol combustion in DF engines containing methanol/HVO traces are showed. Methods for the treatment of HVO-MeOH mixtures are discussed with consequent selection of the most suitable technology.
- **Chapter 3 - Experimental study on phase separation of HVO-methanol mixtures:** The first research gap deriving from literature is tackled in this chapter. It addresses experiments carried out on HVO-methanol mixtures to determine the time required by the fuels to fully separate by gravity. Additionally, these tests ascertain the efficacy of gravity settling tanks for their usage onboard.
- **Chapter 4 - Modelling of a disk-bowl type centrifugal separator:** it presents the development of a disk-bowl type centrifugal separator. This serves as a tool to determine the separator performance when integrated in the multi-fuel system.
- **Chapter 5 - Multi-fuel system modelling:** it covers the modelling of the multi-fuel system to define its schematic variations and the separator working conditions.
- **Chapter 6 - Integrating and sizing the centrifugal separator in the multi-fuel system:** it provides a combination of the centrifugal separator and multi-fuel system models respectively developed in chapter 4 and 5. A final separator design is found, capable of working in the defined yacht's operational profiles in chapter 5. The separator performance and required time are assessed. The results and the mathematical model developed in chapter 4 are validated.

At the end of each chapter conclusions are drawn to summarise the findings. The last chapter provides answers to the above-listed research questions. A discussion of the study outcomes is followed and recommendations are given for future research.

2

Literature review

This chapter contains a literature review concerning the role of HVO-methanol separation. A criteria-driven approach led to the selection of HVO and methanol for the Feadships' decarbonisation by 2030. Their main features and properties are reported in appendix A. In reality, conventional EN 590 diesel (with or without FAME) is still currently used while alternative fuels become increasingly available. Despite the EN 590 diesel and HVO similar properties, HVO and methanol are the preferred fuels in this study due to their potential for emissions reduction. Hence, in this chapter, first, the effects on engines deriving from the usage of these non-pure fuels are covered. Second, the status of the mixed HVO-methanol in the storage tanks is studied and separation techniques are selected.

2.1. Mutual HVO-methanol contamination

When storing multiple fuels in the same storage tanks, variation of the bunkered fuel's concentration occurs. The use of non-pure fuels can impact the energy converters' performance. Effects on port-fuel injection dual-fuel (PFI DF) engines are presented relative to the engine operating modes.

2.1.1. Contamination effects on port-fuel injection dual-fuel engines

Within the scope of this project, PFI DF engines are identified as one of the preferred energy converter technologies enabling a multi-fuel-certified system. Figure 2.1 gives a general overview of the contamination in HVO and methanol for a PFI DF engine. In a PFI DF engine, in dual-fuel mode, at the beginning of the compression stroke, methanol is injected into the intake port and evaporates mixing with the intake air. The mixture reaches the cylinder and near the end of the compression stroke, HVO is injected to ignite the methanol-air mixture [21]. The dual-fuel mode allows switching to single-fuel (HVO) operations.

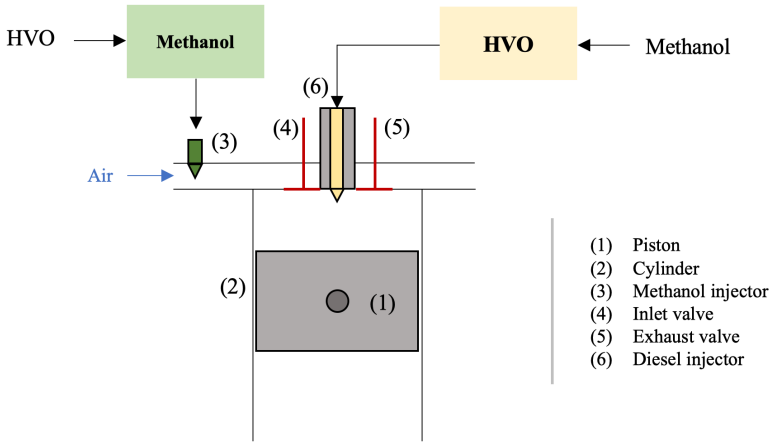

Figure 2.1: Schematic of a methanol-diesel PFI DF engine, adapted from [22, 23]

Figure 2.1 shows the HVO and methanol mutual contamination in single-fuel and dual-fuel modes respectively. In reality, other contaminants than HVO and methanol reciprocal miscibility can yield undesired engine performance. However, regulations compliance of the bunkered fuels and well-established practices onboard do not generate major concerns. For instance, this is the case of sulphur, chlorine, acetone, acetic acid and water.

Consequently, challenges in PFI DF engines associated with MeOH/HVO contamination by HVO/MeOH are discussed with respect to the associated engine mode. A summary of the main effects on engines is shown in figure 2.2. The events with higher risks are reported in blue.

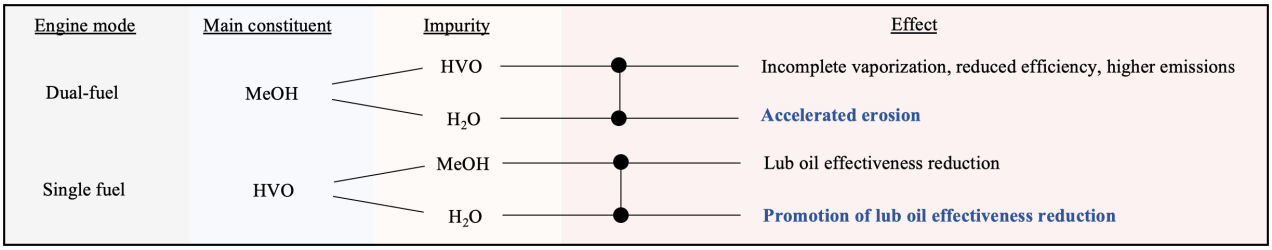

Figure 2.2: Contamination and possible effects of mutual HVO-methanol contamination on PFI DF engines

HVO contamination in dual-fuel mode

Traces of HVO in methanol can lead to incomplete methanol vaporization, reduced engine efficiency and higher emissions. This is due to the methanol properties change. R.S. Tol [24] calculated that if diesel is added to methanol, in an ideal mixture, the methanol density, the gravimetric LHV, viscosity, and stochiometric air-to-fuel ratio increase, while oxygen content and heat of vaporization drop. Nevertheless, it can be expected that the mentioned parameters do not change significantly for small diesel traces. On the other side, incomplete methanol vaporization causes engine wear, unburned hydrocarbons, formaldehyde, and formic acid formation, which are corrosive for the engine [25, 26, 27]. Thus, corrosion represents the main unwanted effect. This is promoted if water is present in the mixture, stemming from condensation in the storage tanks. Water breaks the passively formed metal oxide film [28] and in a diesel-methanol mixture accelerates erosion on engine components like pistons [29, 30, 31]. Droplets of unvaporized methanol and other polar species (e.g. water) strip the lubricant film off the metal surfaces, yielding to the so-called *wall-washing* effect [26].

Methanol contamination in single fuel (HVO) mode
Methanol in HVO causes lube oil efficacy reduction. No concerns arise regarding the engine performance, as the increased methanol content in diesel has been found to result in a slight break thermal efficiency rise and NOx, CO_2 and soot emissions drop [32, 33], due to an increase in heat of vaporization and oxygen content [24]. Conversely, the reduced volumetric energy content can result in power output drop [24, 34, 35]. Hence, the lube oil effectiveness degradation represents the main concern, ought to viscosity and methanol condensation reduction. This trend has been found to cause engine wear. Studies revealed piston rings wear due to partial oxidation at high temperatures [36] and high ring wear given by methanol wall wetting phenomenon [37]. Moreover, the lube oil performance degradation is fostered by water addition due to water condensation. Reduction of anti-wear additives efficacy was observed on zinc, lead, magnesium, aluminium and copper [34, 36].

Overall, it emerges that limits of HVO/MeOH concentration in MeOH/HVO remain undefined, with limited conclusions for PFI DF engines due to a lack of specific mixture studies and marine quality standards. Hence, this study advocates a conservative HVO-methanol full separation. A review of fuels separation methods is followed to achieve this goal.

2.2. Fuels miscibility

The selection of a method for liquids separation depends on the mixture state. To determine this it is fundamental to study the fuels miscibility in the storage tanks.

Miscibility is not a trivial aspect as it depends on the temperature, bonding status of the molecules and volume fractions of the constituents. The HVO-methanol miscibility is studied assuming that the bunkered fuel does not exceed 5% v/v in the storage tank before bunkering. Storage temperature is assumed in the 15-30°C range, for the liquid state of both fuels in this condition and avoidance of crystal formation in the HVO case [38]. No studies exist on this specific fuels mixture. Hence, predictions on the mixture status are defined from the individual fuels nature and available research on similar substances.

A first conclusion can be drawn on the fuels' polarity nature. This is defined by the bonds between positively charged nuclei and negatively charged electrons in atoms or groups of atoms. The distinction between *polar* and *non-polar* molecules respectively lies in the asymmetrical and symmetrical distribution of shared electrons between the atoms. When substances are mixed polar compounds tend to attract each other via *dipole-dipole forces*. Dipoles are formed with one end side of the molecule becoming slightly positive and the other one slightly negative. Thus, the positive end of one dipole and the negative end of another attract each other [39]. This is the case of water and alcohols, namely methanol, where hydrogen bonds with a highly electronegative oxygen atom [39, 40]. Conversely, hydrocarbons, and in this case HVO, are non-polar [41, 42]. Consequently, generally, it can be expected that HVO does not mix with methanol. Miscibility between polar and non-polar molecules is known relatively to water and hydrocarbons [40]. Hydrocarbons are in fact poorly miscible with water since hydrocarbon molecules tend to interfere with the hydrogen bonding in H_2O molecule but the generated intermolecular forces are weak to lead to miscibility.

Miscibility studies on HVO and methanol are absent in the literature. R.W. Kiser [43] studied the solubility of various hydrocarbons in methanol. The closest hydrocarbon to diesel in terms of carbon number is n-decane. It was found that below a temperature slightly higher than 40°C and for a CH_3OH mole fraction ranged 0.11-0.9 methanol and n-decane exist in two liquid phases. Nevertheless, alongside the carbon atoms, the studied diesel differs from HVO in aromatics content.

Maximum aromatics content allowed in conventional diesel is 8% m/m while it accounts for 1.1% m/m in paraffinic fuels [41]. Aromatics can interact with the polar -OH- group of alcohols and form temporary dipoles or weak intermolecular forces [42]. The model developed by Privat et al. [44] predicts alcohols-hydrocarbons miscibility, with hydrocarbons having low-to-high aromatics content. The minimum aromatics content studied equals 8% m/m. At the fuels storage temperature considered, results show that a hydrocarbon-rich phase is achieved for MeOH mass concentration equal to or lower than 18%. A methanol-rich phase is given for methanol mass concentration equal to or greater than 95%. Hence, under the studied conditions it can be expected that a bunkered fuel-rich phase is created in the storage tanks in a blend with up to 5% v/v residual fuel.

2.3. Fuels separation techniques

The literature review on the effects in PFI DF engines from mutual HVO-methanol contamination led to the conclusion that full fuels separation is relevant to be explored. To avoid the effects reported in figure 2.2, anti-wear additives and corrosion inhibitors might be added to the mixture. Nevertheless, no products were found in the literature for this specific analysis. To pursue full fuels separation, separation techniques are reviewed and the most suitable technologies are selected. For the choice of the fuels separation technology, the nature of the treated mixture must be known. A main distinction is made between *heterogeneous* and *homogeneous* mixtures, respectively meaning that generally, the liquids form phase separation or not. Homogeneous and heterogeneous separation techniques are presented in this section.

2.3.1. Separation of homogeneous mixtures

Preliminary conclusions from the HVO-methanol miscibility study indicate that a homogeneous mixture is generated in the storage tanks under the considered conditions. Hence, it can be expected that homogeneous separation techniques are used to separate these fuels. However, the deployment of these methods is excluded from this study. The main reasons behind this choice are reported in figure 2.3 and discussed as follows.

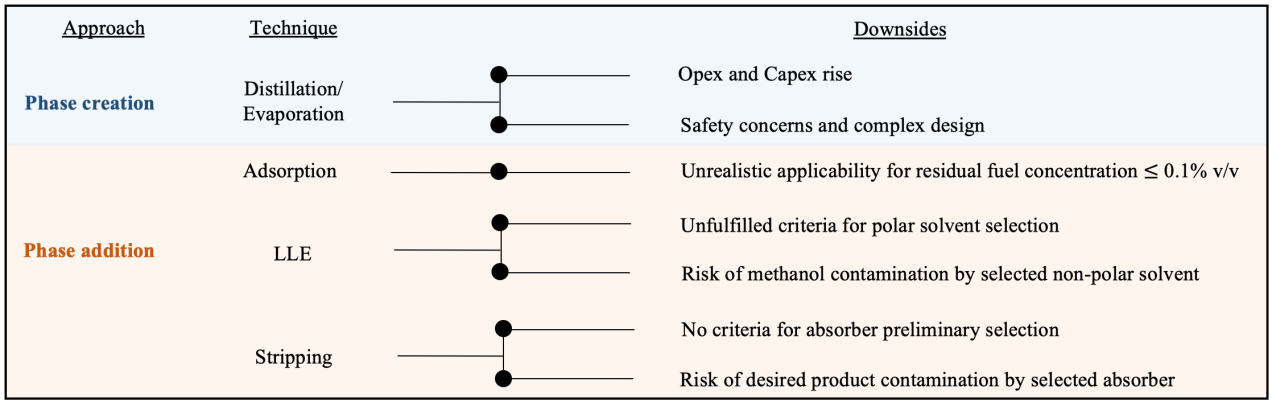

Figure 2.3: Downsides of homogeneous separation techniques for HVO-methanol separation

Homogeneous separation techniques distinguish between *phase creation* and *addition* approaches [45].

Phase creation

It consists of creating a second phase, immiscible with the primary mixture, via energy transfer or pressure reduction. Phase creation methods include *distillation* and *evaporation* [45]. The usage of these two technologies can benefit from small equipment requirements, easy staging, economics of

scale, achievable low energy costs and design and scale-up reliability. However, operational costs grow if concentrations below 20 wt% of exceeding 250°C-boiling point contaminants need to be removed from methanol [46]. This is the case of small HVO concentrations in methanol, with the EN 15940 diesel boiling range reaching 320°C [47]. Additionally, for small applications, the system Capex rise [46]. This applies to yachts wherein only a few hundred fuels cubic meters are processed to meet the yacht's range. Furthermore, it is not advised to change the methanol phase onboard, given that methanol fumes are labelled as toxic [47]. Integration of these separation systems complicates the yacht design and onboard safety.

Phase addition

It consists of adding another fluid which absorbs, extracts or strips certain species from the primary mixture. For liquid mixtures, identified techniques are liquid-liquid extraction (LLE), adsorption and stripping [45]. Adsorption is left out of this analysis since it is applied for residual fuel at a concentration below 0.1% v/v. This scenario is unrealistic for yachts, which are not assumed to bunker with near-empty storage tanks. Hence, LLE and stripping are reviewed.

- **Liquid-liquid extraction**: consists of adding a solvent to the homogeneous mixture such that the solvent and the solute form a separate phase with the main constituent. Next, the two liquid phases are fed in an extractor which separates the purified carrier from the solvent-rich liquid [45]. The added solvent needs to have the same polarity nature as the solute (residual fuel). Criteria for its selection are identified in handbooks, based on the properties of the involved substance [48, 49]. Among a set of solvents [50], no solvents for methanol extraction from HVO are found to meet all the desired criteria for a preliminary selection [51, 49]. Concerning HVO extraction from methanol, pentane and perchloroethylene seem to be suitable [50, 52, 53]. Nevertheless, the addition of the solvent to the mixture can contaminate the desired product. Although solvent recycling is possible, this complicates the operations and design procedures [45]. For example, perchloroethylene is sensitive to oxidative breakdown, thus amine or phenolic-type inhibitors are added as antioxidants [50].
- **Stripping**: it consists of adding a vapour-stripping agent to the liquid mixture. The liquid mixture enters the top of the stripping column while the gas is fed from the bottom. The gas gets in contact with the liquid and selectively removes the undesired components by mass transfer [54]. In this case, there are no criteria for the absorber selection. Screening tests and process modelling are used to determine the absorbent properties and their overall performance [48, 55]. An economic assessment is also suggested to be coupled to these studies [46, 56]. Lastly, similarly to LLE, contamination of the absorbent can occur, yielding complex operations and design, due to the installation of an additional separator to recover the absorber [54].

Consequently, due to the exclusion of homogeneous separation techniques for the aforementioned reasons, other methods are investigated to fully separate HVO/MeOH from MeOH/HVO.

2.3.2. Separation of heterogeneous mixtures

This subsection presents the selected technologies for HVO-methanol separation, which apply to heterogeneous mixtures. The literature review on HVO-methanol miscibility led to the assumption that under the defined conditions, the fuels in the storage tanks create a homogeneous mixture. Hence, deliberate HVO/MeOH addition in the mixture might be performed to use the chosen technologies. In reality, this is an established practice on board ships, as more water is fed in the diesel-water mixture to achieve a more efficient separation [20].

The selected technologies are gravity settling tanks and centrifugal separators. Their usage is in fact a well-established practice onboard ships [19, 20]. Furthermore, concerning centrifuges, Green and

Perry [48] identified centrifugal separation based on the criteria shown in figure 2.4. The criteria stem from shake test observations and are fulfilled by methanol and HVO [35, 41, 50, 57, 58].

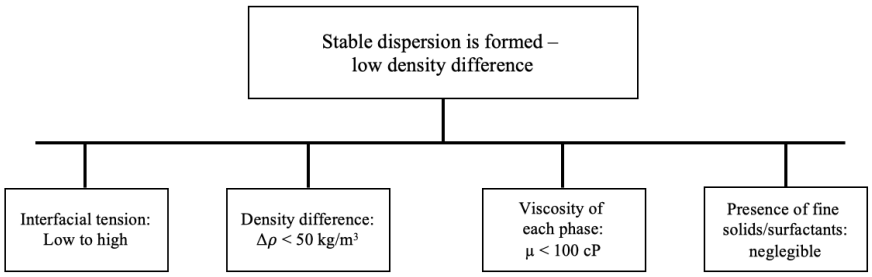

Figure 2.4: Shake test-based criteria for the application of centrifugal separation, adapted from [48]

Concerning gravity, generally, a difference of 0.1 in specific gravity in a mixture of compounds is sufficient to ensure phase separation by gravity [59]. This is not the case for methanol and HVO, whose density is respectively 795.5 kg/m^3 and 765-800 kg/m^3 [35, 41]. Moreover, the time required by a HVO-MeOH mixture to phase separate is not clear. M. Kato et al. [60] stated that a long time is needed for this but a time quantification is not given. This might generate concerns when high flow rates are needed to be processed on board in certain operational profiles. Consequently, if low rates of dropping settling can be expected, centrifuges are identified as an alternative technique [45, 48, 61]. The criteria set by Green and Perry [48] evidence the importance of shake tests to study the mixture phase separation. To not exclude gravity tanks a priori, experiments shall be carried out on the selected fuels. Hence, the fundamentals of gravity separation are presented as follows to predict the mixture's behaviour in view of experimental studies. Next, a centrifugal separator type is chosen and its working principles are discussed for its potential application.

Gravity sedimentation

The theory of gravity sedimentation of droplets in binary liquid mixtures is covered by Green and Perry [48] and T. Frising et al. [62]. Principles of solid particles sedimentation in liquid media can be found in the book by A. De Haan [46]. Although this reference does not specifically address liquid mixtures, some useful insights can be obtained regarding the behaviour of dispersed phases in liquids. Firstly, the nomenclature used in this chapter is briefly mentioned. The droplets of the liquid in the lower concentration are referred to as "dispersed droplets" and therefore the associated liquid substance is named "dispersed phase" (or "droplets' bulk phase"). This is because the dispersed phase exists as dispersed droplets within the "continuous" liquid. The latter usually refers to the liquid at a higher concentration and it is called "continuous phase". A schematic of a gravity settling batch is reported in figure 2.5. When two liquids are mixed, the dispersed droplets tend to move towards the interface formed between the continuous phase and the droplets' bulk phase. This phenomenon is called "sedimentation". At the interface, the droplets move towards the dispersed bulk, because of a film generated by the continuous liquid. The rupture of this film leads the droplets to "coalesce". If sedimentation is faster than droplets' coalescence, a dense-packed zone is formed at the interface between the dispersion and the coalesced phases. Here the droplets collide and merge into each other forming bigger droplets which eventually coalesce. The mixture behaviour can be monitored by plotting the limit between the dispersed bulk and continuous phase over time. The results are the curves in figure 2.5 where the heights of each phase are plotted versus time. It emerges that after a time t_ε two clear light and heavy phases are formed when the interface thickness tends to zero.

The prediction of the mixture's behaviour depends on different fuels' parameters, which are subjected to examination in the ensuing paragraphs.

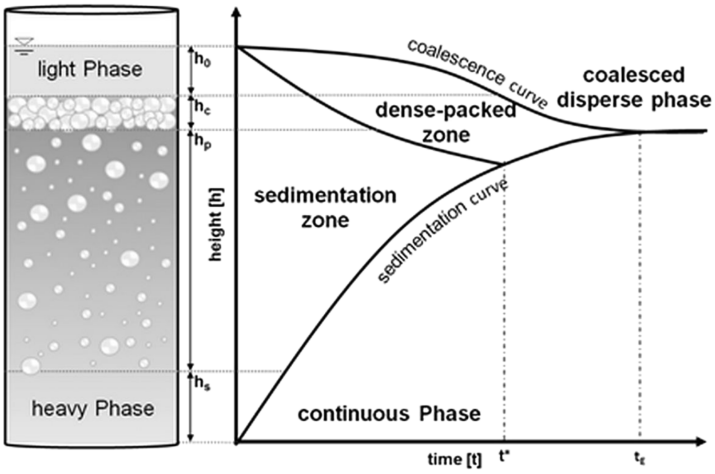

Figure 2.5: Illustration of a gravity settling batch [63]

•Dispersed droplets diameter

The dispersed droplets' diameter was found to impact the time required to achieve full separation. As figure 2.5 illustrates, the thickness of the dense-packed zone can be represented as a function of time. The thickness tends to a limit value which, at a certain time, determines full separation. Some equations are presented in the literature which correlate the time and the heights in figure 2.5. More specifically, the time is expressed by means of the droplet velocity for a certain travelled distance. The first to study sedimentation was Stokes in 1851 which expressed the terminal settling velocity of a single sphere in a viscous fluid. The velocity is calculated by a force balance around the single droplet and for a Reynolds number smaller than 1 the formula becomes [46, 62]:

$$V = \frac{\Delta\rho g d^2}{18\mu_c} \tag{2.1}$$

Where $\Delta\rho$ is the difference between the continuous and dispersed phase densities, d is the droplet diameter and μ_c is the dynamic viscosity of the continuous phase. Nevertheless, this expression becomes more complicated when considering higher Reynolds numbers and the relative concentration of the two liquids in the mixture. To take into consideration corrections for drag and relative velocities between the fluids, different formulas were developed by Ishii and Zuber in 1979 [64] and compared to earlier empirical correlations found by Richardson and Zachi [65]. The equations stemming from both works are still a function of Stokes' velocity. Hence, it emerges that the velocity of the droplets is still proportional to the droplet diameter. Thus, it is evident that the droplet diameter plays an important role in the prediction of the fuels' separation. Consequently, a relation between the settling time of dispersed droplets can be anticipated relative to this parameter. From equation 2.1, it can be said that bigger droplets tend to coalesce faster than smaller ones. However, it shall be pointed out that equation 2.1 is valid for spherical-shaped particles [46, 62]. In the case of deformed particles, the velocity is still proportional to their diameter [66]. Nevertheless, the diameter considered is a nominal diameter which is corrected through the Corey parameter. The latter is a shape factor determined relating the cross-sectional area of an equivalent sphere to the maximum cross-sectional area of an ellipsoidal particle [67]. As a consequence, independently of their shape, it can be expected that bigger droplets in the Stokes regime require less time to coalesce compared to smaller droplets travelling for the same distance.

•Coalescence

Together with the dispersed droplets' diameter, the coalescence phenomenon is important to predict

the mixture's behaviour. As described in the previous subsection, droplets' coalescence consists of the droplets' motion towards their bulk phase. Coalescence depends on the characteristics of a film formed around the dispersed liquid by the interplay of the droplets with the continuous phase. The less time required by bigger droplets to get separated from the continuous phase is further emphasised when droplets cohere into each other, i.e. they coalesce. This is because they form several or one single droplet of larger diameter [68]. Hence, coalescence is described in this subsection to provide some insights into this phenomenon.

The importance of coalescence in gravity separation was highlighted by Frising et al. [62]. Although, more specifically, coalescence is only one stage of the overall process. This is carefully described by J. Kamp et al. [68]. Figure 2.6 depicts a schematic sequence of droplets collision and subsequent events which may occur. These are described in the following paragraphs.

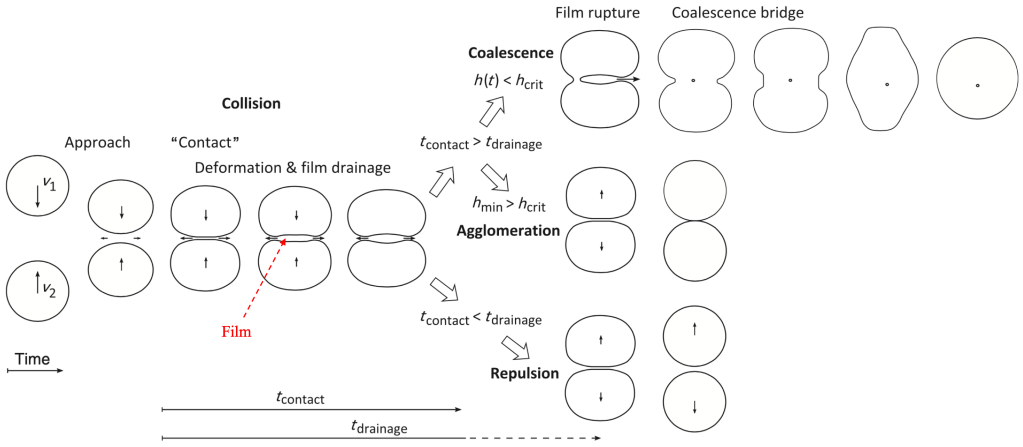

Figure 2.6: Schematic sequence of the droplets collision and subsequent events, adapted from [68]

For the droplets to form bigger geometries they first have to move towards each other. This happens with the droplets having a relative velocity and displacing a certain volume of the continuous phase. This behaviour generates frontal waves which interact with each other and further increase the continuous phase displacement. Nevertheless, the latter is limited by the viscous forces and counterbalanced by the deceleration and deformation of the droplets. Because of the deformation, a thin film is formed between the droplets, as it can be noticed in figure 2.6.

Driven by inertia forces, when the droplets touch each other they get more deformed. At this point, different phenomena can occur. First, if the film between the droplets gets drained it results in the so-called "film drainage" event. This is caused by a drop of pressure from the middle of the film towards the edge of the droplet. The film drainage occurs within a certain time span $t_{drainage}$, measured from the droplets' contact to the end of the film rupture. This ranges from milliseconds to seconds, but it reaches relatively infinity in stable emulsions [68].

If the drainage time exceeds the time during which the droplets are in contact ($t_{contact}$), a repulsion of the droplets occurs. If the film drainage time is smaller than the droplets contact time, coalescence or agglomeration happens. The coalescence results from droplets' conjunction when the droplets are at a distance ($h(t)$) falling below a critical value (h_{crit}, "critical distance"). The drops connect along the region where the film of the continuous phase was located before. This results in a coalescence bridge, as figure 2.6 shows. The interplay between inertia, viscous and interfacial forces dampens the waves

induced by the drops' movement and the droplets turn into a new spherical shape. In case $t_{contact}$ exceeds $t_{drainage}$ but the critical distance is not reached by the droplets, these move apart after having reached maximal deformation due to interfacial tension. And if $t_{contact}$ is smaller than $t_{drainage}$ the film does not have enough time to get rupture. Hence, collision and repulsion take place [68].

Factors were identified influencing coalescence. A higher viscosity of the continuous phase viscosity compared to the one of the dispersed phase increases the resistance of the film to rupture. Hence, coalescence is retarded. Furthermore, a higher density difference between the liquids slows down the film drainage. This is because the droplets get deformed (assuming a flattened shape) and thus the film thickness grows. Additionally, the buoyancy force increases minimising the droplets' interaction [69]. In addition, the higher the interfacial tension the higher resistance of the droplets to deformation [69, 70]. Consequently, the area of the drainage film decreases and therefore the coalescence time [69]. Moreover, external inputs can influence the process. In a scenario where the relative velocity between the droplets and the continuous phase rises, Coulaloglou and Tavlarides [71] found that the contact time between the droplets diminishes and therefore not enough time remains for the film to get drained. However, other authors propose the opposite trend [72, 73]. Lastly, the droplets' shape is found to be one of the most important parameters influencing coalescence. Finely dispersed droplets in the order of magnitude of a few micrometres and smaller stay in spherical shape. For them, in the assumed Stokes flow regime, the coalescence time drops with increased diameter (as already observed from equation 2.1). Nevertheless, with the droplets becoming deformable at a certain size a film with a larger area develops between the droplets. This would require more time to drain, hence the coalescence time increases with the droplets' diameter [68].

In this subsection it was seen that the coalescence plays an important role in the mixture's behaviour. Coalescence depends on the fuels' density difference, interfacial tension, and viscosity of the continuous liquid and dispersed droplets' shape. While density difference, interfacial tension and viscosity of the continuous liquid are inherent properties of the fuels, the dispersed droplets' shape requires discussions in view of the fuels' miscibility projection.

•Dispersed droplets shape

The droplets' geometry is discussed in view of the experimental results interpretations. The settling velocity of droplets is generally independent of their shape. Nevertheless, research showed that the latter indirectly affects the settling velocity as directly impacts the coalescence process. Two criteria were found in the literature allowing the prediction of the droplets' shape moving in liquid media. The first criterion is based on a diagram presented by Clift et al. [74]. This relates the droplet geometry to the Reynolds, Eötvös and Morton numbers. Respectively, these can be calculated as:

$$Re = \frac{\rho_c D v_t}{\mu_c} \tag{2.2}$$

$$E = \frac{g \Delta \rho D^2}{\sigma} \tag{2.3}$$

$$Mo = \frac{g \mu_c^4 \Delta \rho}{\rho_c^2 \sigma^2} \tag{2.4}$$

In all the equations above the subscript c refers to the continuous phase. Re is the Reynolds number expressing the ratio between inertia and viscous forces. In equation 2.2 the term v_t indicates the terminal settling velocity of the droplet. Equation 2.3 is the expression of the Eötvös number and represents the ratio between gravity and interfacial forces, whilst the Morton number (equation 2.4) is representative of a fluid property group. In both equations 2.3 and 2.4 the term σ appears. This

indicates the interfacial tension. An empirical expression for this was found by Girifalco and Good [75] in 1957. The interfacial tension is expressed as the energy of cohesion and adhesion between the two considered phases (a and b). The resulting formula is:

$$\sigma = \sigma_a + \sigma_b - 2\Phi(\sigma_a \sigma_b)^{1/2} \tag{2.5}$$

Where σ_a and σ_b are the interfacial tensions of the two phases, while Φ is an empirical value to be determined experimentally. However, Girifalco and Good provide a theoretical expression for Φ as a function of the molar volume V of the respective liquids:

$$\Phi = \frac{4V_a^{1/3}V_b^{1/3}}{(V_a^{1/3} + V_b^{1/3})^2} \tag{2.6}$$

Consequently, after calculating the value of σ using expression 2.5, it is possible to determine the Morton number with equation 2.4. This value is used to enter the graph presented by Clift et al. [74] to intercept the area where the droplets assume a spherical shape. In this area, for the known Morton number, the Reynolds and Eötvös numbers can be extracted. With the known Eötvös number, the diameter above which the droplets have a deformed shape can be determined from equation 2.3.

Another approach which correlates the droplets' shape with coalescence was derived by Wellek et al. in 1966 [70]. The authors studied the behaviour of non-oscillating droplets in liquid media for a set of binary mixtures. From the experimental results, a relation between the droplet deformation and the properties of the liquids was found. The droplet deformation is expressed as "eccentricity" as the ratio between the horizontal and vertical diameter of the droplet. The droplet deformation increases the lower the dynamic viscosity of the continuous phase and the higher the density difference between the liquids. With reference to the Reynolds and Eötvös numbers (equations 2.2 and 2.3) this means that the inertia forces and gravity are dominant over the viscous and interfacial forces respectively. This results in proportionality between the eccentricity and the droplet diameter, which aligns with the previously described approach. More specifically, a minimum diameter exists above which the droplets assume a deformed shape.

Consequently, both approaches can potentially be used for the droplets' shape prediction. However, the first approach based on the Eötvös number determination is favoured as the diagram developed by Clift et al. [74] provides a more straightforward visualisation of the results to be combined with the observations in the lab. The second approach presented is partially used in this study. The equation by Wellek and Agravwal [70] is not validated as very high-resolution images shall be available for analysis and therefore this approach is used to either confirm or deny the relation between the droplets' deformation and the fuels' properties.

Centrifugal separation

Centrifuges are consolidated technologies used onboard ships for separating water and/or solids from the fuel [19, 20]. The paragraphs below provide the working principle of centrifugal separation and the separator type selected for this work. The latter shall be modelled to provide an alternative to gravity separation.

•Centrifugal separation principle

Centrifugal separators multiply the gravity force acting on the two liquid phases increasing the driving force, which leads to separation, and the speed at which the separation happens [19, 48]. This principle is regulated by the following equations. Equation 2.7 expresses the force separating the liquid constituents by gravity in a settling tank. Equation 2.8 refers to the centrifugal force exerted

in a centrifugal separator. When the two formulas are compared it can be noticed that the gravity acceleration g is replaced by $\omega^2 r$. Hence, as already mentioned, by regulating the rotational speed ω and the effective radius r it is possible to increase the separating force [19]. Low to extreme multiples of gravity accelerations are 50-20,000 [19, 48].

$$F_s = \frac{\pi}{6} D^3 \cdot (\rho_h - \rho_l) g \tag{2.7}$$

$$F_s = \frac{\pi}{6} D^3 \cdot (\rho_h - \rho_l) \omega^2 r \tag{2.8}$$

•Disc stack centrifuge

For this study, disc stack centrifuges are selected. Liquid-liquid separation can be obtained with the same centrifuges used for liquid-solid separations. Sedimentation centrifuges are considered the most suitable for liquid-liquid separation. Although also hydrocyclones can theoretically be used they are not as effective as for solid-liquid separations. Generally, tubular and disc bowl centrifuges are used [76]. However, the tubular design is discarded from this research for handling challenges. More specifically, this design consists of a high-speed vertical shaft driving a tubular bowl [77]. For certain throughput, the sludge retention volume and liquid dwell time can only be increased by extending the bowl's length. This causes balancing and handling concerns on board ships [19]. Thus, disc bowl-type centrifuges are the sole designs discussed and studied here.

Figure 2.7 shows a section of a typical disc stack centrifuge. This design encompasses an electric motor which drives a shaft, on top of which a bowl assembly is mounted. This is surrounded by an outer framework which carries the feed and the discharge connections. The mixture is fed at the top of the bowl. Conical discs are mounted on top of each other, in a number up to 150 and spaced around 2-4 mm [19, 20]. Figure 2.7 depicts the motion of the heavy and light phases within a consecutive discs' section. The discs reduce the settling distance of denser droplets. In this way the separation zone is divided into thin layers such that these droplets have to travel a shorter distance before hitting the upper disc surface [78]. Here, the droplets lose their kinetic energy leading to coalescence [79]. Hence, because of the centrifugal force, the denser droplets get collected at the outer bow's wall and move towards the heavy phase outlet channel. Conversely, the lighter liquid flows upwards along the discs towards the axis and leaves the centrifuge through the light phase outlet channel [19, 20, 78].

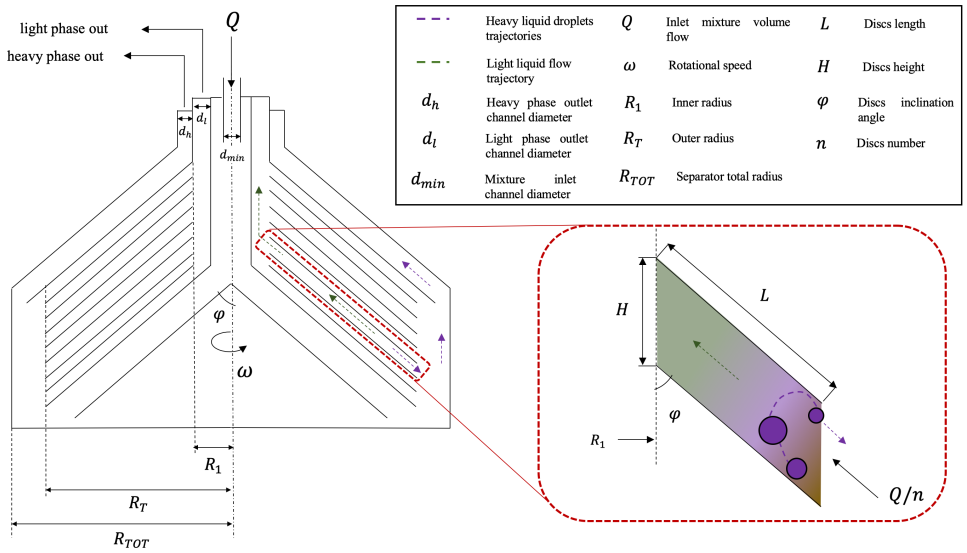

Figure 2.7: Interior of a disc stack centrifugal separator (left) and focused view of the section between consecutive dics (right), adapted from [61, 78, 79]

In section 2.2, the goal of achieving full HVO-methanol separation was defined. For this, the disc stack centrifuge performance shall be assessed if gravity separation fails to fulfil this requirement. The identified challenge for the effective use of disc stack centrifuges relates to the fuels' density. The methanol and EN 15940 densities differ of maximum 30.5 kg/m^3 and can even overlap [35, 41], depending on the bunkered fuel properties. Disc stack centrifuges can be used for biodiesel production to separate glycerol from FAME [80]. Considering glycerol and FAME densities [47], this process proves that it is possible to separate two liquids with a density difference of around 377 kg/m^3. Towler and Sinnott specify that applications for smaller density difference as low as 100 kg/m^3 are possible [76], while it has already seen that Green and Perry [48] recommend centrifuges for even lower density differences, i.e. values below 50 kg/m^3. The discrepancy of minimum allowed density difference leaves uncertainties regarding the effective methanol-EN 15940 diesel separation. This is enforced by the lack of lab tests on these specific fuels and the influence of tailored separator design parameters on its performance [81]. Thus, the separator sizing and the assessment of its performance are fundamental for the separation of HVO-methanol mixtures.

2.4. Literature research conclusions

When storing multiple fuels in the same storage tanks, variation of the bunkered fuel's concentration is expected. Combusted non-pure fuel(s) in PFI DF engines can lead to different challenges, defined from theoretical aspects and performed tests with close to HVO and methanol substances. Due to a lack of standards and research on accepted fuels, techniques were reviewed to achieve full fuels separation. For this, the fuels' mixture status must be known. In the considered storage conditions, one bunkered fuel-rich phase is expected. Thus, a homogeneous mixture is created. However, due to several downsides, technologies for the separation of homogeneous mixtures are not envisaged to be applied and a heterogeneous mixture shall be created to separate the fuels. Gravity tanks and disc stack centrifuges are selected. Regarding gravity, the literature does not quantify the time for HVO-methanol to achieve full gravity separation. This is a fundamental aspect onboard to match the desired throughput and fulfil the yacht's operations. The literature evidenced the importance of shake tests to observe the phase separation of liquid mixtures. Thus, experiments of this type would help to quantify the phase separation efficacy and time of HVO-methanol mixtures. Aspects of the dispersed droplets in the mixture would help correlate the tests observations with the fuels' properties. Coalescence phenomenon, dispersed droplets' diameter and shape are identified as important aspects. Regarding centrifuges, the minimum density difference between the treated liquids required for an effective separation is not well understood within the literature. Hence, a disc stack centrifuge sizing and performance assessment are necessary.

3

Experimental study on phase separation of HVO-methanol mixtures

As emerged from the literature review in chapter 2 no accurate conclusions can be drawn relative to mutual HVO and methanol miscibility. An experiment is carried out to assess the phase separation of HVO-methanol mixtures. In this chapter, the experiment objective is explained. Next, the methodology followed and the description of the tests set-up are covered. Lastly, results are discussed and conclusions are presented.

3.1. Experiment objective

The experiment aims to study the miscibility of HVO-methanol mixtures. The available literature for methanol-hydrocarbons mixtures shows good insights relative to the singular compounds interaction. Nevertheless, the studied binary mixtures are not fully representative of the HVO-methanol case. Moreover, with a further look at the yacht's operations, it is not clear how much time the HVO-methanol mixture needs to phase separate by gravity. Hence, a test is conducted to quantify the time required by the fuels to fully phase separate for different concentration ratios.

3.2. Experiment methodology

The phase separation observation of the liquid mixture is performed at two different levels. On a higher level, the phase separation determination consists of a visual change observation from the cloudy to limpid aspect of the two phases. This denotes a change from a binary to a single homogeneous phase, as highlighted by T. Santos et al. [82]. On a deeper level, the phase separation is tracked at the micro-scale via the utilisation of a microscope. This approach enables the visualization of the potential presence of one fuel's droplets into the other. Moreover, in subsection 2.3.2 the importance of the droplets' diameter on the separation time was discussed. Hence, with the utilisation of the microscope, the diameter of the possibly observed droplets can be measured. Several experts employed microscope imaging to study the behaviour of mixtures. H. Le Ferrand [83] et al. used a cryo-transmission electron microscopy to image the liquid-liquid phase separation of proteins into concentrated microdroplets. Similarly, a light microscope was used to investigate the liquid-liquid phase separation of Tau proteins in vitro [84]. T. Frising et al. [62] used an optical microscope to investigate emulsions of water in oil. Furthermore, X. Zhang et al. [85] reviewed the utilisation of microscopes for intracellular liquid–liquid phase separation. They discussed the potential of a set of microscope types for droplets tracking. The light microscope was found to

process high imaging speed and minimal light exposure, making it a highly promising choice for prolonged observations. Although these studies are quite far from fuels' applications, they underline the relevancy of micro-scale observations.

A research on fuels for ships was performed by G. Doetjes [86]. In this case, the emulsion of F-76 diesel fuel and methanol was studied. First, the liquids were poured into the beaker and they were subsequently stirred for 5 minutes in order to create an emulsion. Liquid samples were extracted at different time intervals with a syringe and observed under a light microscope. The microscope enables the visualisation and size measurement of possible droplets of one fuel into the other. Given the nature of the studied fuels close to HVO and methanol, the methodology of G. Doetjes is followed. Similarly, the fuels mixture is stirred to create a random dispersion of one fuel into the other. Moreover, mixture samples are extracted at time intervals for analysis.

Lastly, because the droplets can be observed and measured under the microscope, mathematical formulas are researched within the literature to predict the mixture's behaviour by finding a relationship between separation time, concentration ratios and droplets diameter. M. Fossen et al. [87] computed a formula to relate the settling and coalescence times with the mixture parameters. In this correlation, the interfacial tension is an unknown parameter. An approximate value can be determined via the already mentioned empirical formula developed by Girifalco and Good [75]. Nevertheless, for an accurate result, the determination of the interfacial tension shall be performed via tests. On the other side, even in case the formula by Girifalco and Good is used, the formulations computed by M. Fossen et al. [87] refer to the Sauter mean diameter (SMD) which is not a representative value of the single droplets' diameter. The SMD is in fact the mean diameter of a distribution of different size droplets [48]. Furthermore, the Stokes formula (equation 2.1) could be deployed with corrections to take into consideration the concentration ratios of the two fuels and the droplets flow regime [64, 65]. Nevertheless, for fixed input parameters these formulas would give only one droplet diameter value. This is not representative of what is derived in reality, since experiments already showed diameter distributions [62, 68, 86]. Hence, the results discussion is limited to the observations in the lab and no equations are used for validation.

As a consequence, the presented methodology encompasses higher and deeper level observations of methanol-HVO mixtures. No equations are used to correlate the required time with the fuels ratio and dispersed droplets diameter. With these information, the experiment setup can then be defined.

3.3. Experiment set-up

The tests were performed in the *Scheikunding Laboratorium Defensie* in Den Helder. The tested HVO and bio-methanol were supplied by *GoodFuels*, whose specifications are reported in table 3.1. The appearance of the pure fuels can be observed in figure 3.1 (a).

The experiment set-up consists of a camera placed in front of the beakers to record the volume level variation relative to a millilitres-scaled beaker and a ruler with a millimetres scale placed on the beaker's side. A picture of the experiment set-up is given in figure 3.1 (b). Moreover, a light microscope is used for the determination of the possible presence of methanol traces in HVO.

The testing procedure consists of pouring the fuels into a beaker at different volume concentrations relative to a fixed mixture's total volume. Second, a magnetic stirrer is deployed to enable the fuels mixing. After stirring is completed, liquid samples are removed from the beaker and transferred to slide chambers to be observed under a light microscope, illustrated in figure 3.1 (d).

The used beaker in which the two fuels are poured has a diameter of 5 cm and a height of 17 cm. The mixture's total volume equals 100 ml and the tests are carried out on methanol at 5, 10, 20, 30, 40, 50, 60 and 70% v/v and room temperature of 20°C. A magnetic stirrer is deployed to enable the fuels to mix at a rotational speed of 1200 rpm. The stirring time is set at one minute following the recommendations by Green and Perry [48]. The utilised magnetic stirrer is illustrated in figure 3.1 (c). To monitor the mixture's behaviour over a time range, samples are extracted after 5, 30 and 60 minutes. The liquid samples are withdrawn with a Pasteur pipette and at a location corresponding to half the height of the light (top) phase for results consistency.

Table 3.1: Tested HVO and methanol main specifications
(* at 15°C, ** at 20°C)

Parameter	Unit	HVO	Methanol
Colour (appearance)	[-]	Colourless (clear and bright)	Colourless (pale)
Relative density	[-]	0.7811*	0.7927**
Purity on dry basis	[% m/m]	-	99.97
Water	[% m/m]	0.04	0.005
Sulfur	[mg/kg]	< 3	4
FAME	[% v/v]	< 0.05	-
Total aromatic hydrocarbons	[% m/m]	< 0.2	-
Kinematic viscosity	[m^2/s]	$3.127 \cdot 10^{-6}$	-
Dynamic viscosity	[Ns/m^2]	-	$0.54 \cdot 10^{-3}$
Flash point	[°C]	86	9.7
Boiling point	[°C]	218.7	64.7

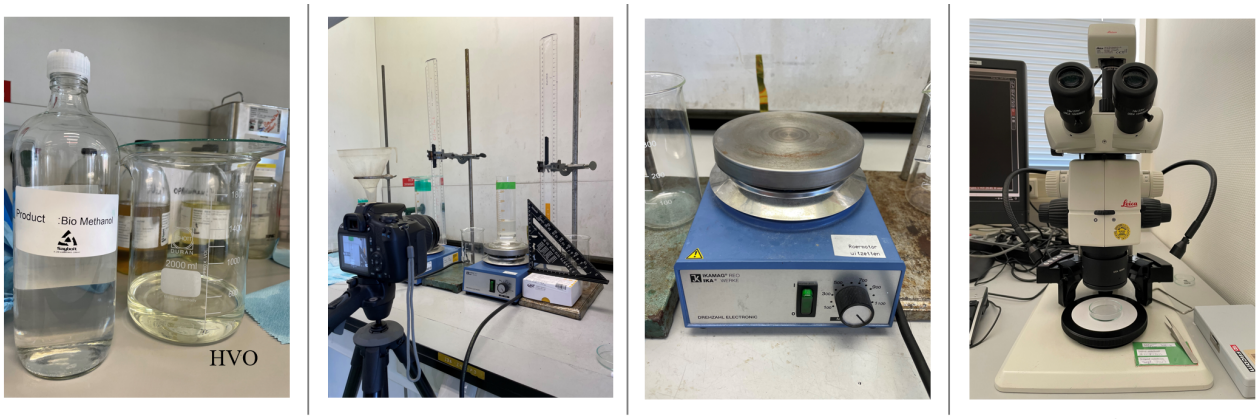

(a) (b) (c) (d)

Figure 3.1: Experiment set-up and equipment
(a: pure bio-methanol and HVO appearance; b: experiment set-up; c: magnetic stirrer; d: light microscope)

3.4. Experiment results

In this section, the experiment results are presented. During the tests, different behaviours were observed for the different methanol concentrations. A relation was found between the separation time and the observations at the microscope. More specifically, these relate to the methanol droplets' size and shape as discussed in subsection 2.3.2. The droplets' shape and diameter distributions are presented in this section.

3.4.1. Droplets shape

In this subsection, the shape of the observed droplets is discussed. Results from the Eötvös number-based approach covered in subsection 2.3.2 are presented and compared to lab observations. Correlations to the presented gravity separation theories in subsection 2.3.2 are presented.

The minimum diameter above which the droplets assume a deformed geometry is calculated following the first approach described in subsection 2.3.2. Furthermore, it has to be pointed out that methanol is treated as the dispersed phase for methanol concentrations up to 50% v/v. For greater values, HVO becomes the dispersed liquid. Firstly, the interfacial tension of the mixture is determined using the empirical formula from Girifalco and Good [75] showed in equation 2.5, with the parameter Φ determined using equation 2.6. Used input values are the ones given from the fuels safety data sheet by the supplier and reported in table 3.1. The resulting minimum diameter of methanol droplets is 9.7 mm applicable for 5-50 % v/v methanol concentrations. For methanol concentrations ranging 60-70% v/v the minimum diameter refers to HVO and its value stands at 8.6 mm. With reference to equation 2.3, the smaller value for HVO stems from the lower Morton number which is due to the smaller dynamic viscosity of methanol.

These results are compared to the observations in the lab. Pictures of the droplets' geometry are displayed in figure 3.2 for different methanol concentrations. The images are captured before the mixing stirrer activation. The pictures reveal spherical droplets at a maximum diameter approximately equal to the calculated values. A possible explanation of this discrepancy lies in the calculated superficial tension stemming from an empirical formulation and the manually read Eötvös and Morton numbers from the diagram presented by R. Clift et al. [74]. Moreover, for methanol ranging 5-50% v/v the bigger methanol droplets can be found towards the bottom of the beaker. For spherical droplets, this behaviour lines up with the Stokes law (see equation 2.1). Deformed methanol droplets are also located at the bottom of the beaker in the 5-50% v/v mixtures, but this is not the case for methanol in the range 60-70% v/v. In the latter situation, in fact, the droplets get deformed at a smaller minimum diameter compared to 5-50% v/v cases. Hence, as discussed in subsection 2.3.2, the methanol droplets require more time to coalesce due to the larger time required by the film to get drained. Furthermore, at very low concentrations (5-10% v/v), the number of visible droplets is significantly fewer than in the other cases. This is because the low concentration of the dispersed phase increases the distance between the droplets. Hence, these do not easily reach the critical minimum distance to get in contact and merge into bigger droplets. Consequently, mainly small and spherical shapes can be visualised. The spherical geometry is also what was observed under the microscope for all samples.

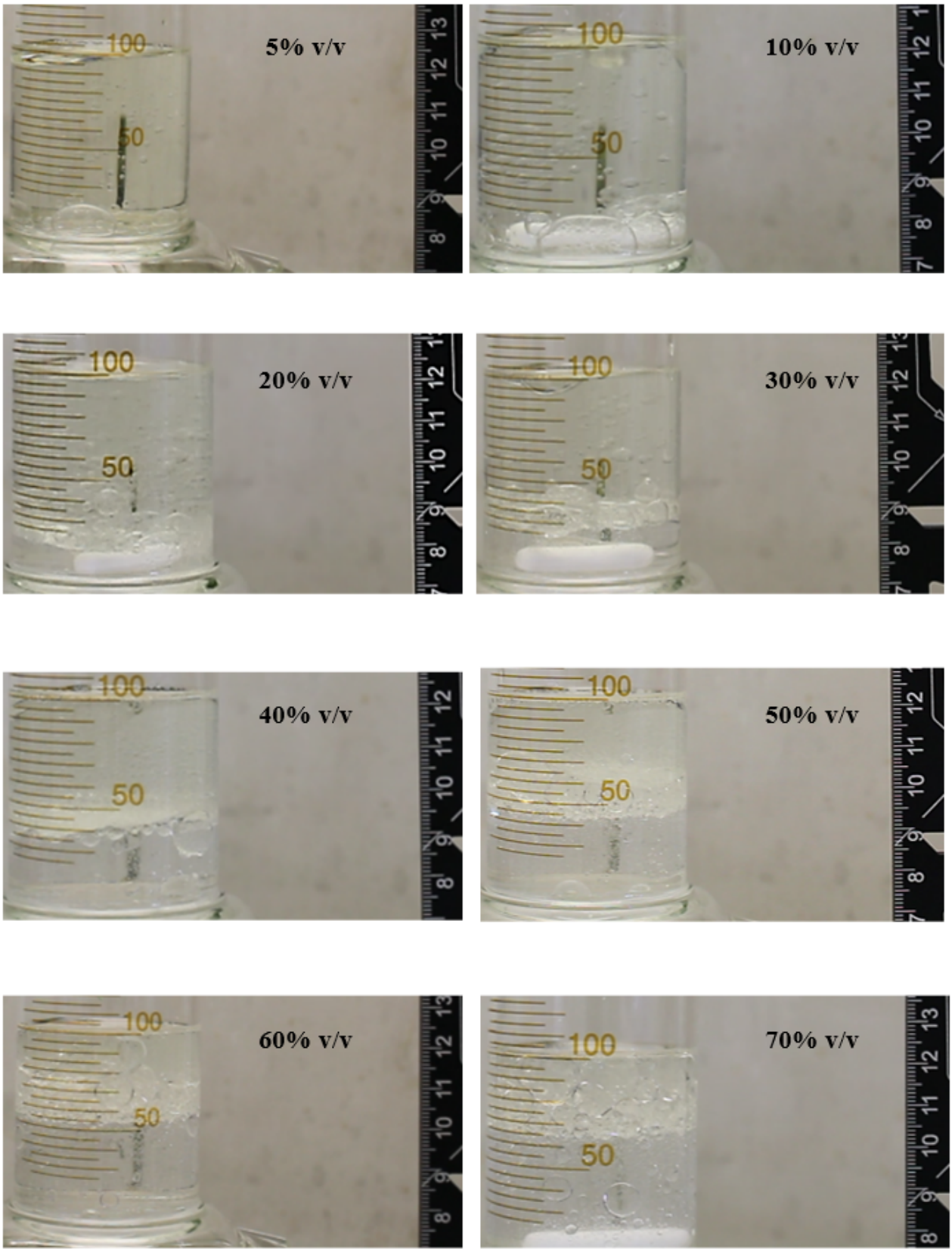

Figure 3.2: Droplets' shape for different methanol volume concentrations (post-mixture stirring time point)

3.4.2. Droplets size distribution

In this subsection, the results relative to the dispersed methanol droplets' size distribution are presented. Results are discussed based on the theory covered in subsection 2.3.2.

The average methanol droplets' diameter and associated standard error are shown in figures 3.4, 3.5, 3.6. The plots are presented for each methanol volume concentration as a percentage of the mixture's total volume and at the time intervals at which the liquid samples were extracted from the beaker.

In general, it resulted that bigger droplets settle down faster compared to smaller ones. This phenomenon can be visualised in a picture taken during the test shown in figure 3.3. The observations refer to the free-surface behaviour neglecting the effect of the beaker walls. Figure 3.3 reveals the dense-packed zone of dispersed methanol droplets at half the total volume height. This result aligns with the predictions for which the Stokes velocity is proportional to the droplet diameter as discussed in subsection 2.3.2.

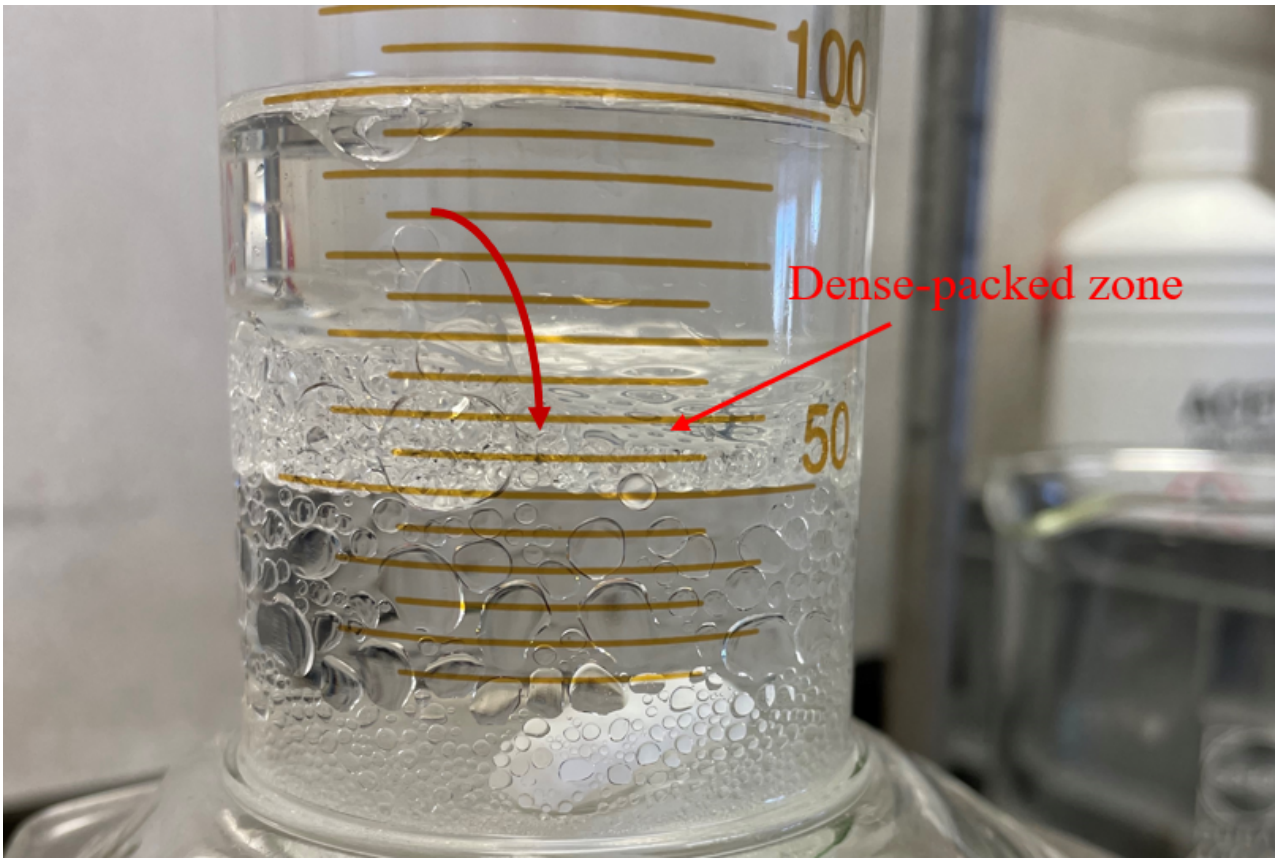

Figure 3.3: Methanol droplets settling

The results analysis can be divided into three different methanol volume groups. The reason behind this classification lies in the different behaviours revealed by the tested mixtures. The first group encompasses the 5-20% v/v range, the second group consists of the 30-50% v/v range and the third covers the 60-70% volumes.

First, with reference to figure 3.4, for methanol at 5-20% v/v, the droplets decrease in size after 30 minutes when compared to the 5-minute case. After 30 minutes the bigger droplets had already settled but smaller droplets remained within the beaker column. Because the methanol ratio is relatively low, the distance between the droplets hardly reaches the minimum critical

value to lead to coalescence. Hence, the probability of the small droplets being encountered by larger ones and merging with each other is also low. The droplets' collision and conjunction occur after 1 hour for the methanol at 5% v/v, in fact, the methanol droplets' diameter grows. Nevertheless, this is not the case for 10-20% volumes. That is to say that after 1 hour the methanol droplets are still smaller compared to the observation at 30 minutes. It can be hypothesized that the droplets have already merged in a time interval between 30 and 60 minutes and therefore the droplets size distribution only shows the tiny droplets remained in the HVO column.

The second case refers to 30-50% methanol volume concentrations. Here the methanol droplets become bigger after 30 minutes, whilst their size decreases after 60 minutes. In fact, it was observed that the larger droplets settle down faster leaving the smaller droplets behind, which explains the relatively small diameter values after 5 minutes plotted in figure 3.5. Subsequently, after 30 minutes these small droplets are merged to form bigger ones. After the latter have settled down, only smaller droplets are left within the HVO volume and they do not have enough distance to cohere into each other. Hence, small droplets remain at the top layer and therefore require a longer time to settle and complete the full separation. However, the effect of droplets' size decrease becomes less pronounced when methanol volume concentration is increased to 50%.

The third group consisting of MeOH at 60-70% v/v shows a slightly different behaviour than the already discussed scenarios. In this situation, it has to be considered that methanol represents the continuous phase. For methanol at 60% of volume, coalescence is faster because visualised HVO droplets after 30 and 60 minutes are smaller than the first observation. This could be explained by the higher HVO dynamic viscosity compared to methanol, which makes the film between droplets vulnerable to rupture. For this reason, the HVO droplets have already merged and coalesced in the 5-30-minute time interval. This trend is followed after 30 minutes, with the HVO droplets becoming even smaller. Regarding methanol at 70% v/v, the HVO droplets become bigger only after 30 minutes. This means that the droplets require a longer time to get in contact and merge into each other compared to the previous case. During the tests, it was observed that an increase in methanol concentration leads to the formation of bigger droplets which mainly locate at the bottom of the beaker. In this way, there is not much space left for the small HVO droplets to pass through.

Lastly, samples with methanol at 1% and 50% v/v were also inspected after three days. The methanol diameter distributions are illustrated in figure 3.7. The droplets become quite tiny compared to all the shown cases, especially in the case of 50% methanol volume (see figures 3.4, 3.5, 3.6). The presence of methanol in HVO after three days indicates that full separation does not happen within three days. In the previous subsection, it was mentioned that all droplets observed under the microscope have a spherical shape. Hence, the incomplete separation after three days resulting from 1% and 50% v/v methanol cases is in line with the fact that small spherical droplets require a long time to coalesce. Overall, this poses a significant challenge in the fuels treatment onboard the yachts, meaning that gravity settling tanks are considered infeasible to be used to separate the mixed fuels, considering a quasi-instantaneous fuel(s) supply to the engines. The reason behind this result might lie in the low-density difference between the fuels (see table 3.1) and the dynamic viscosity of both fuels. Green and Perry [48] identified threshold empirical values under which a stable dispersion is formed ($\Delta\rho = 0.05\,\mathrm{kg/m^3}$ and $\mu = 0.1\,\mathrm{Ns/m^2}$). With reference to table 3.1, the density difference and dynamic viscosity of the tested fuels fall below the threshold values and therefore the presence of dispersed droplets in the continuous phase occurs. Pictures showing the mixture appearance at the tested fuels ratios are reported in appendix B. All the images do not reveal clear phases with cloudiness levels depending on the methanol volume concentration and observation time. Moreover, in all scenarios a variation of the two phases' thickness cannot be quantified if measurements are taken with reference

to the millimetre ruler placed next to the beaker, showing that with time no substantial volume of the dispersed liquid has moved towards its bulk column. As a consequence, it can be stated that the partial separation is ought to the different polarity nature of the liquids, as seen in chapter 2, for which repulsive forces are established to keep the single methanol and HVO droplets apart.

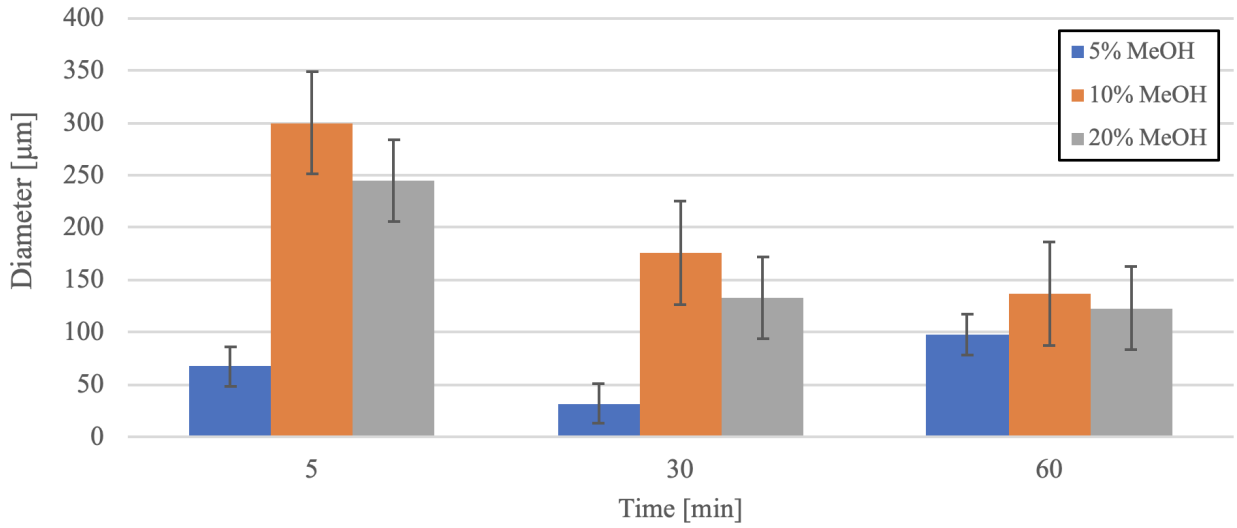

Figure 3.4: Average diameter of methanol droplets for methanol at 5-20% v/v

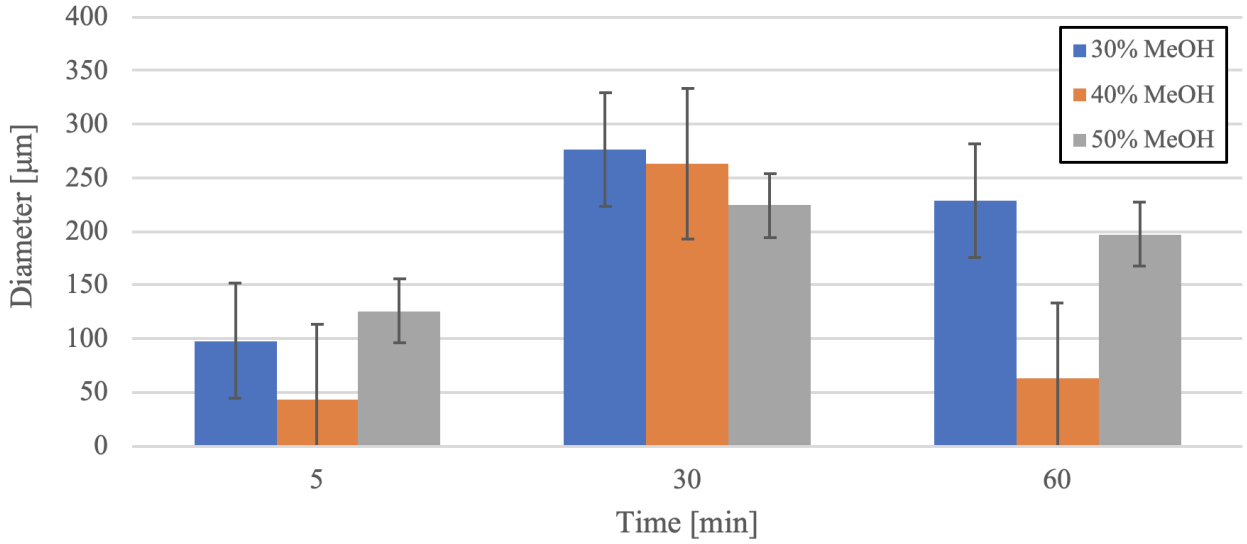

Figure 3.5: Average diameter of methanol droplets for methanol at 30-50% v/v

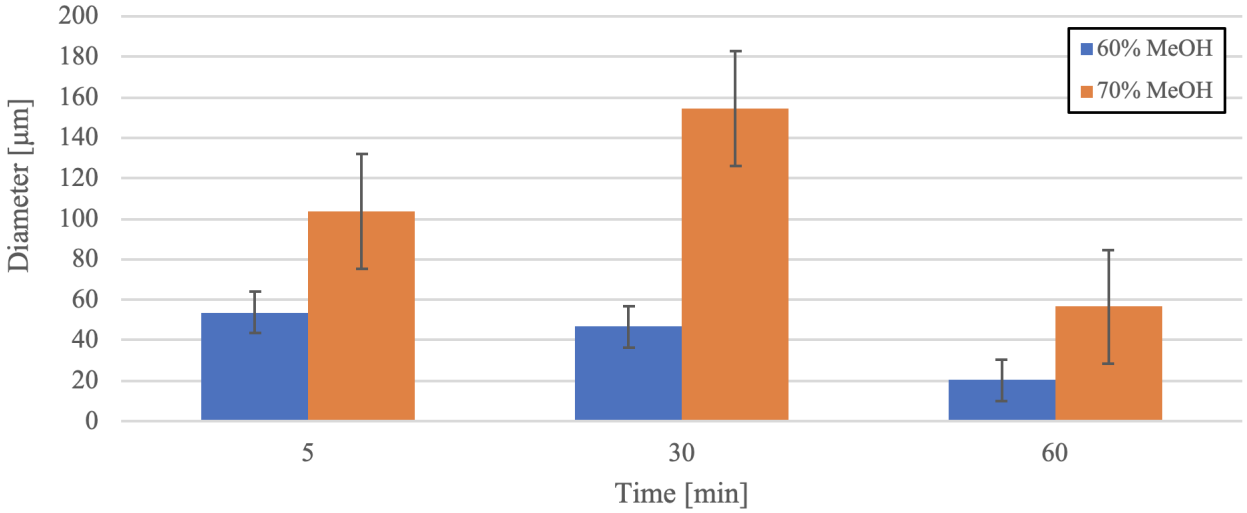

Figure 3.6: Average diameter of methanol droplets for methanol at 60-70% v/v

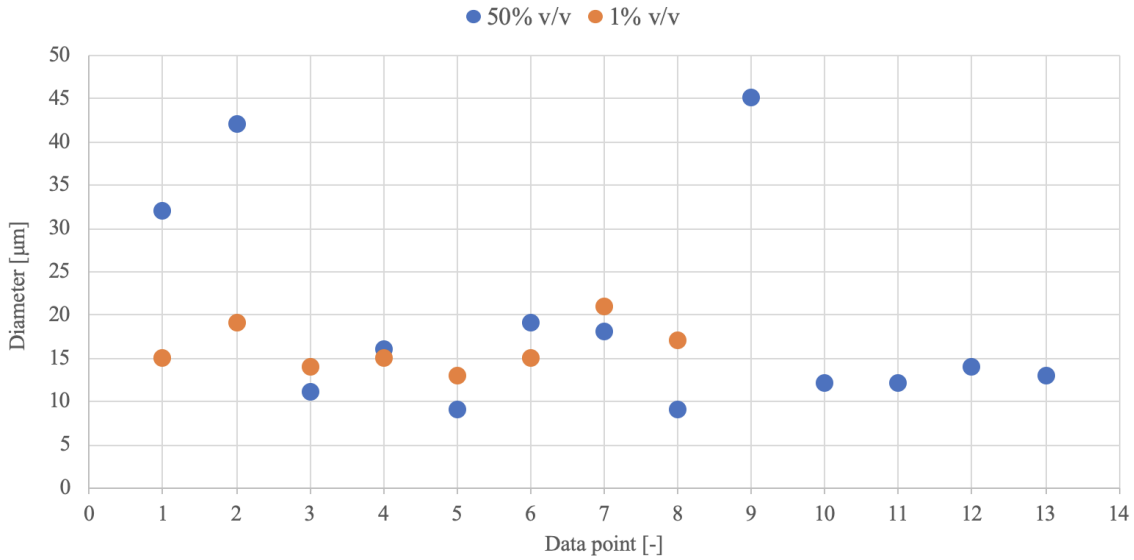

Figure 3.7: Methanol droplets' diameter distribution after three days

A last test was carried out with methanol at 30% v/v with a variation of the mixture's total volume. This methanol concentration was selected because from the resulting behaviours, the separation slows down compared to higher concentrations but it is quicker than lower methanol ratios. The total volume of the mixture was doubled to 200 ml. The diameter distribution is represented in figure 3.8. It can be noticed that the diameter reduces overall. However, the reduction becomes more evident after 1 hour. This phenomenon can have a significant impact on the mixture behaviour in the storage or gravity settling tanks onboard. In fact, it can be assumed that for fuels in storage or settling tanks with a capacity substantially higher than the beakers used in the lab, the formation of tiny droplets gets more pronounced. Consequently, separation by gravity would require a longer time than 1 hour. This time might further extend, considering that from the tested samples full separation after three days could not be detected.

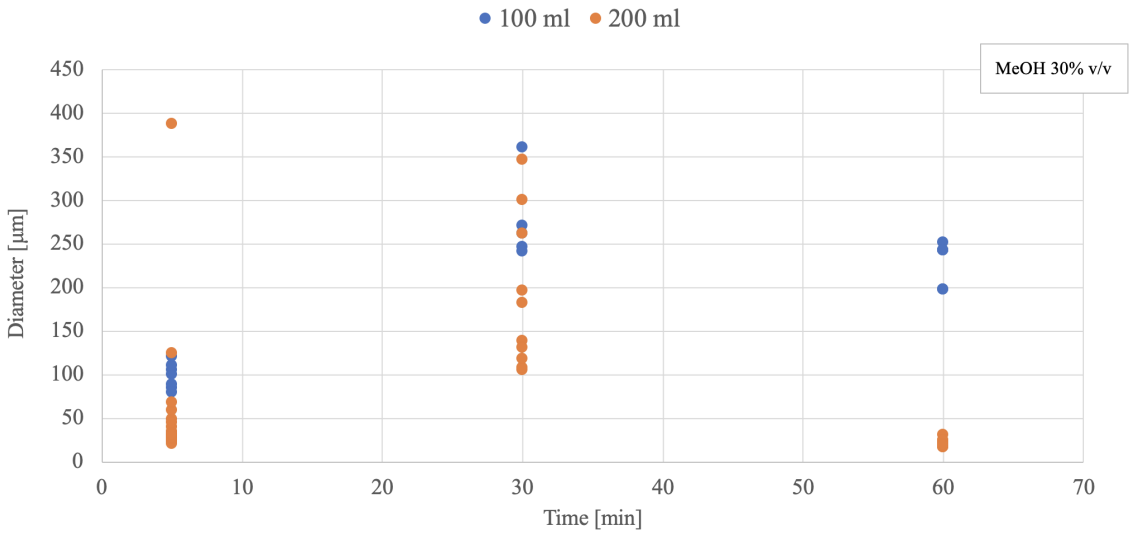

Figure 3.8: Methanol droplets' diameter distribution for total mixture volume variation (MeOH at 30% v/v)

3.5. Chapter conclusion

This chapter discussed the experiments conducted on HVO-methanol mixtures at different relative concentrations. The importance of the tests lies in the quantification of the time and relative volume ratios of the fuels to achieve full separation. The dispersed droplets' diameter and shape were found to be relevant parameters to be observed. Three groups were identified based on the methanol volume in the mixture, due to the same behaviours observed within the group. Overall, the results were found to be in agreement with the presented theoretical background. The most striking outcome is represented by the non-achieved full separation of all the tested mixtures after 1 hour. This time is further extended to 3 days for methanol at 1% and 50% of volume. This conclusion is assumed to be valid for the other mixtures under the tests conditions. Consequently, the usage of gravity settling tanks is found to be unfeasible for the fuels separation onboard considering a quasi-instantaneous clean fuel supply to energy converters.

4

Modelling of a disk-bowl type centrifugal separator

The tests carried out on HVO-methanol mixtures revealed the unfeasibility of the fuels separation via gravity in view of a quasi-instantaneous clean fuel supply to energy converters. Hence, centrifugal separators are to be investigated to overcome this challenge while achieving full separation. This chapter covers the description of a mathematical model of a disc-stacked centrifugal separator. Firstly, the approach followed for the mathematical model development is given. Next, the model hypotheses are presented. Lastly, an analysis is shown to assess the sensitivity of the model to input parameters.

4.1. Mathematical model approach

The mathematical model aims to get an understanding of a disk-stacked centrifugal separator for the HVO-methanol separation and in the optic of the centrifuge integration in the multi-fuel system. In this section the approach to tackle the presented analysis is presented, followed by the hypothesis made to facilitate the modelling.

For this analysis the output parameters are the time required by the separator to start its operations and the separator performance. The separation time is calculated and referred to as the starting time as the centrifuge is selected to work continuously, supplying fuel to the energy converters onboard quasi-instantaneously. Thus, the starting time would be the only parameter to cause possible delays to the yacht's operations. Regarding the separator performance, this is assessed aiming at achieving complete separation. Furthermore, the separator outlet volume flows represent inputs for this problem. More specifically, they are design constraints as the volume flow of the fuels exiting the separator must match the fuel volume flows required by the energy converters onboard.

In chapter 2 it was seen that the disc stack centrifuge selected for this study is a separator bowl-type consisting of a series of discs vertically arranged and with controlled interspacing. The fed mixture enters the discs section and separation of the two constituent liquids occurs. An illustration of this geometry is given in figure 2.7. For this analysis, the focus is directed towards the motion of the individual heavy fuel droplets within the separator discs' sections. This is because the centrifuge macro behaviour does not give any indications of the identified output parameter and centrifuge performance. Some studies, in fact, highlighted the importance of the dispersed droplets observation for the settling time and performance [78, 79, 88]. The settling time and separation performance are determined by the dispersed droplets' motion within consecutive discs' sections. Regarding

the separation time, no universal equations exist for the settling time of the dispersed droplets in a centrifugal environment, given the non-linearity of the problem. A list of equations for the gravity coalescence time exists [78] where the gravity contribution can be thought to be replaced with the centrifugal force. However, the equations are in disagreement and the presence of other unknown parameters makes the usage of these equations harder. Some mathematical models of centrifugal solid-liquid mixtures separation were developed [78, 89, 90, 91, 92]. While they represent relevant investigations within a centrifugal modelling approach, they refer to tubular designs. For this reason, they are not fully representative of the disc-stacked bowl. Nevertheless, some of these works [89, 90, 91] show that the separation time can be determined by computing the equations of motion of the dispersed droplets. Hence, this approach is considered valid for the calculation of the centrifuge starting time. Furthermore, by knowing the single droplet motion, the separator performance can be assessed. More specifically, the droplet trajectory can be determined to observe whether the dispersed fuel droplet follows the desired path. Lastly, relative to the centrifuge efficiency, it shall also be investigated whether this is influenced by the considered model parameters.

The motion of the dispersed fuel droplets in a centrifugal separator is a typical two-phase flow problem. This means that the two liquids in two thermodynamic phases exist in a simultaneous flow [93]. In this model, the equations of motion are computed for the heavy phase droplets, meaning the fuel with the higher density. This relates to actual marine separator designs, for which the heavy phase represents the dispersed liquid [94].

Furthermore, reference can be made to figure 2.7 for the computation of the motion equations of the heavy fuel droplets. These are formulated in a manner that confines their trajectories to the interstitial region between successive discs. This formulation presupposes the scenario wherein droplets of the denser phase undergo separation upon collision with the upper disc surface [79]. Other areas of the separator, namely inlet and discharge sections, are not analytically modelled since it is assumed that the single droplet follows a regular trajectory in the direction of the inlet/outlet flow.

4.2. Mathematical model hypotheses

The approach followed to compute the equations of motion between two consecutive discs' section is based on the forces balance. The model built by H.P. Greenspan [88] suggests a balance between drag and centrifugal 'gravity' forces, which represent the main forces acting on the droplet. In fact, gravity per se is negligible compared to centrifugal force, considering that the centrifugal force is ranged from 5000-8000g in centrifugal separators [19]. In reality, other forces are exerted on the denser droplets, such as Coriolis and shear forces, and thermal energy. However, the contribution of the first two forces is considered to be negligible relative to the centrifugal force, whilst the thermal energy can be ignored due to its uncertain effect within a centrifugal environment [78].

The model is based on the following assumptions:

1. Binary mixture: water and/or solids can be found in the bunkered fuel, representing added substances to the binary fuels mixture. However, to facilitate the analysis, HVO and methanol are the only mixture constituents considered in this work.
2. Incompressible fluids.
3. Ideal separation: full removal of HVO/methanol from methanol/HVO. An equation was written by J.P van der Linden [95] to calculate the separation efficiencies based on the inlet and outlet volume flows, with the values of the latter measured in the lab. Following the mass balance approach, an ideal separation simply means that the outlet volume flow equals the

inlet throughput. In reality, other approaches were used to determine the separation efficiency as a function of the droplet diameter [78, 79]. However, in this case, the droplet diameter is selected as a parameter constraining the separator space design.

4. The heavy phase droplet is a perfect sphere and its shape and size remain unchanged from the inlet to the outlet condition. This assumption follows the hypothesis of negligible shear stress which can alter the droplets' shape and size via break-up and deformation.
5. The flow through the discs' section is uniform, i.e. no flow variations are considered. This stems from the assumption of no droplets break-up as the motion is representative of a single droplet.
6. When the droplets hit the upper disc they slide along it with no friction.

4.3. Equations of motion

The description of the mathematical model leading to the final equations of motion is presented in different subsections to enhance clarity and prevent confusion for the reader.

4.3.1. Reference system and forces equilibrium

In section 4.1 it was said that the critical section to be considered is the space between two consecutive discs. A representation of this section is illustrated in figure 4.1, while a section of the entire separator is presented in figure 2.7. In principle, with reference to figure 4.1, the dispersed droplets enter the discs' section travelling a certain distance before hitting the upper disc. Here, they coalesce towards the outer bow's wall and get discharged.

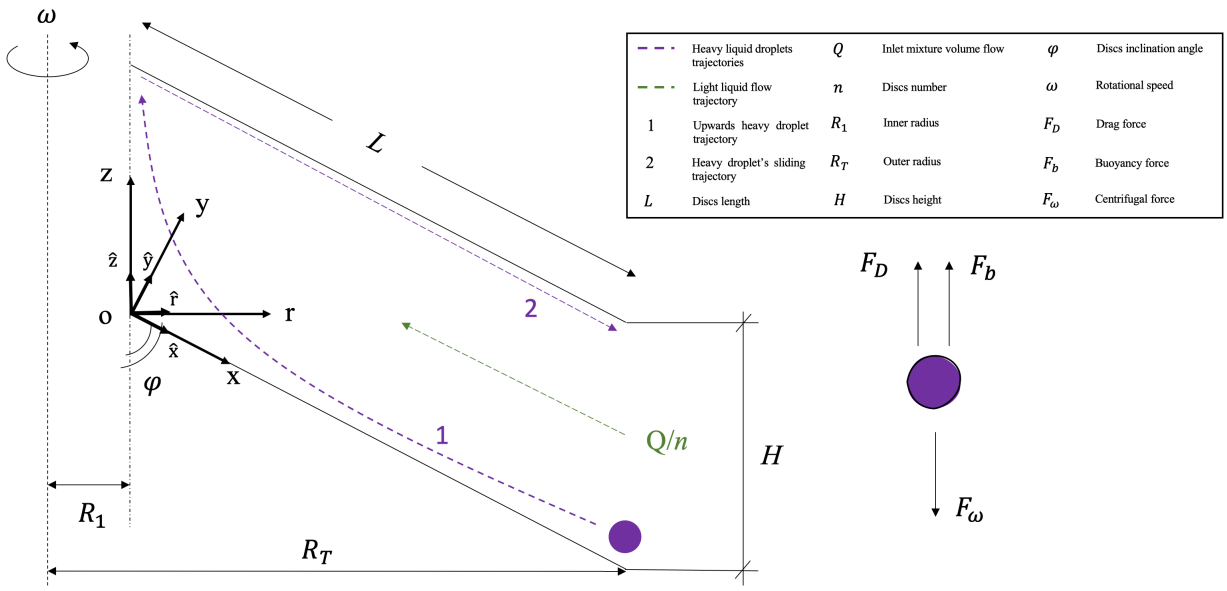

Figure 4.1: Fuels' trajectories within a consecutive discs' section and forces on the heavy fuel droplet

In figure 4.1 it can be observed that a reference system with the same inclination of the discs was selected. Such a rotating reference frame enables a two-dimensional analysis, embedding the circular motion of the droplet due to the centrifugal force. The equations describing the rotation of this reference system with respect to the rz coordinate system are presented below:

$$\begin{cases} x = r\ sin\varphi - z\ cos\varphi \\ y = r\ cos\varphi + z\ sin\varphi \end{cases} \tag{4.1}$$

$$\begin{cases} r = x\ sin\varphi + y\ cos\varphi \\ z = -x\ cos\varphi + y\ sin\varphi \end{cases} \tag{4.2}$$

$$\begin{cases} \hat{x} = \hat{r}\ sin\varphi - \hat{z}\ cos\varphi \\ \hat{y} = \hat{r}\ cos\varphi + \hat{z}\ sin\varphi \end{cases} \tag{4.3}$$

$$\begin{cases} \hat{r} = \hat{x}\ sin\varphi + \hat{y}\ cos\varphi \\ \hat{z} = -\hat{x}\ cos\varphi + \hat{y}\ sin\varphi \end{cases} \tag{4.4}$$

From the equations above it is possible to compute the velocity and acceleration for each direction as a function of time. For a conservative approach, it is assumed that the droplets enter at the bottom edge with an acceleration in the x-direction. From the equations above the acceleration in the x-direction can be decomposed as:

$$\ddot{\vec{x}}_d = \ddot{x}\hat{x} + \ddot{y}\hat{y} \tag{4.5}$$

The acceleration in the x-direction is determined to manipulate Newton's second law:

$$\sum \vec{F} = m_d \ddot{\vec{x}}_d \tag{4.6}$$

Where m_d is the droplet mass which for spherical shapes is expressed as [46, 78]:

$$m_d = \frac{\pi}{6}\rho_h D^3 \tag{4.7}$$

In the equation above ρ_h is the density of the heavy fuel whilst D is the denser droplet diameter.

The forces vector is the summation of the considered buoyancy, centrifugal and drag forces experienced by the droplet. Respectively their expressions are [19, 46, 78]:

$$\vec{F}_b = -\frac{\pi}{6}D^3\rho_h r\omega^2\hat{r} \tag{4.8}$$

$$\vec{F}_\omega = \frac{\pi}{6}D^3\rho_l r\omega^2\hat{r} \tag{4.9}$$

$$\vec{F}_D = C_D\frac{\pi D^2}{4}\frac{1}{2}(\vec{V}_F - \vec{V}_d) \tag{4.10}$$

Where, in equations 4.8 and 4.9, ρ_h and ρ_l are the density of the heavy and light fuel respectively. In equation 4.10 the vectors $\vec{V}_F$ and $\vec{V}_d$ respectively indicate the velocity of the flow entering the single discs' section and the velocity of the heavy liquid droplet. The expression for $\vec{V}_F$ is presented in the next section, whilst the term C_D represents the drag coefficient and it is a function of the Reynolds number. The expression for C_D [46] is given below:

$$\mathrm{C_D} = \begin{cases} \dfrac{24}{Re} & Re < 1 \\ \dfrac{24}{Re}(1 + \dfrac{3}{16}Re) & 1 \leq Re < 5 \\ 1.85Re^{-0.6} & 5 \leq Re < 5000 \end{cases} \tag{4.11}$$

With the Reynolds number of the droplet expressed as [93]:

$$Re = \frac{\rho_l D}{\mu_l}(\dot{x} + V_F) \tag{4.12}$$

Where μ_l is the dynamic viscosity of the light fuel expressed in kg/ms. Now, writing the equilibrium of the forces from equation 4.6 it results:

$$m_d \ddot{\vec{x}}_d = \vec{F}_b + \vec{F_\omega} + \vec{F}_D \tag{4.13}$$

$$m_d(\ddot{x}\hat{x} + \ddot{y}\hat{y}) = \frac{\pi}{6}D^3\Delta\rho(x\ sin\varphi + y\ cos\varphi)\omega^2(sin\varphi\hat{x} + cos\varphi\hat{y}) - \frac{1}{2}\rho_l C_D \frac{\pi}{4}D^2(\dot{x}\hat{x} + \dot{y}\hat{y} + V_F\hat{x}) \tag{4.14}$$

Manipulating the equation above, the motion equations are obtained:

$$\ddot{x} = \frac{\pi}{6}\frac{D^3\Delta\rho}{m_d}(x\ sin\varphi + y\ cos\varphi)\omega^2 sin\varphi - \frac{N}{m_d}(\dot{x} + V_F) \tag{4.15}$$

$$\ddot{y} = \frac{\pi}{6}\frac{D^3\Delta\rho}{m_d}(x\ sin\varphi + y\ cos\varphi)\omega^2 cos\varphi - \frac{N}{m_d}\dot{y} \tag{4.16}$$

In the equations of motion the term N is a function of the Reynolds number. The calculations for N are reported in appendix C. The results are shown below:

$$\mathrm{N} = \begin{cases} -3\pi\mu_l D & Re < 1 \\ \left(\frac{3\pi\mu_l D}{\dot{x} + V_F} + \frac{9}{16}\pi\rho_l D^2\right) \cdot \left(\sqrt{(\dot{x} + V_F)^2 + \dot{y}^2}\right) & 1 \leq Re < 5 \\ \frac{\pi}{8}\rho_l D^2 \cdot 1.85\left(\frac{\rho_l D}{\mu_l}(\dot{x} + V_F)\right)^{-0.6} & 5 \leq Re < 5000 \end{cases} \tag{4.17}$$

4.3.2. Initial conditions and velocity profile

The obtained motion equations of the heavy fuel droplet require further considerations to be resolved. Firstly, they represent a system of ordinary differential equations and therefore initial conditions shall be imposed. The initial conditions also serve to confine the spatial domain of the droplet movement within a distinct section between two successive discs, as discussed in section 4.1. Furthermore, in the same subsection, it was mentioned that this study is a typical two-phase flow problem. Hence, the velocity profile of the mixture entering the separator shall be researched in view of the relative velocity existing between the two liquids. The initial conditions and the velocity profile are covered in the next paragraphs.

Initial conditions

The equations of motion obtained represent a system of ordinary differential equations. In order to solve them initial conditions shall be imposed. These relate to the initial states of the heavy fuel droplet with respect to its trajectories and contribute to limiting the spatial domain to a discs section. That is to say, as figure 4.1 depicts, the droplet entering at the bottom edge ($x = L$) follows a first path (trajectory 1) according to which the droplet flows towards the discs end section ($x = 0$). Depending on the set input data the droplet can either hit the upper disc or not. In the first case, a second path (trajectory 2) is followed. During this motion, the droplet slides along the upper disc ($y = H\ sin\varphi$) moving towards $x = L$. At this condition, the droplet enters the outlet channel and gets discharged. If at the end of trajectory 1 the droplet reaches $x < 0$ values it means it gets discharged with the light

fuel. Consequently, the discharged light fuel will contain heavy fuel traces.

The initial conditions are imposed for both trajectories 1 and 2. Regarding the notation, the initial conditions are indicated with two subscripts *i,j* where *i* refers to either the first ($i = 1$) or the second trajectory ($i = 2$). The subscript *j* equals 0, meaning that that condition is set for the relative time $t = 0$. The initial conditions for the first trajectory are:

$$\begin{cases} x_{10} = L \\ y_{10} = 0 \\ \dot{x}_{10} = \dot{x}_{10} \\ \dot{y}_{10} = 0 \end{cases} \tag{4.18}$$

The assumption that the droplet enters at the lower disc edge is given by the conditions at x and y. While the initial velocity in the vertical direction equals zero, particular is the case of the initial velocity in the x-direction. To determine its value, it could be assumed that the droplet enters with the velocity of the fed mixture [79]. Nevertheless, this approach does not consider the dynamic of the problem. Hence, $\dot{x}_{10}$ can be determined by imposing the forces equilibrium at the initial position along x:

$$\vec{F}_{b,x} + \vec{F}_{\omega,x} + \vec{F}_{D,x} = \underline{0} \tag{4.19}$$

Substituting the formulas of the buoyancy, centrifugal and drag forces from equations 4.8, 4.9 and 4.10, projected on x:

$$\frac{\pi}{6} D^3 \Delta\rho x \, sin^2\varphi - \frac{1}{2}\rho_l C_D \frac{\pi}{4} D^2 (\dot{x}_{10} + V_F) = 0 \tag{4.20}$$

In the equation above the drag coefficient is present. The expression used for C_D is the one associated with $1 \leq Re < 5$. Here Re is the Reynolds number of the fed mixture flow, determined via iterations with variations of input parameters. Substituting the drag coefficient expression in the equation above, the velocity $\dot{x}_{10}$ equals:

$$\dot{x}_{10} = \frac{16\mu_l}{3\rho_l D}\left(-1 + \frac{D^2 \Delta\rho\omega^2 L \, sin^2\varphi}{18\mu_l}\right) \tag{4.21}$$

Regarding the initial conditions for trajectory 2, the droplet assumes the final position of trajectory 1 at the time $t = \tau$. Because it was said that trajectory 2 exists only if the droplet hits the upper disc, the droplet's vertical position equals $H \, sin\varphi$. Regarding the velocity, in the x-direction, it equals the horizontal velocity at the time $t = \tau$ of trajectory 1. Lastly, because the droplet coalesces when it hits the upper disc, the droplet slides along it. This means that its vertical position remains equal to $H \, sin\varphi$. Hence, the initial conditions for trajectory 2 are:

$$\begin{cases} x_{20} = x_{1,\tau} \\ y_{20} = y_{1,\tau} = H \, sin\varphi \\ \dot{x}_{20} = \dot{x}_{1,\tau} \\ \dot{y}_{20} = 0 \end{cases} \tag{4.22}$$

Velocity profile

The velocity of the fed mixture flow V_F is calculated to determine the relative velocity subsisting between the two liquids. The velocity V_F is calculated by Di Pretoro and Manenti [79] as volume flow divided by the cross-sectional area of the space between the consecutive discs. Nevertheless,

this expression does not consider the dynamic of the flow. The velocity of the mixture entering the space between the discs is a function of the Reynolds number of the flow. More specifically, there is a build-up of a boundary layer at the discs' surface leading to parabolic velocity profile [78]. The thickness of the boundary layer can be assumed to be $\delta = 1/2 \cdot h$, where $h = H\ sin\varphi$. From this, it can be verified that [74]:

$$\frac{\delta(x)}{Hsin\varphi} = \frac{0.5}{Hsin\varphi}\left(\frac{2\pi n\ sin\varphi\ vL^3}{Q}\right)^{0.5}\left(\frac{x}{L}\right)^{1.5} \tag{4.23}$$

The expression for the velocity V_F assuming a parabolic profile can now be found as in [78]. The mixture flow velocity $\tilde{V}_F$ can be expressed as function of x [79]:

$$\tilde{V}_F = \frac{Q}{2\pi nxH\ sin\varphi} \tag{4.24}$$

Now, for a parabolic velocity profile ($\delta = 1/2H\ sin\varphi$) and for $0 \leq y \leq H\ sin\varphi$:

$$V_F(x,y) = \tilde{V}_F(x)\frac{y}{H\ sin\varphi}\left(1 - \frac{y}{H\ sin\varphi}\right) \tag{4.25}$$

Integrating between 0 and $H\ sin\varphi$:

$$H\ sin\varphi\ \tilde{V}_F \int_0^{H\ sin\varphi} y(1-y)\,dy = \frac{Q}{2\pi nx} \tag{4.26}$$

It results that:

$$\tilde{V}_F = \frac{6Q}{2\pi nxH\ sin\varphi} \tag{4.27}$$

Substituting this expression in equation 4.25, the mixture flow velocity equals:

$$V_F(x,y) = \frac{3QL}{\pi nxH^2 sin^2\varphi} yL\left(1 - \frac{y}{H\ sin\varphi}\right) \tag{4.28}$$

4.4. Sensitivity analysis

In this section, an analysis is reported to show the sensitivity of the developed model to input parameters. Given its mathematical nature, first, the model validation is done by collecting data from the literature. First, the resolution method of the motion equations is briefly described. Second, results are discussed given a set of input parameters.

4.4.1. Resolution approach

The resolution approach for the sensitivity analysis is depicted in figure 4.2. The approach is divided into three main blocks whose description is covered in the following paragraphs.

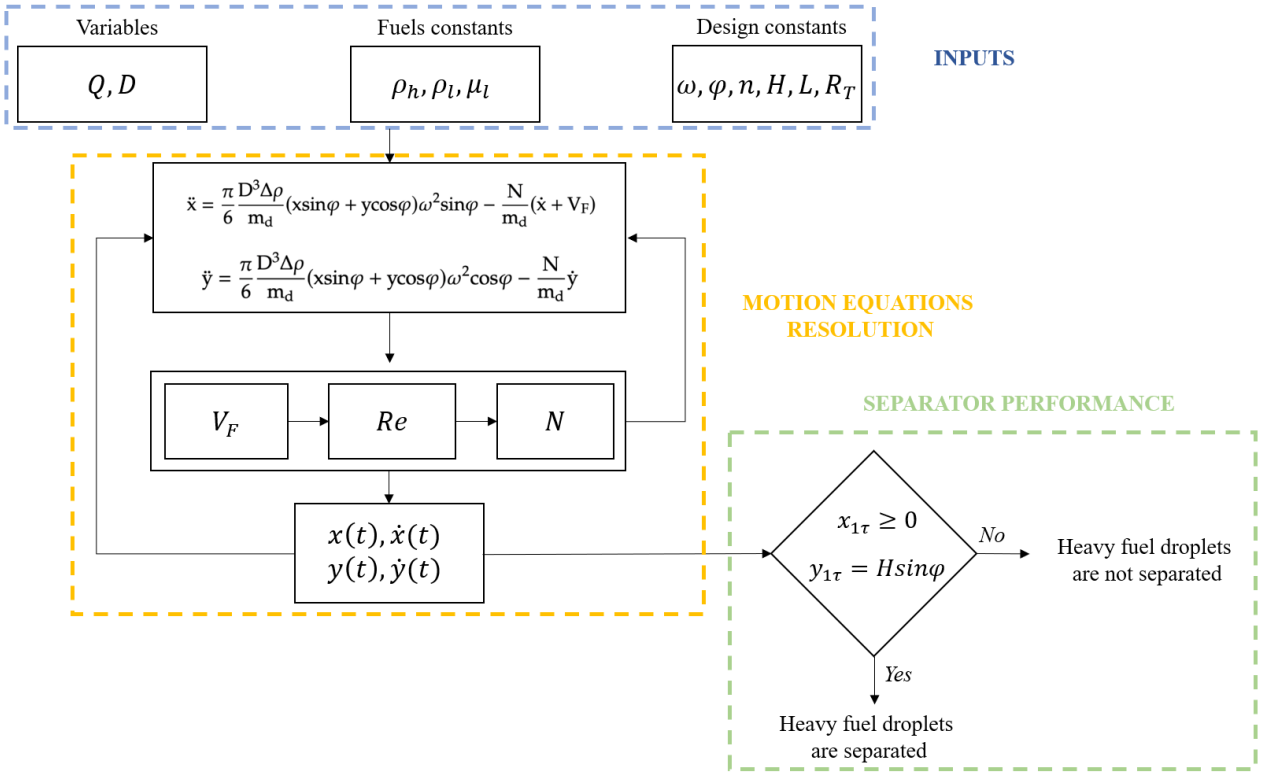

Figure 4.2: Flow chart of the motion equations resolution

This approach aims at observing the droplet trajectory variation by changing the fed mixture volume flow. The latter is the most important parameter in view of the separator integration in the multi-fuel system to match the desired fuel(s) volume flows by the energy converters. Hence, as figure 4.2 shows, the other inputs are kept constant in this part of the study, namely the fuel properties and the separator design parameters. Furthermore, the droplet diameter is considered a variable given that a unique value cannot be established a priori.

The motion equations 4.15 and 4.16 are solved with the Runge-Kutta (RK4) numerical method calculating the values of x, y, $\dot{x}$ and $\dot{y}$ at each time step. Here, the fed mixture flow velocity V_F is calculated according to equation 4.28. This value is used to identify the droplet's Reynolds number (see equation 4.12). At each step, the Reynolds number is assessed to determine the formula for N to be used (see equation 4.17). The values of V_F, Re and N are plugged into the equations of motion again to start the Runge-Kutta resolution at the next time step.

At each time step the motion and velocity of the droplet are given. First, it is verified whether, at the end time, the droplet has hit the upper disc. Conditions for this to be verified can be read in figure 4.2. If the conditions are met the droplet coalesces and the approach just described is followed to determine the horizontal position of the droplet as a function of the time. If the conditions are not met the droplet travels towards the section end reaching negative x values. This means that the droplet of the heavy fuel enters the light fuel discharge channel. In this case, it can be concluded that fuels separation does not fully occur. This check gives insights into the separator performance by just observing the droplets' trajectory for a fixed droplet diameter. Nevertheless, since it is hard to determine the concentration of droplets with a given diameter without experiments, a further analysis of the separator performance is performed which is described next.

A more in-depth explanation of the main coloured blocks depicted in figure 4.2 is given in the following paragraphs.

Sensitivity analysis input parameters

The inputs for the sensitivity analysis are reported in table 4.1. From this, it can be observed that methanol represents the heavy liquid. This is because the HVO density ranges from 765-800 kg/m^3 [41] while the methanol density equals 795.5 kg/m^3 [35]. Hence, to ensure the maximum density difference between the two liquids HVO is selected with its lowest density. Furthermore, the separator design inputs, namely the number of discs, discs inclination angle, length and vertical distance, are taken from typical centrifugal separator design parameters [78, 95]. The angular velocity was calculated considering that angular velocity values for typical centrifuges are 5000-8000 g, calculated as $\omega^2 R_{TOT}$, where R_{TOT} is the total radius of the centrifuge [19].

Table 4.1: Centrifuge model input parameters

Parameter	Symbol	Unit	Value
Methanol density [35]	ρ_h	[kg/m^3]	795.5
HVO density [41]	ρ_l	[kg/m^3]	765
Methanol dynamic viscosity at 40°C [35]	μ_h	[Ns/m^2]	$461.39 \cdot 10^{-6}$
HVO dynamic viscosity at 40°C [41]	μ_l	[Ns/m^2]	$1530 \cdot 10^{-6}$
Discs inclination angle [78, 95]	φ	[deg]	45
Angular velocity	ω	[rad/s]	273
Number of discs [78, 95]	n	[-]	34
Discs vertical distance [78]	H	[m]	$0.35 \cdot 10^{-3}$
Discs' length [78]	L	[m]	0.07
Separator total radius [78]	R_{TOT}	[m]	0.107
HVO outlet section diameter [79]	d_l	[m]	0.01
Methanol outlet section diameter [79]	d_h	[m]	0.01

Motion equations resolution method

The equations of motion obtained (equations 4.15 and 4.16) are solved numerically, given the complexity of the system. In fact, this comprises coupled second-order differential equations. Furthermore, due to the presence of the term N, the unknown velocities in the x- and y-direction appear at the denominator for $Re \geq 1$, making the resolution of the mentioned equations more complex to be solved analytically. Consequently, the numerical RK4 method was selected to solve the droplet's motion. This is also known as the Runge-Kutta method. The selection of RK4 over other numerical methods lies in its robustness. In solving non-linear differential equations, RK4 is less dissipative in terms of numerical errors, yielding a more accurate approximation of the actual solution. A description of the Runge-Kutta method is given in appendix D.

Separator performance

The separator performance is assessed by observing the heavy-phase droplets' trajectory. However, another approach shall be established alongside this. By obtaining the trajectories of the denser droplets from the mathematical model, it can be observed if the heavy fuel droplets coalesce towards the heavy fuel outlet channel or not. This is done by checking the conditions shown in figure 4.2. This analysis is based on a certain droplet diameter but in reality, it is hard to determine the concentration of the droplets with a particular size. Hence, alongside the droplets' trajectory observation, another method to assess the separator performance is found.

One way to assess the separation performance is by determining its efficiency. In his work, R. Plat calculated the separation efficiency [78] as a function of the critical droplet diameter of the heavy liquid droplet, i.e. the minimum droplet diameter that the droplet has to have in order to get separated. The efficiency is then defined as the ratio between the actual droplet diameter of the droplet and the critical diameter. Nevertheless, this method is discarded from this analysis since R. Plat assumes that the droplets entering the discs' section at the bottom edge do not get separated. This hypothesis is in contrast with the developed mathematical model.

Another approach to determining the separation efficiency is given by J.P. van der Linden [95] and it is based on the mass balance. More specifically, the efficiency is equal to:

$$\beta = 1 - \frac{f_{out}}{f_{in}} \tag{4.29}$$

Where f_{out} and f_{in} are the inlet and outlet mass flow respectively. However, this efficiency was calculated via measurements of f_{out} and f_{in} in the laboratory and therefore they are not parameters stemming from formulations. Hence, this approach cannot be directly implemented in this study.

Similarly, the European Committee for Standardisation (CEN) [96] provides a formula for the separation efficiency based on the number of particles in cleaned oil before and after the separator. Their associated values can only be determined via tests, hence limiting the applicability of this approach at this stage. Other experimental works concerning the efficiency of centrifuges can be found [97, 98].

The last approach to evaluate the separator performance consists of the determination of the interface position. Excluding the already discussed methods for the reasons presented above, this approach is used in this study alongside the trajectory observation of the heavy fuel droplets. An illustration of the interface position measured from the centrifuge rotational axis is given in figure 4.3.

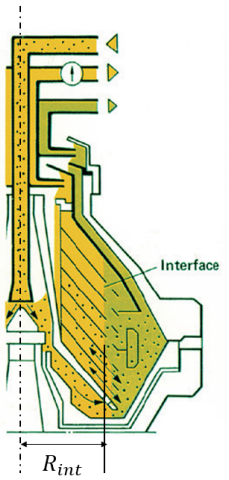

Figure 4.3: Interference position, adapted from [61]

The interface position establishes a section formed by the two liquids and its correct location ensures that the light phase can enter the narrow channels of the disk stack along its entire height [61]. In 1952, Ambler concluded that the interface must align with the holes in the disc stack where the mixture is distributed [99]. Contrasting viewpoints advocate for siting the light-heavy phases demarcation right outside the disc stack. A stance motivated by concerns related to

fouling challenges [61, 95]. Nevertheless, an interface located outside the discs' section would lead to contamination of the heavy phase by the light liquid [100]. Hence, it remains clear that the interface region shall be as close as possible to the disc periphery, as also remarked by *Westfalia* [100].

An engineering approach is employed for the calculation of the interface position [79]. The equation specifying its location is presented herewith, stemming from the pressure difference characterizing this boundary:

$$R_{int} = \sqrt{R_T^2 + \frac{\rho_l}{\rho_h}\left(\frac{Q_l^2}{S_l^2\omega^2}\right) - \frac{Q_h^2}{S_h^2\omega^2}} \tag{4.30}$$

Where Q_l and Q_h are the discharged volume flows of the light and heavy liquid respectively, which, for an ideal separation are calculated based on the relative percentage concentrations in the fed mixture X_l and X_h:

$$Q_l = X_l \cdot Q \tag{4.31}$$

$$Q_h = X_h \cdot Q \tag{4.32}$$

Assumed methanol concentration in the mixture is 10% v/v, based on the maximum concentration of the denser phase in actual centrifuges [94]. Moreover, in equation 4.30, R_T is the position of the outer edge of the disc-stack as shown in figure 4.1, while S_l and S_h are the outlet cross sections of the light and heavy phase respectively. These are calculated as:

$$S_l = \frac{\pi d_l^2}{4} \tag{4.33}$$

$$S_h = \frac{\pi d_h^2}{4} \tag{4.34}$$

Where d_l and d_h are the outlet diameters of the light and heavy liquids respectively.

4.4.2. Results

The first results of the mathematical model are shown in figures 4.4 and 4.5 for a fed volume flow equal to 0.01 m^3/s and 0.02 m^3/s respectively. These values are taken from existing separator designs. A volume flow of 0.01 m^3/s is representative of an alcohol-biodiesel separation, utilised for biodiesel production [101], hence falling within the purpose of this study. The higher volume flow is instead typical of a high-capacity marine separator [94]. The droplets diameter range is assumed to be 5-100 μm, as typical of solid-liquid centrifugal separators [77, 102]. Figures 4.4 and 4.5 give a representation of the non-dimensional section between two consecutive discs. The lines defined by $y/(H\ sin\varphi) = 0$ and $y/(H\ sin\varphi) = 1$ respectively represent the lower and upper disc. As discussed in section 4.3, the methanol droplets enter the depicted region at $x/L = 1$. Hence, the vertical line for $x/L = 1$ delineates the entering section of the mixture. Furthermore, it designates the section through which the methanol droplets must traverse to get discharged in the heavy phase outlet channel situated at $x > 1$.

Figures 4.4 and 4.5 depict the motion in the x- and y-direction of the methanol fuel droplets. Regarding the latter, only the minimum and maximum value of the collected diameter is plotted. Therefore, the values below the minimum plotted diameter get discharged in the HVO outlet channel, thus they reach $X/L < 0$. This indicates that these droplets are too small to hit the upper disc and

coalesce because their acceleration in the x-direction dominates over the acceleration in the vertical direction. Looking at the equations of motion along x (equation 4.15), the right end term prevails over the first one, given that the right end term is inversely proportional to droplet diameter, whilst the first term is diameter-independent. Consequently, for a given volume flow the acceleration associated with the relative velocity term dominates the equation. Conversely, for bigger droplets the first term of the equations of motion (equation 4.15 and 4.16) is ruled by the centrifugal force, which is strong enough to force the methanol droplets towards the side wall. It is worth pointing out that the droplets with diameters bigger than the maximum values showed in figures 4.4 and 4.5 are also collected at the methanol outlet channel. Nevertheless, they would not hit the upper disc but quite instantaneously change their direction towards the centrifuge's wall. However, their behaviour is not shown here for more efficient graph readability.

When comparing figures 4.4 and 4.5 it can be noticed that for a higher volume flow entering the discs section, the droplets travel a bigger distance than the case of lower volume flow. This is because, according to equations 4.28, 4.15 and 4.16, the volume flow velocity increases proportionally and therefore the right end term in the equations of motion rises. This behaviour is more pronounced for smaller droplets' diameter for the reasons stated above.

A further aspect to consider is the travelled time by the methanol droplets. This time is fundamental to determine the starting time of the centrifuge, assuming that as soon as the first fuel batch is discharged the process becomes continuous. Consistently with the fact that smaller droplets travel for a longer distance within the discs' section, their time to get discharged is higher than in the case of bigger droplets. For the minimum droplets' diameter and $Q = 0.01$ m^3/s the residence time within the discs' section equals 35 seconds, whilst this value becomes very small and equal to 2.5 seconds for $Q = 0.02$ m^3/s. In addition to this, the time required by the first batch to flow inside and outside the separator shall be considered. This time will be added when a centrifugal separator sized to meet the yacht's operational profile will be integrated into the fuel system. This is because specific parameters, such as inlet and outlet discharge channel diameters need to be calculated.

Lastly, from figures 4.4 and 4.5 the location of the interface position (purple line) relative to the discs' section can be observed. For a higher volume flow the value of R_{int} decreases. As it can be noticed in equation 4.30, the negative right end term dominates. From both figure 4.4 and 4.5 emerges that the interface position is not at the edge of the disc-stack as it would be in the identified ideal situation. Consequently, the plots are not representative of an ideal design. Furthermore, as observed by J.P. van der Linden [95], the interface position must take into consideration other factors, such as the rotational speed and the outlet radius. Another sensitive parameter is the diameter of the light and heavy phase outlet channels [79]. As a consequence, a more in-depth analysis is necessary when the centrifugal separator is integrated into the yacht's fuel system later in this work.

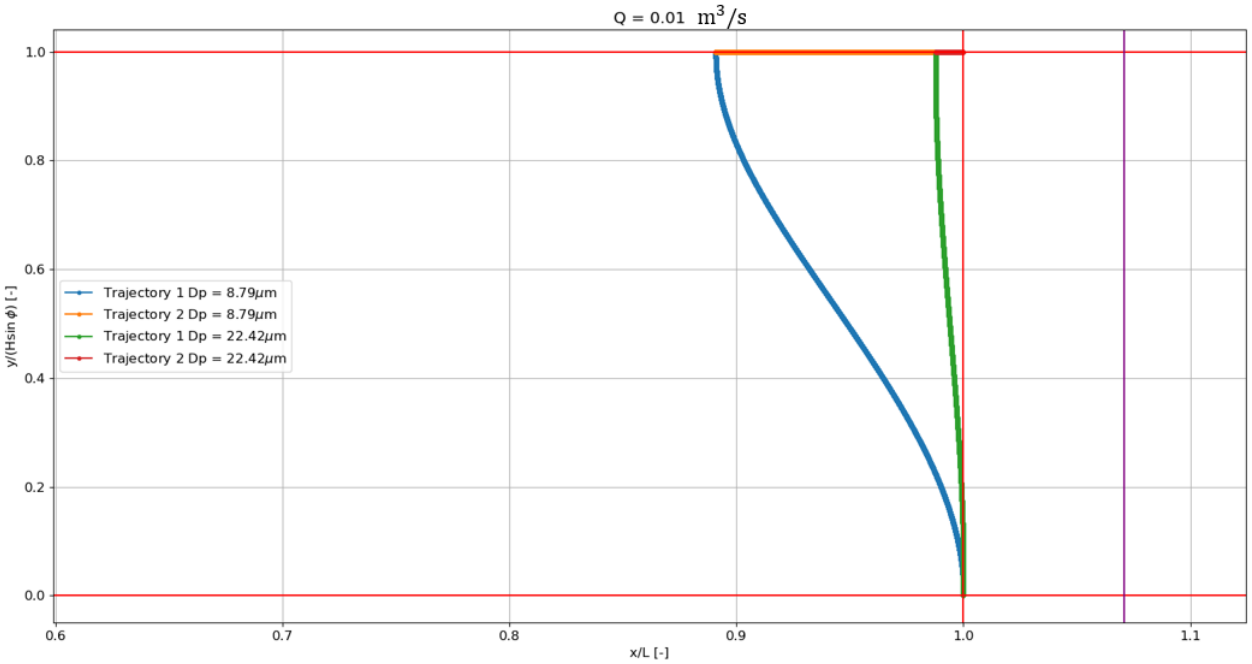

Figure 4.4: Methanol droplets motion within a consecutive discs' section at fed Q = 0.01 m^3/s

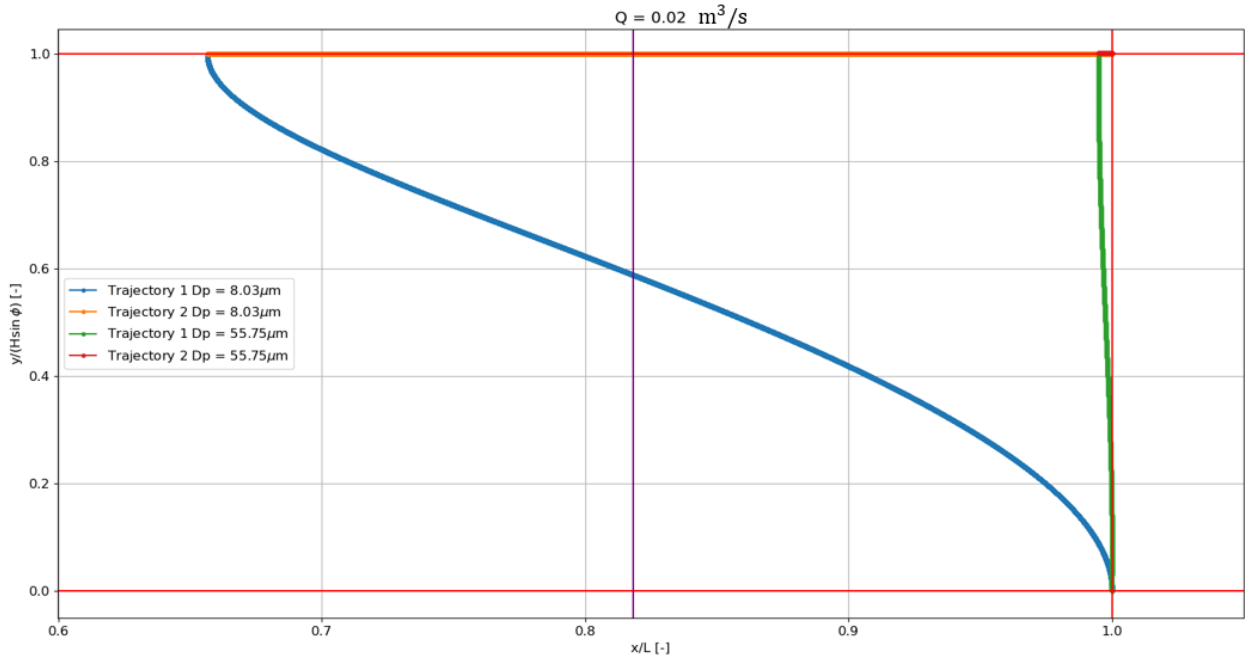

Figure 4.5: Methanol droplets motion within a consecutive discs' section at fed Q = 0.02 m^3/s

4.5. Chapter conclusion

In conclusion, this chapter described the developed mathematical model of a disk-bowl type centrifugal separator. The outputs of this study encompass the performance of the separator and its startup time. The calculation of the equations governing the motion of individual heavy fuel droplets within the interspace of the separator discs emerged as the sole avenue to ascertain these outputs. The model was built based on the forces exerted on the heavy liquid droplets under a set of assumptions. This approach resulted in coupled second-order differential equations describing the motion of the mentioned droplets within the disc-stack sections. The equations are solved numerically via the Runge-Kutta approach. A sensitivity analysis showed that for a range of droplets diameter and a higher fed volume flow the separator collects a wider range of droplet diameters. Smaller droplets require more time to get collected, hence they have a higher residence time within the discs' section. Furthermore, the performance of the centrifuge is assessed based on the interface position. This tends to move towards the disc-stack inner section with higher throughput. Additional analysis is required when the centrifuge is sized for its use in the fuel system in order to ensure an ideal allocation of the interface.

5

Multi-fuel system modelling

In the previous chapter, a mathematical model of a centrifugal separator was developed to overcome the partial HVO-methanol separation observed with the carried experiments. To assess the separator performance its working conditions need to be defined. These are mainly dictated by the yacht's operations, as the centrifuge is an integral component of the multi-fuel system. Hence, the latter is modelled under certain yacht's operations. First, the multi-fuel system modelling approach is presented. Second, calculations are shown for the identified yacht's operational profiles. Next, results are presented to show the difference stemming from the operating modes.

5.1. Multi-fuel system model

This section covers the multi-fuel system modelling. First, the scope and methodology are presented. Next, calculations are shown for the studied cases and associated results are presented.

5.1.1. Modelling scope and approach

The scope of the multi-fuel system model is to calculate the volume flow to be fed to the centrifugal separator to serve the ICEs for certain operational profiles. Alongside this, the fuel system schematic must be defined accordingly. In fact, in the previous chapter, it was seen that the centrifugal separator performance depends on a set of input variables. These represent design parameters to be determined when sizing the separator. Nevertheless, the separator capacity, measured relative to its inlet volume flow, is dictated by the required fuel(s) by the installed energy converters onboard.

To pursue the mentioned scope, the methodology illustrated in figure 5.1 is followed. It consists of an iterative process which takes the diesel fuel system of an average Feadship as a starting point. This is modified based on the yacht's operational profile, for which the yacht for the *MENENS* future use case [103] is considered and whose main specifications are reported in table 5.1. The input for the system schematic is the fuel volume flow required by the engines at each operational condition. The yacht's operational conditions are indicated in figure 5.1 with their associated abbreviation enclosed in a circle. The fuel system lines are iteratively defined to ensure mass balance within the considered sections of the system. A brief description of the Feadship's fuel system and multi-fuel system difference, operational profile and mass balance is given below.

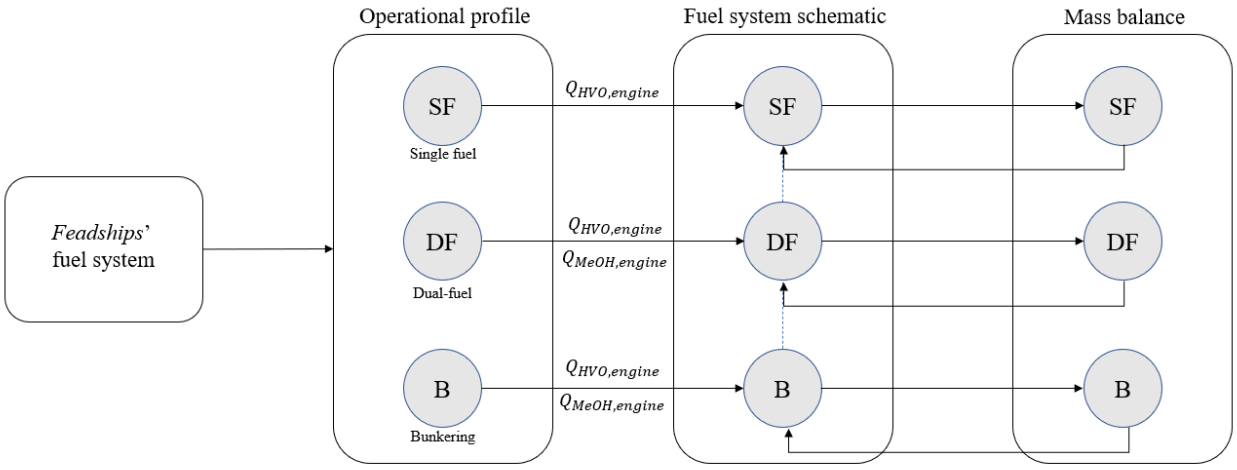

Figure 5.1: Methodology of the multi-fuel system modelling

Table 5.1: Yacht's main specifications (MENENS future use case) [103]

Parameter	Symbol	Unit	Value
Length	L	[m]	87
Beam	B	[m]	13.5
Draught	T	[m]	3.9
Displacement	Δ	[t]	2470
Range	d_{range}	[nm]	5000
Range speed	v_{range}	[kn]	12
Maximum speed	v_{max}	[kn]	18
Mean auxiliary load	$P_{aux,m}$	[kW]	280

(Multi-)Fuel system schematic

The fuel system considered as a starting point for the iteration process is typical of a diesel fuel system. A full description of a diesel fuel system can be found in appendix E. The diesel fuel system considered as the starting point of this study with its main components is shown in figure 5.2.

The fuels are alternatively stored in prismatic storage tanks, designed to accommodate a fuel volume to guarantee the yacht's range [104]. Transfer pumps allow the fuel to be circulated from one tank to another to regulate the yacht's trim and list [19].

From the storage tanks the fuel is firstly transferred to the treatment systems. Regarding the fuel treatment, this encompasses settling tanks and/or centrifugal separators. Onboard Feadships one treatment stage removes impurities from the fuel via a centrifuge. The cleaned fuel flows towards the service tanks. Two service tanks are usually required such that one can keep supplying fuel to the energy converters while the other is being cleaned or repaired [19]. To SOLAS Regulation II-1/26.11 [105] each service tank has a capacity of at least 8 hours at the maximum power of the propulsion plant.
Lastly, the fuel is pumped out from the service tanks to be used in energy converters and dedicated stripping lines can be installed.

Regarding the energy converters, this analysis is constrained to internal combustion engines (ICEs). More specifically, port-fuel injection dual-fuel (PFI DF) engines. The power generation of the studied

yacht comprises 4 electrical generators, referred to as gensets. They are assumed to be capable of working in both single-fuel (HVO) and dual-fuel (HVO-MeOH) modes [103]. The input data from the engine manufacturers are reported in table 5.2.

The two operational modes define the main difference between a single diesel and a multi-fuel system. The latter does not differ much from a typical diesel system in terms of system components. The most striking dissimilarity lies in the fuels handling operations. In the multi-fuel system, HVO and methanol are alternatively stored in the same storage tanks, with the type of fuel bunkered depending on the yacht's route and consequent engines operation. Hence, the yacht's operational profile dictates the design choices of the fuel system modelling.

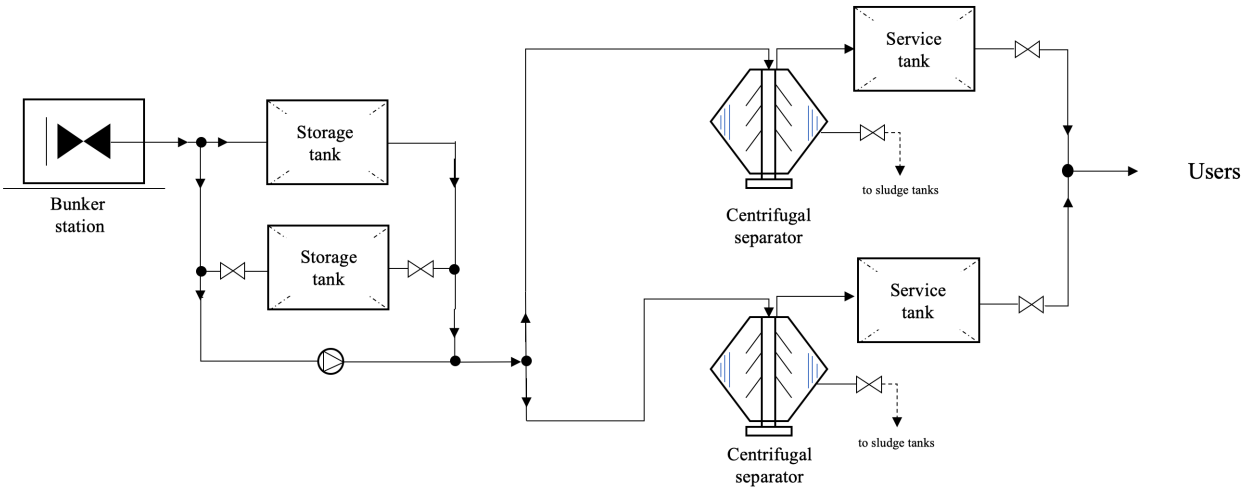

Figure 5.2: Diesel fuel system and its main components - reference design

Table 5.2: Gensets main specifications (*sfc* refers to MDO with LHV = 42780 kJ/kg) [106, 107]

			Genset 1	Genset 2
Parameter	Symbol	Unit	Value	
Units installed	-	[-]	2	2
Electrical power	P_e	[kW]	1461	873
Break power 100% MCR	$P_{b,genset,max}$	[kW]	1491	895
Specific fuel consumption 100% MCR	*sfc*	[g/kWh]	227	227
Specific fuel consumption 75% MCR	*sfc*	[g/kWh]	227	227
Specific fuel consumption 50% MCR	*sfc*	[g/kWh]	228	228
Specific fuel consumption 25% MCR	*sfc*	[g/kWh]	228	228

Operational profile

The fuel system is designed based on the yacht's operational profile to determine the volume flow required by the engine of a specific deployed fuel and consequently the separator capacity. From the operational profile, the required power by the engines for auxiliary and propulsion loads can be extracted. Furthermore, the operational profile offers insights into the yacht's history. Low electric power ranging from 280-800 kW is in fact representative of stationary (anchoring) mode. Higher power indicates manoeuvring, slow cruising or fast sailing [11]. This is fundamental to determining the fuel to be utilised onboard. More specifically, the built-in flexibility concept of the multi-fuel system enables the switch from one fuel to another depending on sailing areas and range. For instance,

the yacht is designed to cover its full range using HVO, given its higher LHV when compared to methanol. For example, this is the case of transatlantic trips when higher power is required. However, for lower ranges or when the yacht sails in the Nitrogen Emissions Control Areas (NECAs), a switch to dual-fuel mode shall be made to cut the GHG emissions by starting to deploy methanol alongside HVO. An illustration of the day average total shaft power of the yacht is depicted in figure 5.3. The single-fuel and dual-fuel modes are indicated as areas in the graph. The power and the operational time in the defined areas are used for the fuel system modelling.

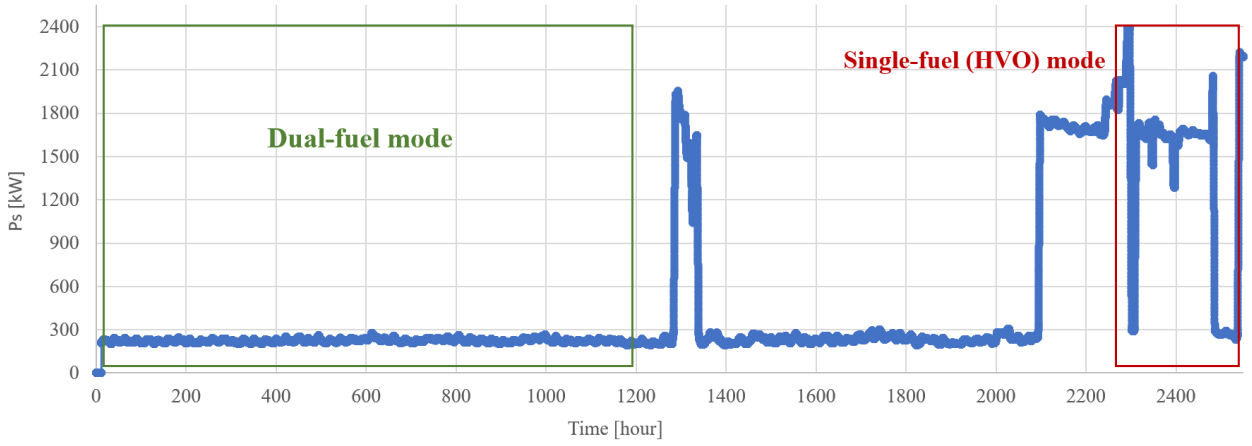

Figure 5.3: Yacht's day average shaft power and operational modes [*source: De Voogt Naval Architects B.V.*]

Lastly, because operations on multiple fuels are possible, figure 5.4 illustrates all the potential and selected scenarios for this study. The picture shows the bunkered and residual fuels in the storage tanks prior to starting operations with the mentioned engine modes. Considering that the mutual fuels' miscibility is the pivotal aspect of this study, the selected scenarios consist of bunkered fuel different from the residual one in the storage tank. Hence, the studied cases comprise:

1. Single-fuel (HVO) ICEs mode: bunkered HVO with residual methanol in the storage tanks
2. Dual-fuel (HVO-MeOH) ICEs mode: bunkered methanol with residual HVO in the storage tanks

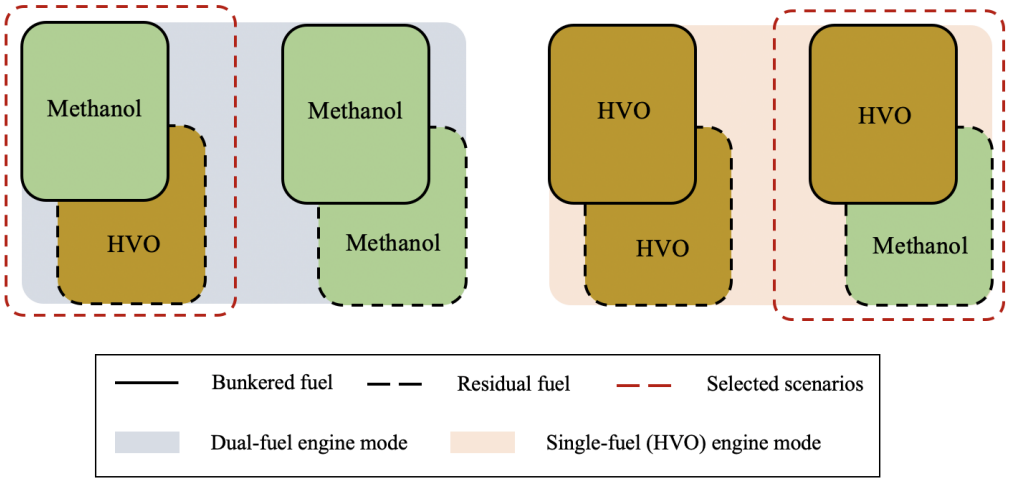

Figure 5.4: Potential and selected HVO-methanol mix scenarios in the storage tanks during bunkering

Volume balance

The principle of mass conservation is applied to define the fuel system schematic. This principle is used to balance the fuel(s) volume flows at each system section. While it is true that the fuel is burned in ICEs and therefore the available volume onboard decreases with time, the volume rate flowing through each system component must be balanced. Hence, at each inlet/outlet section of the centrifugal separator, tanks and fuel lines, the used formula in this work is:

$$\sum Q_{in} = \sum Q_{out} \tag{5.1}$$

Where Q_{in} and Q_{out} respectively are the inlet and outlet volume flows of a studied system section, expressed in m^3/s. Thus, for a certain time, the volume entering the considered section must be equal to the one which flows out. Equation 5.1 stems from the assumption of incompressible flows. Its computation can be found in appendix F. The density of the specific fuels is in fact assumed constant, as no variations of the environmental conditions are considered. Furthermore, no significant change in the fuels mixture is foreseen. This is due to the close densities of HVO and methanol, coupled with the circumstance wherein the bunkered fuel mixes with a limited quantity of residual fuel.

Thus, equation 5.1 is used to impose the volume flow conservation within the fuel system. The application of the described approach for the studied cases is addressed in the next subsections.

5.1.2. Single-fuel mode

In this study, both single and dual-fuel modes are considered to determine the separator capacity and the multi-fuel system schematic. In this subsection, the single-fuel (HVO) operation is investigated. The following assumptions are made:

- HVO is bunkered. The exclusive employment of HVO constitutes the operational mode wherein the yacht's engines operate solely on this fuel type. This configuration is notably characteristic of transatlantic voyages, wherein the yacht can cover its full range at range speed while utilizing HVO as the sole fuel source. This operational mode is also informally referred to as "transatlantic trip".
- Methanol at 5% v/v is left in the storage tanks at the time of bunkering, as a conservative estimate: residual fuel different than the bunkered one is the core of this study, representing an initial design condition for the fuels handling challenge stemming from the mutual fuels' miscibility.
- Dedicated service tanks as to SOLAS Reg. II [105].
- Both methanol and HVO service tanks are full at the time of bunkering.
- The mixture fed to the separator consists of methanol at 10% v/v and HVO at 90% v/v. This ratio is kept constant in the design and based on the maximum concentration of the heavy phase that the actual centrifuges are designed for [94].

Engines volume flow

The first step in the analysis consists of determining the volume flow required by the gensets. In this case, the fuel demanded is only HVO. Firstly, the total shaft power in kW is given from Feadships' data monitoring which already takes into consideration the sea margin. The shaft power is converted to the break power delivered by the gensets. This is done by dividing the shaft power by the transmission efficiency [108]:

$$P_b = \frac{P_S}{\eta_{TRM}} \tag{5.2}$$

The assumed η_{TRM} equals 0.98 [6].

Secondly, since the specific fuel consumption is known for % MCR equal and greater than 25, conditions on the delivered power by each engine are set such that the MCR does not assume values below 25%. The MCR percentage for each genset is calculated as:

$$\%MCR = 100\frac{P_{b,genset}}{P_{b,genset,max}} \tag{5.3}$$

Interpolation is done among the *sfc* data reported in table 5.2 to extrapolate the specific fuel consumption. Given that this refers to diesel, a correction is applied. It considers the different lower heating values between the two fuels [6] and a tolerance of 5% to consider possible deviations from the *sfc* declared values:

$$sfc_{HVO} = sfc_{diesel}(1 + 0.05) \cdot \frac{LHV_{diesel}}{LHV_{HVO}} \tag{5.4}$$

Next, for each engine i the HVO volume flow in m^3/s is calculated as [108]:

$$Q_{HVO,eng(i)} = \frac{P_b \cdot sfc_{HVO}}{3600\rho_{HVO}} \tag{5.5}$$

Where ρ_{HVO} is the HVO density in kg/m^3 and sfc_{HVO} is the HVO specific fuel consumption in g/kWh. Hence, the total HVO volume flow required by the engine at each time interval is:

$$Q_{HVO,eng} = \sum_{i}^{k_e} Q_{HVO,eng(i)} \tag{5.6}$$

Where k_e is the total number of gensets. The calculated required fuel volume flow can then be used to quantify the fed volume to the centrifugal separator. Additionally, $Q_{HVO,eng}$ is used to determine the amount of possible fuel recirculating and system schematic changes.

Fuel system volume balance

In order to fulfill the requested HVO volume flow by the ICEs, the capacity of the centrifugal separator delivering clean fuel must be determined. Moreover, the volume flowing through each system component must be balanced to define the final multi-fuel system schematic. The volume conservation equation 5.1 is applied at each considered section of the fuel system.

Starting from the centrifugal separator, the separator outlet volume flow has to match the required HVO by gensets at each time. As a conservative approach, it is assumed that the centrifuge works at the maximum capacity required. Hence, the maximum HVO volume required by the ICEs must be delivered by the separator. With reference to figure 5.5, imposing volume conservation at the separator inlet and outlet sections:

$$Q_{sep} = \frac{Q_{HVO,eng,max}}{X_{HVO}} \tag{5.7}$$

$$Q_{MeOH,eng} = Q_{sep} \cdot X_{MeOH} \tag{5.8}$$

Where Q_{sep} is the mixture volume flow fed to the separator in m^3/s and $Q_{HVO,eng,max}$ is the maximum HVO volume flow required by the ICEs during the considered operational time. $Q_{MeOH,eng}$ is the methanol volume flow discharged by the separator, while X_{HVO} and X_{MeOH} respectively are the HVO and methanol concentrations as a percentage of the mixture volume fed to the centrifuge.

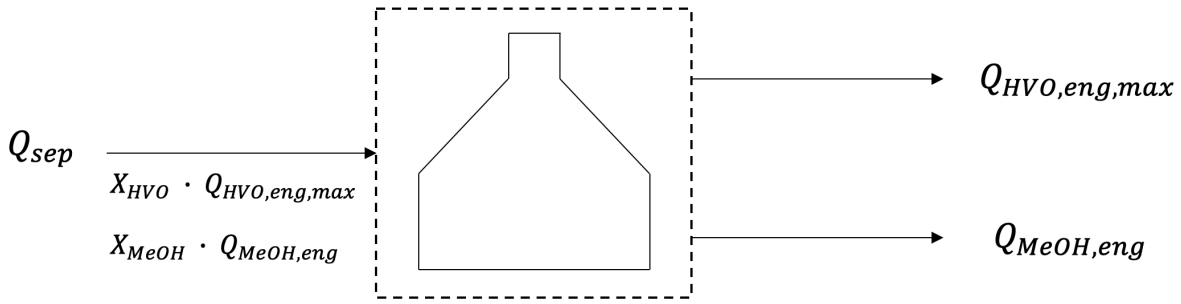

Figure 5.5: Volume balance at the centrifugal separator sections (single-fuel mode)

Now it is considered that the suction line in the storage tanks is usually located at the bottom of the tanks. The experiments presented in chapter 3 revealed that, although a full HVO-MeOH gravity separation requires more than 3 days, a consistent methanol volume settles at the container bottom as soon as mixture stirring terminates. Thus, it can be expected that bottom suction lines extract a mixture mainly composed of methanol from the storage tanks, whose exact value could not be predicted with the performed experiments. Therefore, the HVO-MeOH ratio is assumed to be kept constant in the storage tanks to facilitate the analysis. A mixer can be installed in the storage tanks to create a random fuels dispersion. Based on the assumptions made, methanol is present at 5% v/v in the storage tanks but 10% v/v is required in the mixture to be fed in the separator. A deliberate addition of methanol is done to bridge this difference, with MeOH stemming from the outlet separator. This is in fact a methanol volume that is not required by the engines and that cannot flow towards the methanol service tank, as this is considered to be full within this approach. Hence, with reference to figure 5.6 the volume flow pumped out from the storage tanks $Q_{ST,OUT}$ and the methanol recirculating $Q_{MeOH,rec}$ can be calculated as:

$$Q_{ST,OUT} = \frac{X_{HVO}}{X_{HVO,ST}} \cdot Q_{sep} \tag{5.9}$$

$$Q_{MeOH,rec} = \left(X_{MeOH} - X_{MeOH,ST} \cdot \frac{X_{HVO}}{X_{HVO,ST}} \right) \cdot Q_{sep} \tag{5.10}$$

Where $X_{HVO,ST}$ and $X_{MeOH,ST}$ respectively are the HVO and methanol volume concentrations as a percentage of the mixture in the storage tanks.

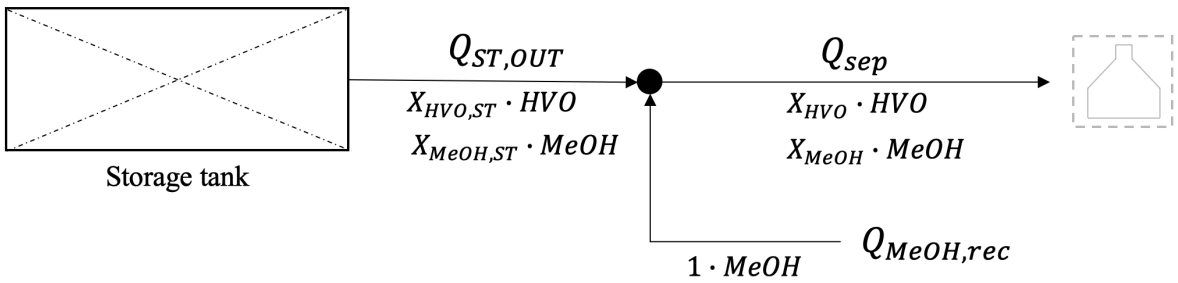

Figure 5.6: Volume balance at the inlet centrifugal separator and outlet storage tanks sections (single-fuel mode)

At this point, because not all the methanol recirculating from the service tanks is used to restore the HVO-MeOH ratios at the separator inlet, a certain MeOH volume flows towards the storage tanks.

Together with this, a certain HVO volume is pumped back to the storage tanks in the operational conditions where the supplied HVO by the separator is greater than the fuel required by the ICEs. The MeOH and HVO volume flows ($Q_{ST,MeOH,in}$ and $Q_{ST,HVO,in}$) recirculating to the storage tanks are calculated with reference to figure 5.7 and 5.8 respectively.

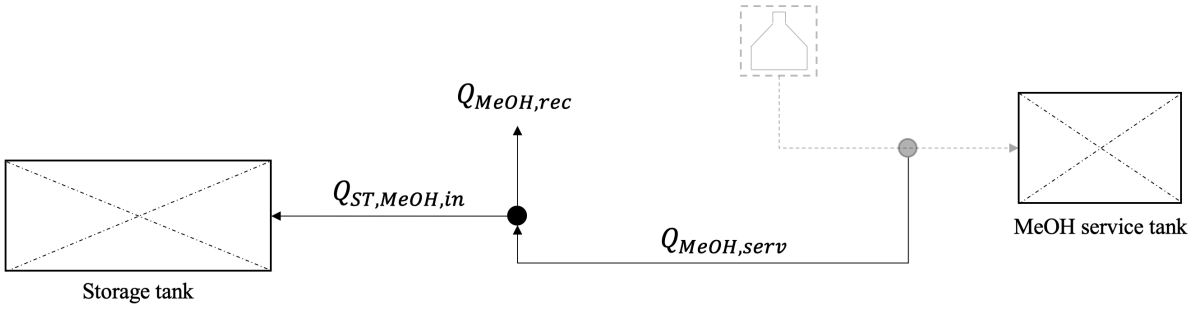

Figure 5.7: Methanol volume balance at the outlet centrifugal separator and inlet storage tanks sections

$$Q_{ST,MeOH,in} = Q_{MeOH,serv} - Q_{MeOH,rec} \tag{5.11}$$

Where $Q_{MeOH,serv}$ is the volume flow recirculating from the methanol service tank.

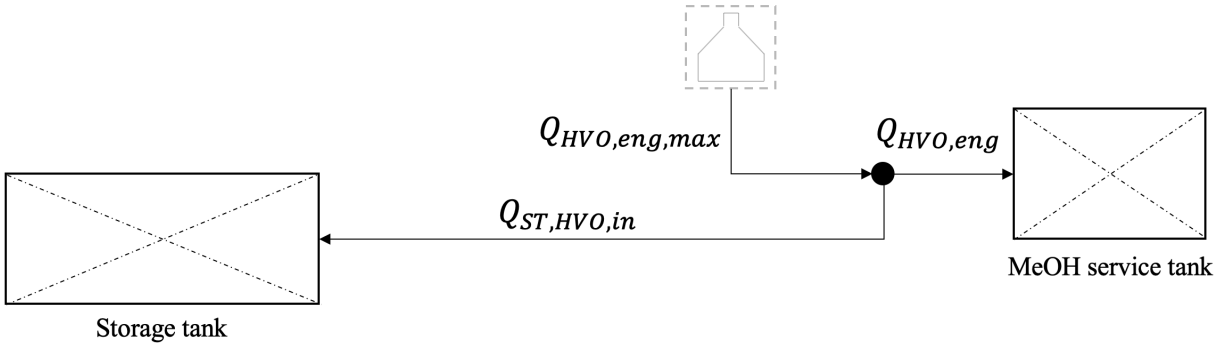

Figure 5.8: HVO volume balance at the outlet centrifugal separator and inlet storage tanks sections (single-fuel mode)

$$Q_{ST,HVO,in} = Q_{HVO,eng,max} - Q_{HVO,eng} \tag{5.12}$$

Nevertheless, the approach followed leads to a rise of methanol concentration in the storage tanks, while the latter get discharged over time. The increasing methanol concentration in the storage tanks is due to the bigger methanol volume pumped back compared to the HVO recirculating volume. More specifically, the HVO-MeOH ratio recirculated back in the storage tanks is smaller than $X_{HVO,ST}/X_{MeOH,ST}$ (95-5 v/v) for certain delivered power by the ICEs. The methanol concentration in the storage tanks at time t is calculated as:

$$X^{(t)}_{MeOH,ST} = \frac{V^{(t)}_{MeOH,ST}}{V^{(t)}_{MeOH,ST} + V^{(t)}_{HVO,ST}} \cdot 100 \tag{5.13}$$

Where $V^{(t)}_{MeOH,ST}$ and $V^{(t)}_{HVO,ST}$ are the methanol and HVO volumes in the storage tanks at time t, calculated as:

$$V_{MeOH,ST}^{(t)} = X_{MeOH,ST} \cdot V_{ST}^{(t)} + (Q_{ST,MeOH,in} - X_{MeOH,ST} \cdot Q_{ST,OUT})\,\Delta t \tag{5.14}$$

$$V_{HVO,ST}^{(t)} = X_{HVO,ST} \cdot V_{ST}^{(t)} + (Q_{HVO,rec} + Q_{HVO,ST,in} - X_{HVO,ST} \cdot Q_{ST,OUT})\,\Delta t \tag{5.15}$$

Where $V_{ST}^{(t)}$ is the fuel volume in the storage tanks at the time t determined from the storage tanks capacity C_{ST}. $V_{ST}^{(t)}$ equals:

$$V_{ST}^{(t)} = C_{ST} + (-Q_{ST,OUT} + Q_{MeOH,rec} + Q_{ST,HVO,in})\,\Delta t \tag{5.16}$$

The capacity of the storage tanks is calculated to fulfill the yacht's range distance at range speed. Knowing these parameters the range duration in hours is:

$$t_{range} = \frac{d_{range}}{v_{range}} \tag{5.17}$$

With d_{range} in nautical miles and v_{range} in knots. The required delivered energy E in kWh is then the summation of the required energy by propulsion and auxiliary systems [6]:

$$E = E_{prop} + E_{aux} = (P_{prop} + P_{aux}) \cdot t_{range} \tag{5.18}$$

Where P is the power required at range speed in kW. Hence, the required fuel capacity in m^3 is:

$$C_{ST} = \frac{3600 \cdot E}{\rho_{HVO} \cdot LHV} \tag{5.19}$$

To keep the methanol concentration steady at 5% v/v in the storage tanks, the methanol volume flow must be equal to:

$$Q_{ST,MeOH,in} = \frac{X_{MeOH,ST}}{X_{HVO,ST}} \cdot Q_{ST,HVO,in} \tag{5.20}$$

The equation above shows the dependency of $Q_{ST,MeOH,in}$ on $Q_{ST,HVO,in}$. The latter is the HVO volume flow pumped back to the storage tanks and it is dictated by the available HVO to be recirculated. To match the required $Q_{ST,MeOH,in}$, the possible methanol in excess must be removed. This in case $Q_{ST,MeOH,in}$ calculated with equation 5.11 is greater than the one determined with equation 5.20. The methanol in excess is indicated with $Q_{MeOH,buff}$ and it is pumped towards a methanol buffer tank. With reference to figure 5.9, $Q_{MeOH,buff}$ equals:

$$Q_{MeOH,buff} = Q_{MeOH,serv} - Q_{MeOH,rec} - Q_{ST,MeOH,in} \tag{5.21}$$

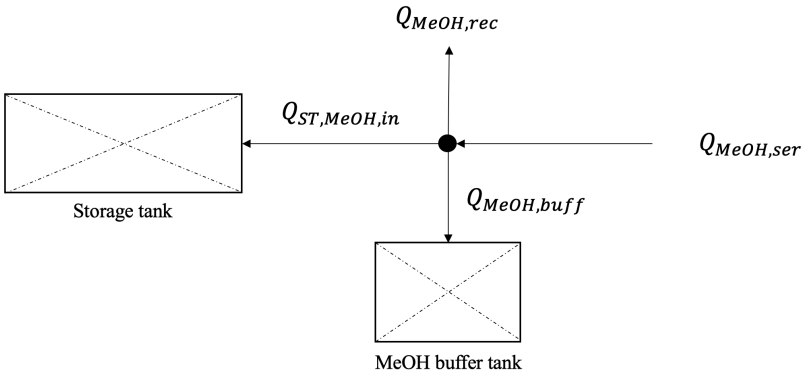

Figure 5.9: Methanol volume balance at the inlet storage tanks and MeOH buffer tank sections

The capacity of the methanol buffer tank in m^3 is calculated in the time interval corresponding to the transatlantic trip as:

$$C_{MeOH,buff} = \left(Q_{MeOH,buff_{(t-1)}} + Q_{MeOH,buff_{(t)}}\right)(t_i - t_{i-1}) \tag{5.22}$$

With $i \in [0; t_{end}]$, where t_{end} is the end time of the transatlantic trip at the moment the storage tanks have to be filled again.

5.1.3. Dual-fuel mode

In this subsection, the modelling for the dual-fuel (HVO-MeOH) operation is covered. Similarly to the single fuel (HVO) operations, the following assumptions are made:

- Methanol is the bunkered fuel.
- HVO at 5% v/v is left in the storage tanks at the time of bunkering, as a conservative estimate: residual fuel different than the bunkered is the core of this study, representing an initial design condition for the fuels handling challenge stemming from the mutual fuels' miscibility.
- Dedicated service tanks are installed as to SOLAS Reg. II [105].
- Both methanol and HVO service tanks are full at the time of bunkering.
- The mixture fed to the separator consists of methanol at 10% v/v and HVO at 90% v/v. This ratio is fixed in the design and based on the maximum concentration of the heavy phase that the marine centrifuges are designed for [94].

Engines volume flows

The volume flow required by the ICEs is calculated. Because in this case the gensets operate in dual-fuel mode, both HVO and methanol volume flows must be determined. Hence, the approach used here slightly differs from the one covered in subsection 5.1.2.

Dual-fuel operation is characterised by the combustion of two fuels. Generally, the amount of one fuel injected in the engine is expressed in function of the amount of the other. Other formulas correlate the quantity of fuel used in dual-fuel (DF) operation to single-fuel mode. These formulas are a function of mass, volume or energy released by the combustion of a single fuel. This study addresses PFI DF ICEs and values of the amount of methanol which can be injected in the air intake were provided by engine manufacturers to *De Voogt Naval Architects*. These values specifically refer to the *diesel substitution ratio* (DSR). This indicates how much diesel is being replaced by methanol in dual-fuel (DF) mode compared to diesel-only (DO) operations. The DSR is expressed in terms of mass flow as [109]:

$$DSR = \frac{\dot{m}_{d,DO} - \dot{m}_{d,DF}}{\dot{m}_{d,DO}} \tag{5.23}$$

Where $\dot{m}$ is the mass flow in kg/s and the subscript d indicates "diesel". Within the literature review, presented in chapter 2, it was found that the DSR depends on different engine parameters, namely thermal efficiency, emissions and load. Trends show that the NO_2 and NOx emissions decrease the higher the injected methanol content, while the break thermal efficiency drops for low loads and remains approximately constant for high loads [109]. In subsection 5.1.2 it was seen that the selected engines' load is always higher than 25% MCR. Hence, within the range provided by the engines' manufacturers, the highest DSR was selected yielding efficiency drop avoidance. The value of DSR assumed is 85%. Thus, rewriting equation 5.23 is possible to compute the HVO mass flow in DF mode:

$$\dot{m}_{HVO,DF} = \dot{m}_{HVO,SF} \cdot (1 - DSR) \tag{5.24}$$

With the subscript "SF" indicating "single fuel" mode. Including equations 5.4 and 5.5 the required HVO volume flow by each gensets in DF mode is:

$$Q_{HVO,DF,eng(i)} = \frac{P_b \cdot sfc_{HVO,SF}}{3600 \cdot \rho_{HVO}} \cdot \frac{LHV_{diesel}}{LHV_{HVO}} \cdot (1 - DRS) \tag{5.25}$$

With P_b calculated as in equation 5.2. Now, to determine the methanol volume flow it is necessary to know any parameter which correlates the HVO and MeOH volumes in DF mode. No values were provided by the engine manufacturers and therefore an assumption can be made on the *replacement ratio* (RR) which gives insights into the HVO replacement efficiency. Recommendations are given by J. Dierickx et al. [109] on having close to stochiometric operations not to decrease the engine efficiency. Considering the ratio between MeOH and HVO lower heating values (LHV), the ideal RR value is 2.16 which is therefore assumed in this study. Thus, from the RR equation [109], the methanol volume flow required in DF mode by the genset i is:

$$Q_{MeOH,eng(i)} = RR \cdot (Q_{HVO,SF} - Q_{HVO,DF,eng(i)}) \tag{5.26}$$

For the operating engines, the total HVO and MeOH volume flows required are:

$$Q_{HVO,DF,eng} = \sum_{i}^{k_e} Q_{HVO,DF,eng(i)} \tag{5.27}$$

$$Q_{MeOH,eng} = \sum_{i}^{k_e} Q_{MeOH,eng(i)} \tag{5.28}$$

The calculated required HVO and MeOH volume flows by the engines can be used to determine the fed volume to the centrifugal separator and the multi-fuel system schematic.

Fuel system volume balance

To fulfill the required HVO and methanol volumes by the ICEs, the separator outlet volume flows must be calculated. The system schematic shall be defined accordingly, meeting the volume conservation at each fuel system section. These calculations are covered in this section. Nevertheless, the approach followed is analogous to the one presented in subsection 5.1.2 for single fuel mode. Hence, equations are presented in each section to show dissimilarities with the single fuel mode.

Starting with the centrifugal separator, the outlet methanol and HVO flows must meet the ICEs requirements. For the considerations mentioned in the previous subsection, the methanol volume to be fed to the engines is expected to be higher than the HVO volume. Consequently, the mixture volume flow entering the centrifuge (Q_{sep}) is calculated based on the methanol volume flow demanded by the gensets ($Q_{MeOH,eng}$). For a conservative approach, $Q_{MeOH,eng}$ is assumed at its maximum value. Referring to figure 5.10 it turns:

$$Q_{sep} = \frac{Q_{MeOH,eng,max}}{X_{MeOH}} \tag{5.29}$$

$$Q_{HVO,eng,DF} = Q_{sep} \cdot X_{HVO} \tag{5.30}$$

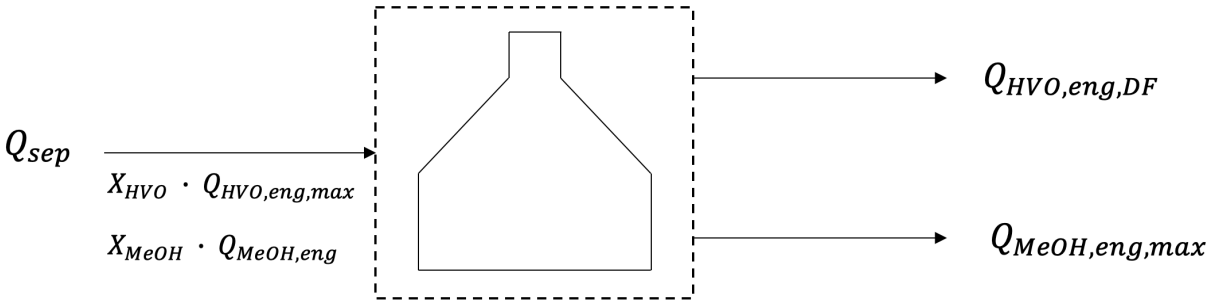

Figure 5.10: Volume balance at the centrifugal separator sections (dual-fuel mode)

Among the hypotheses of this case, residual HVO is found at 5% v/v in the storage tanks at the moment of bunkering methanol. Furthermore, it is assumed that HVO enters the centrifuge in a mixture with methanol at 90% v/v. As discussed in subsection 5.1.2, HVO shall be deliberately added within the fuel line connecting the storage tanks and the centrifugal separator. This is under the assumption that the extracted mixture from the storage tanks consists of a fixed HVO-MeOH volume ratio. The volume flows of the mixture pumped out from the storage tanks ($Q_{ST,OUT}$) and HVO ($Q_{HVO,rec}$) deliberately added to this are:

$$Q_{ST,OUT} = \frac{X_{MeOH} \cdot Q_{sep}}{X_{MeOH,ST}} \tag{5.31}$$

$$Q_{HVO,rec} = \left(X_{HVO} - X_{HVO,ST} \cdot \frac{X_{MeOH}}{X_{MeOH,ST}} \right) \cdot Q_{sep} \tag{5.32}$$

For the equations above reference can be made to figure 5.11.

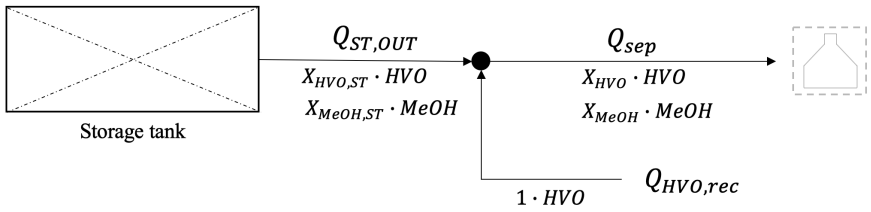

Figure 5.11: Volume balance at the inlet centrifugal separator and outlet storage tanks sections (dual-fuel mode)

The HVO volume recirculating to restore the HVO-MeOH at the separator inlet stems from the HVO volume which comes out from the separator. The recirculating HVO is derived from the HVO which cannot be completely burned in the engines when these do not work at full power. A representation is given in figure 5.12. The extra HVO volume flow is:

$$Q_{HVO,ser} = Q_{HVO,eng,DF,max} - Q_{HVO,eng,DF} \tag{5.33}$$

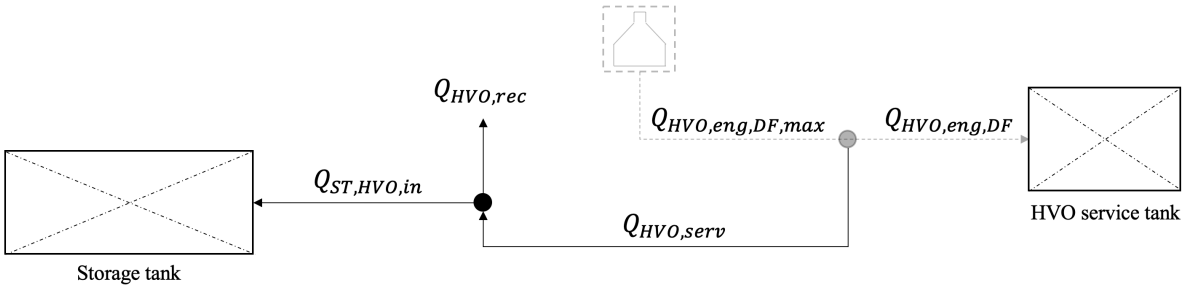

Figure 5.12: HVO volume balance at the outlet centrifugal separator and inlet storage tanks sections (dual-fuel mode)

As figure 5.12 depicts, in the cases where $Q_{HVO,ser} > Q_{HVO,rec}$, a certain HVO volume is pumped back in the storage tanks. This amount equals:

$$Q_{ST,HVO,in} = Q_{HVO,ser} - Q_{HVO,rec} \tag{5.34}$$

The identical situation occurs for methanol when the ICEs power is below 100% MCR. In these cases, methanol is directly pumped back into the storage tanks. An illustration is given in figure 5.13. The methanol flowing back to the storage tanks is:

$$Q_{MeOH,rec} = Q_{MeOH,eng,max} - Q_{MeOH,eng} \tag{5.35}$$

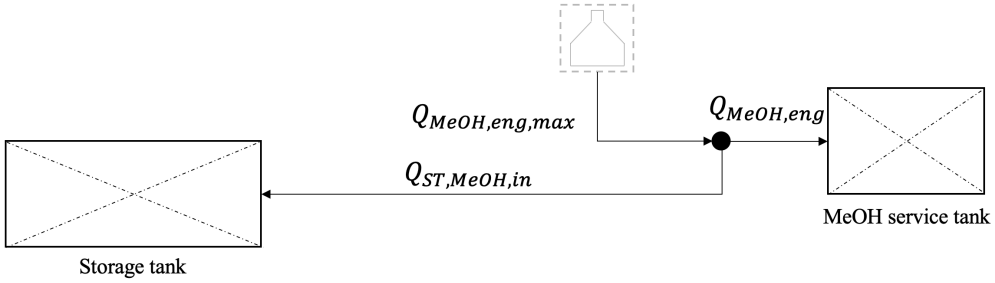

Figure 5.13: Methanol volume balance at the outlet centrifugal separator and inlet storage tanks sections (dual-fuel mode)

Next, as for the single fuel case, the varying HVO-MeOH ratio in the storage tanks shall be considered. In this study, it is hypothesised that the mixture pumped out from the storage tanks consists of a fixed fuels ratio, i.e. HVO-MeOH at 95-5% v/v. This is possible by installing a mixer in the storage tanks. Nevertheless, the changing fuels concentrations in the storage tanks might stem from the recirculating fuels. To keep the fuels ratio at the desired value, $Q_{ST,MeOH,in}$ and $Q_{ST,HVO,in}$ must meet the following correlation:

$$Q_{ST,HVO,in} = \frac{X_{HVO,ST}}{X_{MeOH,ST}} \cdot Q_{ST,MeOH,rec} \tag{5.36}$$

Equations 5.13 to 5.19 can be used to check the fuels' ratio in the storage tanks. Equation 5.36 shows the dependency of $Q_{ST,HVO,in}$ on $Q_{ST,MeOH,rec}$, meaning that the HVO stream entering the storage tanks depends on the available methanol recirculating from the service tanks. $Q_{ST,HVO,in}$ from the equation 5.34 must equal the value calculated with the equation above. Otherwise, an HVO buffer

tank might be necessary to install to either accommodate or pump out the fuel. Referring to figure 5.14, the volume flowing towards or from the HVO buffer tank is:

$$Q_{HVO,buff} = \pm(Q_{ST,HVO,in} + Q_{HVO,rec} - Q_{HVO,ser}) \tag{5.37}$$

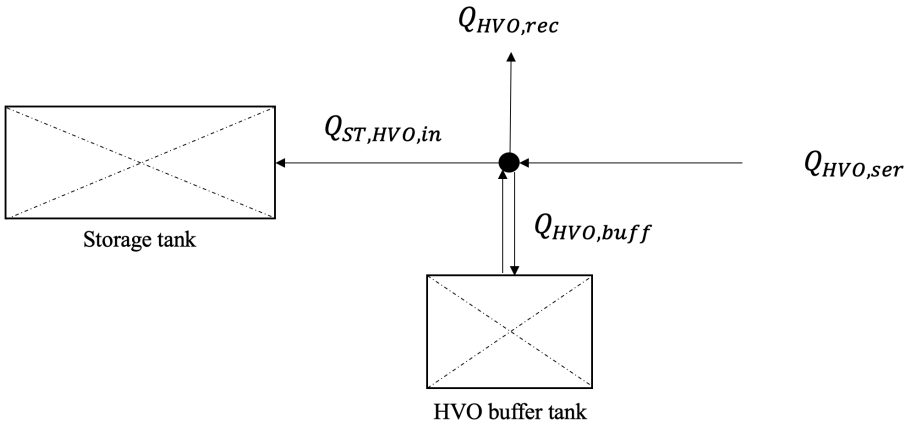

Figure 5.14: HVO volume balance at the inlet storage tanks and HVO buffer tank sections

The capacity of the HVO buffer tank in m^3 is calculated in the time interval corresponding to the duration of the dual-fuel operations:

$$C_{HVO,buff} = \left(Q_{HVO,buff_{(t-1)}} + Q_{MeOH,buff_{(t)}}\right)(t_i - t_{i-1}) \tag{5.38}$$

With $i \in [0; t_{end}]$, where t_{end} is the end time of the dual-fuel operations right before refuelling.

5.1.4. Bunkering operations

This subsection addresses the fuel bunkering scenario prior to starting single-fuel and dual-fuel operations. This scenario is fundamental to assess the impact of the sized centrifugal separator on the buffer tanks capacity.

This case assumes that both methanol and HVO service tanks are empty. In reality, it was seen in the previous sections that a certain HVO/MeOH volume is needed to control the mixture inlet composition for the separator. Here, it is assumed that the buffer tanks are already provided with the minimum demanded HVO/MeOH to fulfill this requirement at the separator inlet. Hence, the empty service tanks indicate an extreme bunkering scenario. Equations 5.18 and 5.19 can be used to determine their capacity, with t equal to 8 hours and P at maximum power as to SOLAS [105]. From this, the time required to fill HVO and methanol service tanks is respectively:

$$t_{ser,HVO} = \frac{C_{ser,HVO}}{Q_{HVO,eng,max}} \tag{5.39}$$

$$t_{ser,MeOH} = \frac{C_{ser,MeOH}}{Q_{MeOH,eng,max}} \tag{5.40}$$

Where C_{ser} is the capacity of each service tank in m^3. Equation 5.39 is valid for the single fuel mode, whilst equation 5.40 for the dual-fuel operations. In both cases, $C_{ser,MeOH} > C_{ser,HVO}$, for the same engine power and 8 hours sailing time required by SOLAS. Furthermore, methanol is the fuel in the

lower concentration in the mixture fed to the centrifuge. Hence, the HVO service tank requires less time to be filled than the methanol service tank. However, the separator keeps working to keep filling the MeOH service tank and therefore an extra HVO volume shall be stored in a buffer tank when the HVO service tank gets full. The capacity of the HVO buffer tank then becomes:

$$C_{buff,HVO} = {C_{buff,HVO}}^{(0)} + {C_{buff,HVO}}^{(1)} \tag{5.41}$$

Where ${C_{buff,HVO}}^{(0)}$ is the HVO buffer tank capacity at the first iteration calculated as in equation 5.38. ${C_{buff,HVO}}^{(1)}$ is determined as follows:

$${C_{buff,HVO}}^{(1)} = Q_{HVO,eng,max} \cdot (t_{ser,MeOH} - t_{ser,HVO}) \tag{5.42}$$

Lastly, to reduce the HVO buffer tank capacity and minimise the required space onboard, it can be considered that HVO is pumped out from its service tank during the yacht's operations. Hence, equation 5.41 becomes:

$$C_{buff,HVO} = {C_{buff,HVO}}^{(0)} + {C_{buff,HVO}}^{(1)} - C_{ser,HVO} \tag{5.43}$$

The remaining fuel in HVO service and buffer tanks is calculated as in figure 5.15.

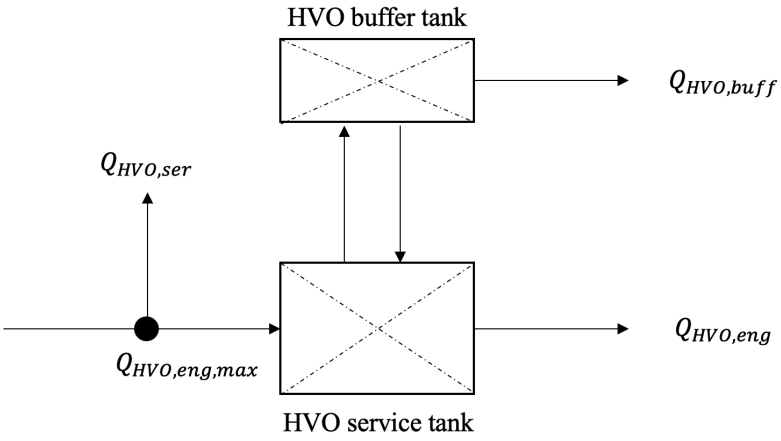

Figure 5.15: HVO volume balance at the inlet and outlet sections of the HVO service and buffer tank sections

5.1.5. Results

This section presents the results of the multi-fuel system modelling for both single-fuel (HVO) and dual-fuel modes.

Single-fuel mode

Figures 5.16 to 5.18 show the results for the single fuel (HVO) model case. Figures 5.16 and 5.17 respectively depict the first and last iteration of the fuel system modelling for the studied single fuel case in subsection 5.1.2. All the volume flows are reported following the nomenclature used in the previous section. The most striking difference between the illustrated system schematics lies in the presence of a methanol buffer tank. This stems from the increasing methanol concentration in the storage tanks. As figure 5.18 illustrates, the methanol ratio in the storage tanks rises over time, due to the bigger methanol volume flowing back to the storage tanks compared to the recirculating HVO. As explained in the previous section, the HVO-methanol ratio circulating to the storage tanks, indicated with $Q_{ST,HVO,in}/Q_{ST,MeOH,in}$, shall be at 95-5 % v/v. However, this value is not met within single fuel operations and it is caused by two reasons. First, the engine operates in single-fuel mode, meaning that only HVO is required. Consequently, with the methanol service tanks full, the separated methanol from the centrifuge is a fuel volume which is not used onboard. Its usage is constrained to restore the HVO-MeOH ratio at the separator inlet. However, an excess methanol volume remains. The second reason for the increasing methanol concentration in the storage tanks is the increasing shaft power and therefore the HVO consumption. When the engine's HVO consumption increases, the recirculating HVO volume flow drops. Consequently, the HVO volume entering the storage tanks decreases while methanol is still unused onboard. The increasing shaft power can be noticed in the rising curve of figure 5.18 in the range of hours 2250-2485. From 2485 to 2538 the power decreases and remains approximately constant and therefore the methanol concentration shows a levelized curve in the graph. The growing trend of power-MeOH concentration restarts after 2485 hours. Hence, to keep the HVO-MeOH ratio at the fixed 95-5 % v/v in the storage tanks, a methanol buffer tank is installed. This stores unused methanol during single-fuel operations. The curve of the fixed methanol concentration versus time is shown in figure 5.18.

Moreover, comparing the system schematic in figure 5.16 and 5.17, the number variation of the service tanks can be noticed. The initial number was set to two per fuel, as to SOLAS Reg. II [105] for a conservative approach following redundancy. Nevertheless, the number was reduced to one to lower the required space onboard.

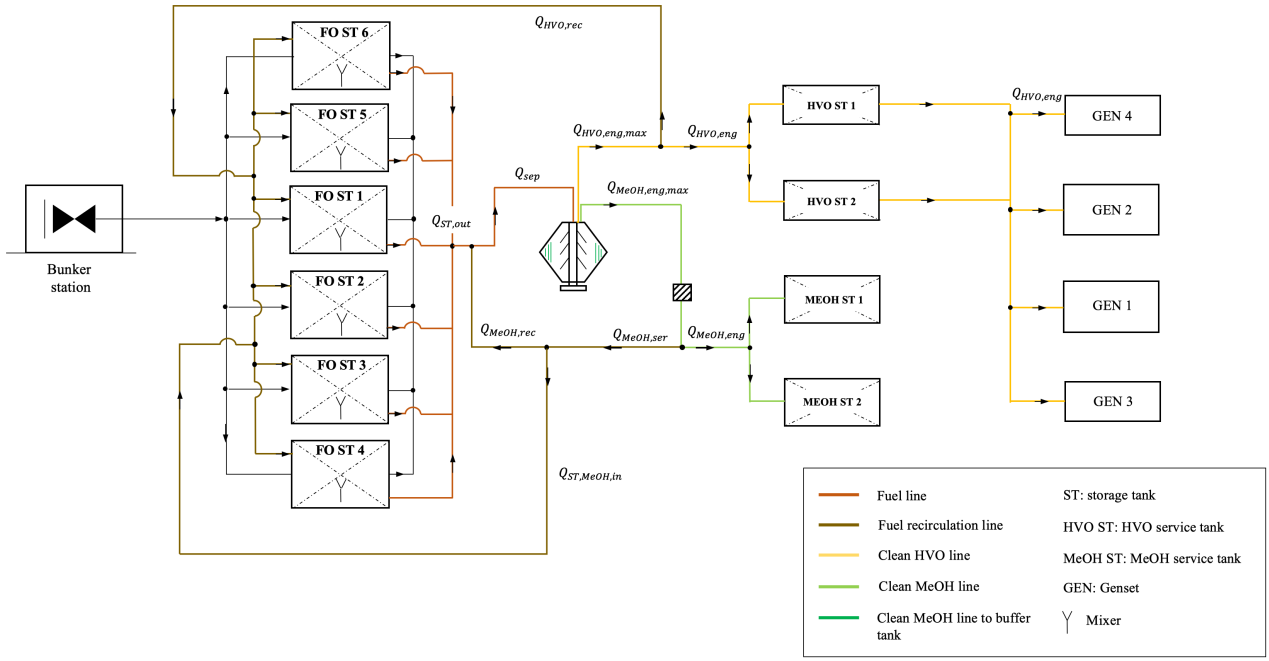

Figure 5.16: Multi-fuel system schematic in single-fuel mode operation. First design iteration (design 1)

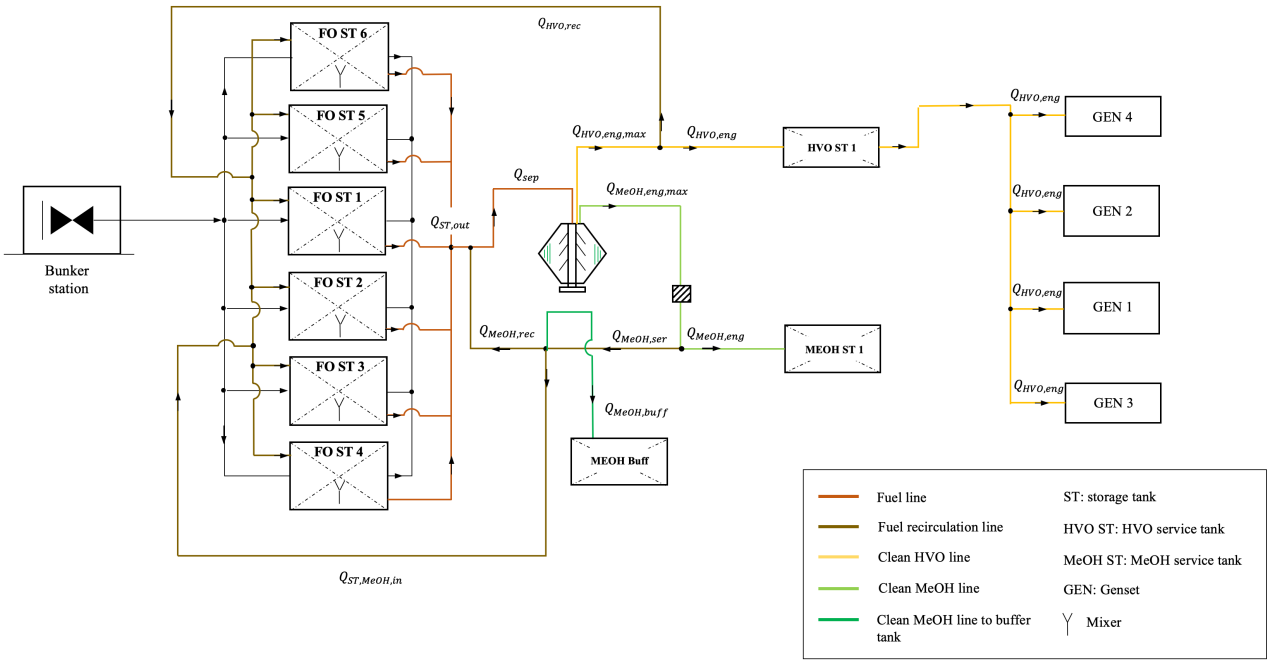

Figure 5.17: Multi-fuel system schematic in single-fuel mode operation. First design iteration (design 2)

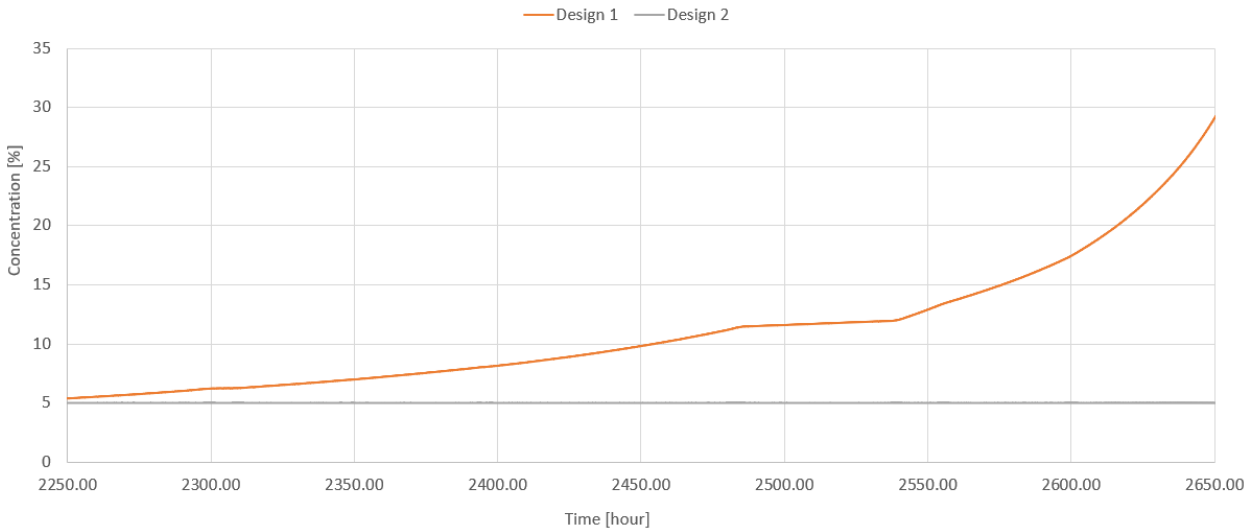

Figure 5.18: Methanol volume concentration change in storage tanks in single-fuel mode operation (Design 1: First design iteration; Design 2: Last design iteration)

Dual-fuel mode

Results of the fuel system schematic for the dual-fuel mode discussed in subsection 5.1.3 are presented in figures 5.19 and 5.20. All the volume flows are indicated following the nomenclature used in the previous section. Similarly to the single fuel case, the most striking difference between the presented schematics results in the HVO buffer tank. The choice of installing a buffer tank is dictated by the HVO-methanol volume ratio variation in the storage tanks. This can be observed in figure 5.21. At the moment right after bunkering, methanol is at 95% v/v in the storage tanks. Its volume slightly grows over time because there is no HVO recirculating back to the storage tanks. In dual-fuel operations, with reference to figures 5.19 and 5.20, $Q_{HVO,rec} > Q_{HVO,ser}$, meaning that to adjust the HVO-MeOH ratio at the separator inlet all the extra HVO exiting the centrifuge and that is not demanded by the engines is used. This is because this study assumes that a mixture is extracted from the storage tanks with a fixed HVO-MeOH volume ratio of 5-95. Nevertheless, the centrifugal separator is designed to receive a mixture composed of HVO-MeOH at 90-10% v/v. Hence, deliberate addition of HVO must be performed at the storage tanks outlet section to fulfill the centrifuge mixture requirement. If no HVO buffer tank is installed, methanol flow $Q_{MeOH,rec}$ is the sole fuel volume entering the storage tanks and therefore its volume concentration therein increases. Thus, an HVO buffer tank is installed to compensate for the fuels ratios mismatch in the storage tanks, while controlling the mixture ratio entering the centrifuge.

Additionally, as for the single fuel case, the number of service tanks is reduced to one per fuel to minimise the required space onboard. Alongside this, it was decided to pump the recirculating HVO out from its service tank. In this way, the HVO buffer tank capacity is further reduced. A return line from the HVO buffer tank to its service tank is installed to keep the service tank at a sufficient level to inject fuel into the engines.

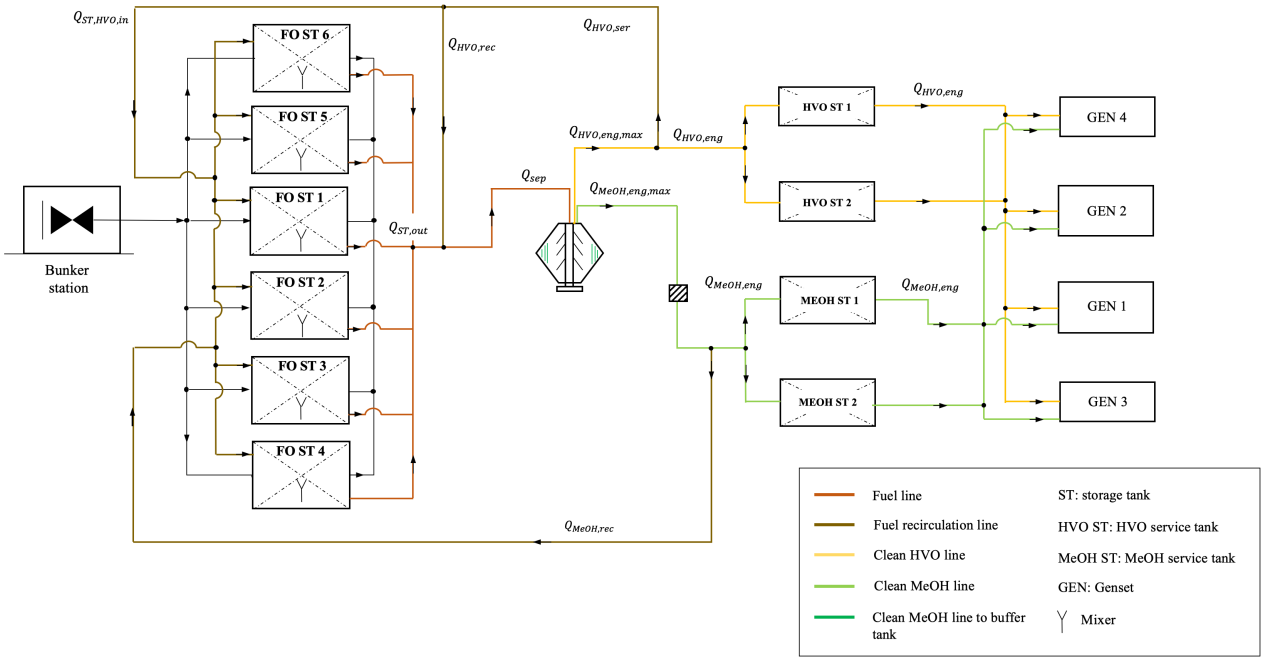

Figure 5.19: Multi-fuel system schematic in dual-fuel mode operation. First design iteration (design 1)

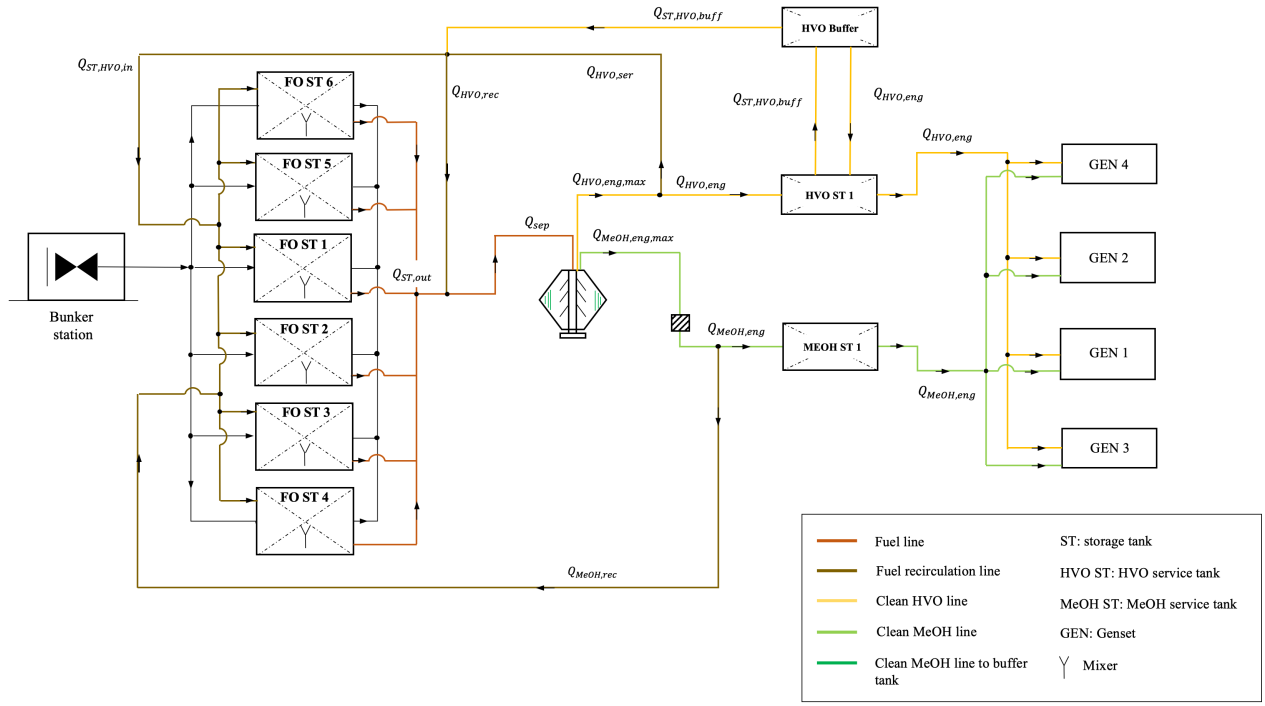

Figure 5.20: Multi-fuel system schematic in dual-fuel mode operation. Last design iteration (design 2)

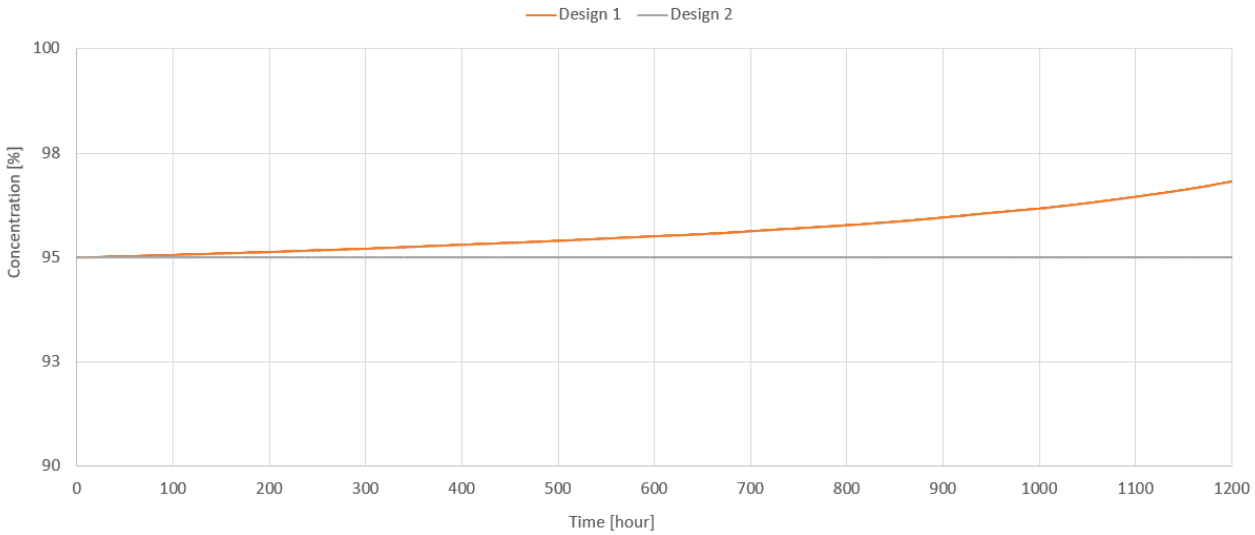

Figure 5.21: Methanol volume concentration change in storage tanks in dual-fuel mode operation (Design 1: First design iteration; Design 2: Last design iteration)

The combination of the systems in figures 5.17 and 5.16 leads to the final multi-fuel system schematic of figure 5.22. The results of the tanks' capacity and required volume flow by the centrifugal separator are reported in table 5.3. The resulting fed volume flows to the separator can then be utilised as inputs for the developed mathematical model of the centrifuge for its integration in the multi-fuel system.

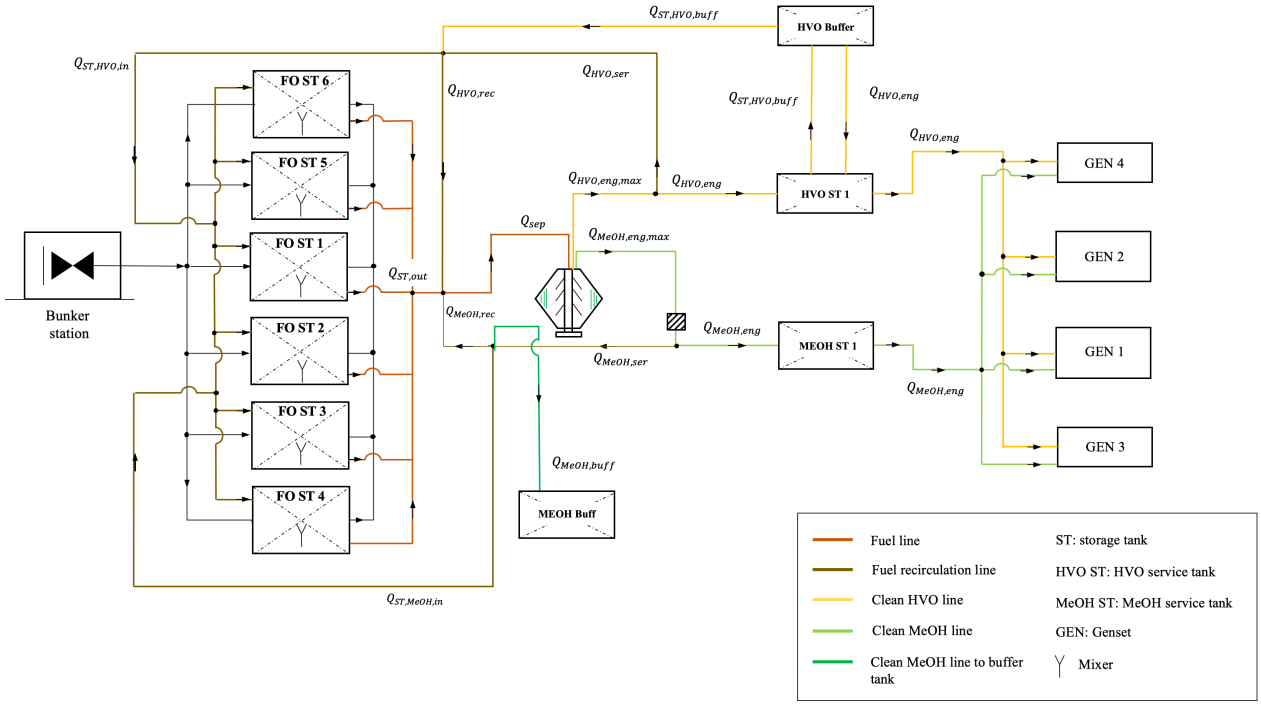

Figure 5.22: Final multi-fuel system schematic for single-fuel and dual-fuel operations

Table 5.3: Main results of the multi-fuel system model

Parameter	Symbol	Unit	Value
Storage tanks capacity	C_{ST}	[m^3]	241.281
HVO buffer tank capacity	$C_{HVO,buff}$	[m^3]	78.014
MeOH buffer tank capacity	$C_{MeOH,buff}$	[m^3]	11.460
Installed service tanks for each fuel	n_{ser}	[-]	1
HVO service tank capacity	$C_{HVO,ser}$	[m^3]	4.278
MeOH service tank capacity	$C_{MeOH,ser}$	[m^3]	9.096
Fed volume flow to the separator (single-fuel mode)	$Q_{sep,SF}$	[m^3/s]	$2.241 \cdot 10^{-4}$
Fed volume flow to the separator (dual-fuel mode)	$Q_{sep,DF}$	[m^3/s]	$4.076 \cdot 10^{-4}$

5.2. Chapter conclusion

This chapter discussed the modelling of the multi-fuel system aiming at identifying the centrifugal separator working conditions. This entailed a study on the yacht's operational profile directed towards ascertaining the fed mixture volume flows to the centrifugal separator and delineating alterations in the fuel system schematic under defined yacht's operations. Single-fuel (HVO) and dual-fuel (HVO-MeOH) engine modes were defined. Calculations were performed using the mass conservation principle as a basis. The obtained separator entering volume flows are $4.076 \cdot 10^{-4}$ m^3/s and $2.241 \cdot 10^{-4}$ m^3/s in dual-fuel mode and single-fuel mode respectively. Furthermore, due to uncertainties stemming from the performed experiments, the residual-to-bunkered fuels volume ratio was set as constant in the storage tanks, specifically at 5-95. A constant HVO-MeOH volume concentrations ratio was retained at 90-10 at the separator inlet following a conservative approach. To adhere to these conditions buffer tanks are needed, whose capacity is calculated by analysing the bunkering operations and minimised by installing one service tank for each fuel. More specifically, to keep the fuels ratio invariable in the storage tanks, a MeOH buffer tank with 1/20 storage tanks capacity is needed in HVO mode to strip the methanol off from the recirculating line. An HVO buffer tank with around 1/3 storage tanks capacity is required in dual-fuel mode to compensate for the mismatch in the mixture flowing between the storage tanks outlet and the centrifuge inlet sections.

6

Integrating and sizing the centrifugal separator in the multi-fuel system

In the previous chapter the centrifugal separator working conditions were identified, corresponding to the separator-fed mixture volume flow in single-fuel and dual-fuel operations. These working conditions are used to evaluate the separator performance to overcome the incomplete HVO-methanol phase separation observed with the conducted experiments. Hence, in this chapter, the results from the multi-fuel system modelling are integrated with the developed mathematical model discussed in chapter 4. First, the integration approach is presented. Next, a separator's final design is determined by optimizing its performance for both single-fuel and dual-fuel operations. Lastly, a results validation and an evaluation of the centrifuge mathematical model are presented.

6.1. Scope and approach

The scope of the centrifugal separator and the multi-fuel system models integration aims at assessing the separator's performance while defining its size. Overall, the objective is to find a separator design which guarantees complete fuels separation in both single-fuel (SF) and dual-fuel (DF) engine modes. In fact, in the previous sections, two different fed mixture volume flows were found, corresponding to the two yacht's operational modes. The centrifuge performance was defined in chapter 4 and consists of observation of the dispersed droplets' trajectory and interface position variation. More precisely, the trajectory observation gives direct insights into whether the dispersed denser droplets coalesce towards the heavy phase outlet channel or not under the design conditions. The interface position represents a further aspect yielding a more reliable design. Regarding the separator size, this analysis points to assessing the influence of the working conditions on the final design whilst finding correlations with existing centrifuges.

To achieve the defined scope the approach illustrated in figure 6.1 is followed.

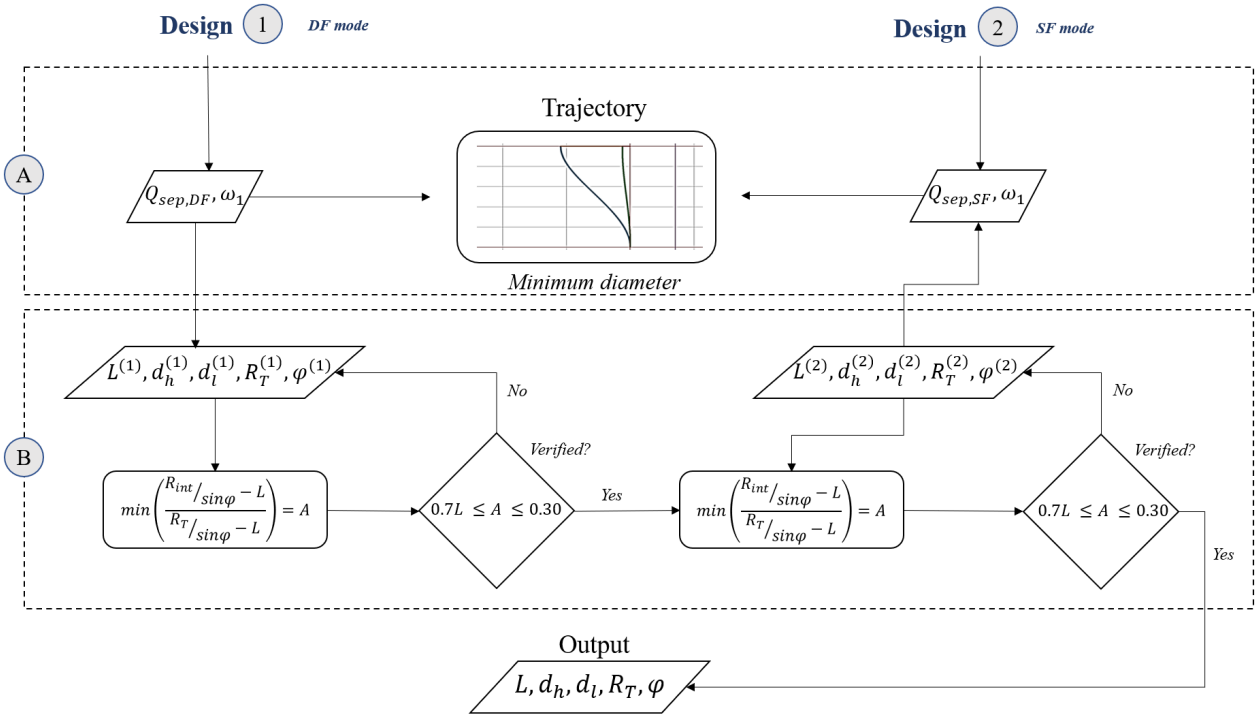

Figure 6.1: Methodology of the centrifugal separator performance assessment and sizing

Because the main objective is finding a unique separator design capable of guaranteeing full separation, a main distinction in figure 6.1 is done between designs 1 and 2. They are representative of DF and SF yacht's operations respectively. This means that these designs simulate the corresponding operational modes by receiving the associated fed mixture volume flow as calculated in the previous sections. This first simulation belongs to the named "block A" which aims at determining the minimum diameter of the dispersed droplets above which all the other droplets get separated. This is achieved by observing the droplets' trajectories within the centrifuge discs' sections as modelled in chapter 4. Additionally, the time required by the droplets to get discharged is measured. This is referred to as coalescence time t_c and it is used to determine the separator starting time in view of the fuel bunkering operation. The starting time is then the summation of t_c, the time required by the mixture to fill the discs sections and the outlet light and heavy phase channels to flow out the centrifuge. With reference to the geometry in figure 2.7, the mixture and the heavy and light liquids are assumed to have the velocity of the associated flow. Hence these times are determined as the ratio between the volume of the associated section and the volume flow:

$$t_{m,in} = \left(1.3nH \cdot \frac{\pi}{4} d_{min}^2\right) \frac{1}{Q} \tag{6.1}$$

$$t_{h,o} = \left[(L + 0.3nH)\,\frac{\pi}{4} {d_h}^2\right] \frac{1}{Q_h} \tag{6.2}$$

$$t_{l,o} = 0.3nH \frac{\pi}{4} {d_l}^2 \cdot \frac{1}{Q_l} \tag{6.3}$$

Where the diameter d_{min} of the mixture inlet is assumed to equal 65 mm from literature [110], as no formulas are found for its calculation. Similarly, in the case of the vertical distance between the upper disc and the top separator section, assumed being equal to 30% of the distance nH.

With reference to figure 6.1, regarding the block of iterations A, Q_{sep} and the rotational speed are inputs for the mathematical model. However, its value is varied to determine the correct interface position. For this, the steps presented in block B of figure 6.1 are followed. A single-objective constrained optimization problem is set. Generally, this assumes the form [111]:

$$\begin{aligned} &min\ f(x), \\ &x \in S \end{aligned} \tag{6.4}$$

With $x \in \mathbb{R}^n$ and $S \subset \mathbb{R}^n$ is the set of the constraining functions $g(x) \in \mathbb{R}^n$. In this study, the function to be minimised is:

$$f = \frac{\frac{R_{int}}{sin\varphi} - L}{\frac{R_T}{sin\varphi} - L} \tag{6.5}$$

This means that the interface position R_{int} is as much close as possible to the end discs section to avoid fouling and contamination of heavy phase by the light fuel, as discussed in chapter 4. Nevertheless, the available literature is limited to a qualitative description of the interface location. In this study, an acceptable interface position range is given as follows:

$$0.7 \cdot L \leq min\ f \leq 0.3 \tag{6.6}$$

This means that the interface can fall inside the discs' section but not assuming values below 70% of the discs' length L. Furthermore, the interface can be positioned outside the discs' section but without exceeding 30% of the total outer radius measured with respect to the discs' end section, i.e. $R_T/sin\varphi - L$. With reference to figure 6.1 the optimization function depends on a set of input parameters, namely discs' length and inclination angle, heavy and light phase outlet diameters, and centrifuge total outer radius. This is because R_{int} is dependent on these parameters, as equations 4.30 to 4.34 show. Hence, equation 6.4 becomes:

$$min\ f(R_{int}, L, d_h, d_l, R_T, \varphi) \text{ subject to :}$$

$$\begin{aligned} R_{int} &= \sqrt{R_T^2 + \frac{\rho_l}{\rho_h}\left(\frac{Q_l^2}{S_l^2\omega^2}\right) - \frac{Q_h^2}{S_h^2\omega^2}} \\ L &\in S_L \\ R_T &\in S_{R_T} \\ d_h &\in S_{d_h} \\ d_l &\in S_{d_l} \\ \varphi &\in S_\varphi \end{aligned} \tag{6.7}$$

Where S_i is the set of the variable i, which defines a range of existing variable values. Thus, the optimization problem finds the minimum of the function f among all possible combinations of the input parameters. The values of the parameters for which the condition in equation 6.6 is satisfied determine the separator design for the block B iteration loop. As it can be noticed in figure 6.1, these values are then the inputs for the droplets' trajectory simulation. The trajectories are generated to check whether variations of the minimum collected diameter occur compared to the first iteration process. The overall process is considered concluded when no variations are observed and the values assumed by the above-listed parameters determine the final separator design. In addition, the separator total diameter can be calculated with reference to figure 2.7 as:

$$D_{TOT} = 2 \cdot \left(\frac{d_l}{2} + R_T\right) \tag{6.8}$$

6.2. Results

This section presents the results of the centrifugal separator mathematical model integration in the multi-fuel system. Relatively to the followed methodology of figure 6.1, the results from iterations in block B are shown first. Next, based on this, block A outcomes are discussed.

6.2.1. Interface position

Starting with iterations in block B of figure 6.1, a first set of input values must be given to the model to calculate the minimum of the f function as in equation 6.7. Based on the literature [19, 78, 79, 95, 100, 101], the first assigned values are:

$$\begin{aligned} L[m] &\in [0.07; 0.1] = S_L \\ R_T[m] &\in [0.1; 0.3] = S_{R_T} \\ d_h[m] &\in [0.006; 0.09] = S_{d_h} \\ d_l[m] &\in [0.07; 0.09] = S_{d_l} \\ \varphi[deg] &\in [45; 65] = S_\varphi \end{aligned} \tag{6.9}$$

It can be noticed that $d_l > d_h$. This is because the dimensions of the outlet light phase diameter are determined with the regulating ring. This is a ring mounted on top of the light liquid outlet channel and its diameter impacts the interface position. As a general rule of thumb, this diameter is bigger for lighter liquids [100], i.e. it falls in the above-reported values for compounds having a relative density approximately equal to the one of HVO.

The generated model is simulated for the two yacht's operational modes, i.e. for two volume flows of the fed mixture ($Q_{sep,DF}$, $Q_{sep,SF}$) two designs are generated. Results are presented in parallel plots showing variations of the five best input values for each separator design. The results of the first iteration process are depicted in figure 6.2.

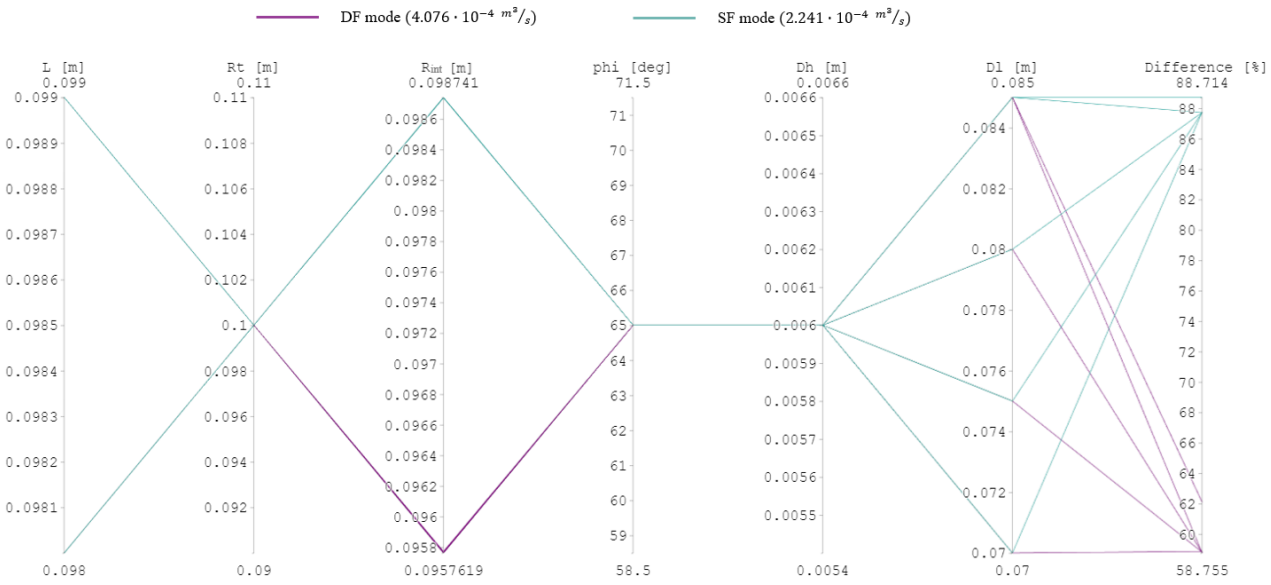

Figure 6.2: Five best combinations of centrifugal separator design parameters for optimal interface position. Results from the first iteration process for dual-fuel and single-fuel engine modes

From the figure above it can be noticed that the minimum value of the f function, expressed in terms of percentage difference, is not in the desired range as in equation 6.6. Hence, a new values

range is assigned to the input parameters. To define this, some observations from the illustrated graph shall be made. Firstly, the discs' length assumes values close to the highest in the given range, whilst R_T scores the lowest. With reference to equation 6.7, this is due to the small values assumed by the terms added to R_T. In fact, for the close densities, the term ρ_l/ρ_h is close to 1, hence it can be imagined that the R_{int} variation is dictated by the volume flow, the diameter of the outlet sections and the rotational speed. Regarding the volume flow, the plot does not show extreme variations between the input values. However, it is true that the percentage difference is lower for the dual-fuel mode case, hence for higher volume flow. The cause might lie in the pressure difference variation at the interface as well as in the higher mixture flow velocity entering the separator, which drags the dispersed droplets more towards the discs section rather than the centrifuge external wall, as seen in equation 4.28 and section 4.4.1. However, this observation is not highly relevant for the purpose of this iteration process of this study. This is because, although the volume flow is varied to simulate the two engine modes, the assumed value is a constant within the separator design. Hence, ω, d_h and d_l are the dictating parameters for the variation of the added terms to R_T in equation 6.7. Nevertheless, the rotational speed is a constant stemming from block A of the iterative process, as seen in figure 6.1. Hence, regarding the diameter of the outlet sections, it shall be considered that, for heavy phase at fixed 10% v/v concentration, $Q_l > Q_h$. Moreover, $d_l > d_h$ in existing separators, with d_h taking the smallest range value. Hence, this compensates the difference between Q_l and Q_h, as both d_l and d_h are present at the denominator of the equation for R_{int}. Consequently, given two fuels with small densities difference, the value of R_{int} strictly depends on the discs' length and the total outer radius. For this reason, and with reference to equation 6.5, the assumed value of the discs' inclination in figure 6.2 is the highest in the given range.

As a consequence of these observations, L, R_T and d_l ranges were enlarged, d_h values were decreased, whilst the range for φ was kept constant. The new assigned ranges are:

$$\begin{gathered} L[m] \in [0.07; 0.19] = S_L \\ R_T[m] \in [0.19; 0.3] = S_{R_T} \\ d_h[m] \in [0.004; 0.07] = S_{d_h} \\ d_l[m] \in [0.007; 0.9] = S_{d_l} \\ \varphi[deg] \in [45; 65] = S_\varphi \end{gathered} \tag{6.10}$$

The results from the last iteration are presented in figure 6.3. It can be noticed that the percentage difference equals 0.038 and 11.558 for dual-fuel and single-fuel mode respectively. Both results fall in the desired range and therefore the final centrifuge design is selected. These outcomes stem from a rotational speed value fixed at 50 rad/s. This was checked in the iteration process referred to as "block A" in figure 6.1, with respect to the methanol droplets trajectories within the modelled centrifuge discs section.

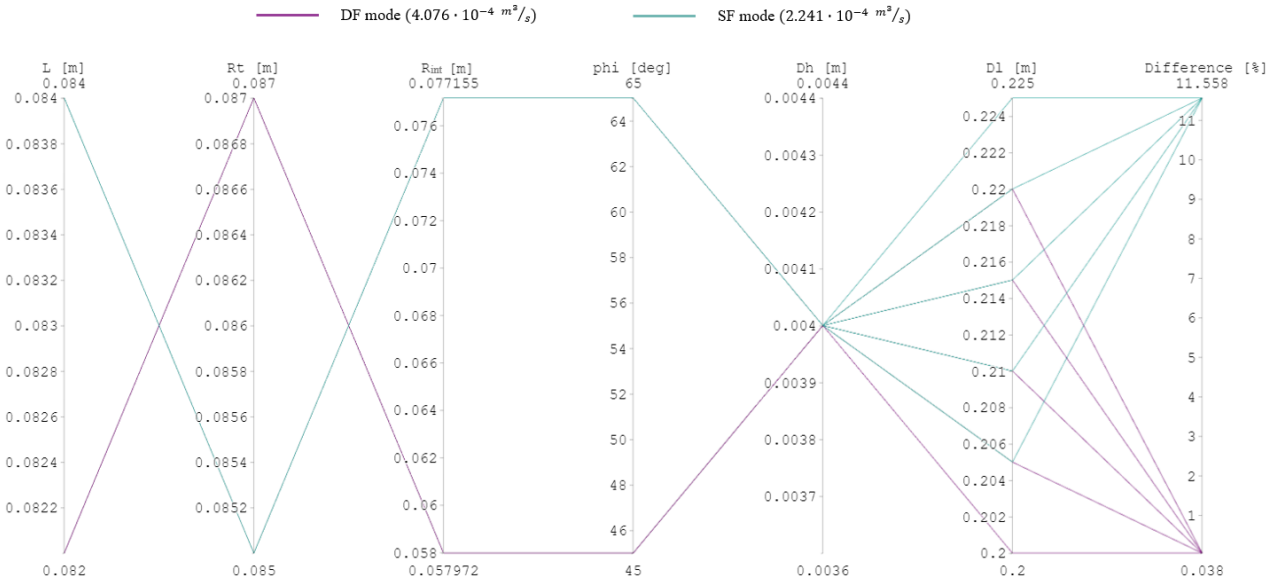

Figure 6.3: Five best combinations of centrifugal separator design parameters for optimal interface position. Results from the last iteration process for dual-fuel and single-fuel engine modes

6.2.2. Droplets trajectory

In this subsection, the results of the methanol droplets' trajectories are shown. The centrifuge specifications resulting from the iterations presented in the previous subsections are used as inputs for the mathematical model developed in chapter 4. The trajectories of the methanol droplets were assessed for a fixed rotational speed fixed at 50 rad/s.

The results from this study are illustrated in figures 6.4 to 6.7. The results are reported for a separator working at both single-fuel and dual-fuel yacht's modes. This means that the fed mixture volume flow respectively equals $2.241 \cdot 10^{-4}$ and $4.076 \cdot 10^{-4}$ m^3/s. The trajectories are plotted for different droplet diameter values. These were selected in the range 5-100 μm as typical of industrial cases [62, 78]. To simplify the discussion of the results, the droplets with diameter values for which they hit the upper disc are referred to as "medium droplets". The droplets with diameter values above this range are called "big droplets". The graphs portray the methanol (heavy phase) droplets' trajectories within a single separator discs' section. Hence, the abscissa represents the non-dimensional horizontal coordinate, expressed as the ratio between the x-coordinate and the disc's length L. The ordinate is the non-dimensional vertical axis, i.e. the ratio between the y-coordinate and the vertical distance between two adjacent discs. This is indicated with h and equals $Hsin\varphi$, with respect to the chosen reference system as in chapter 4.

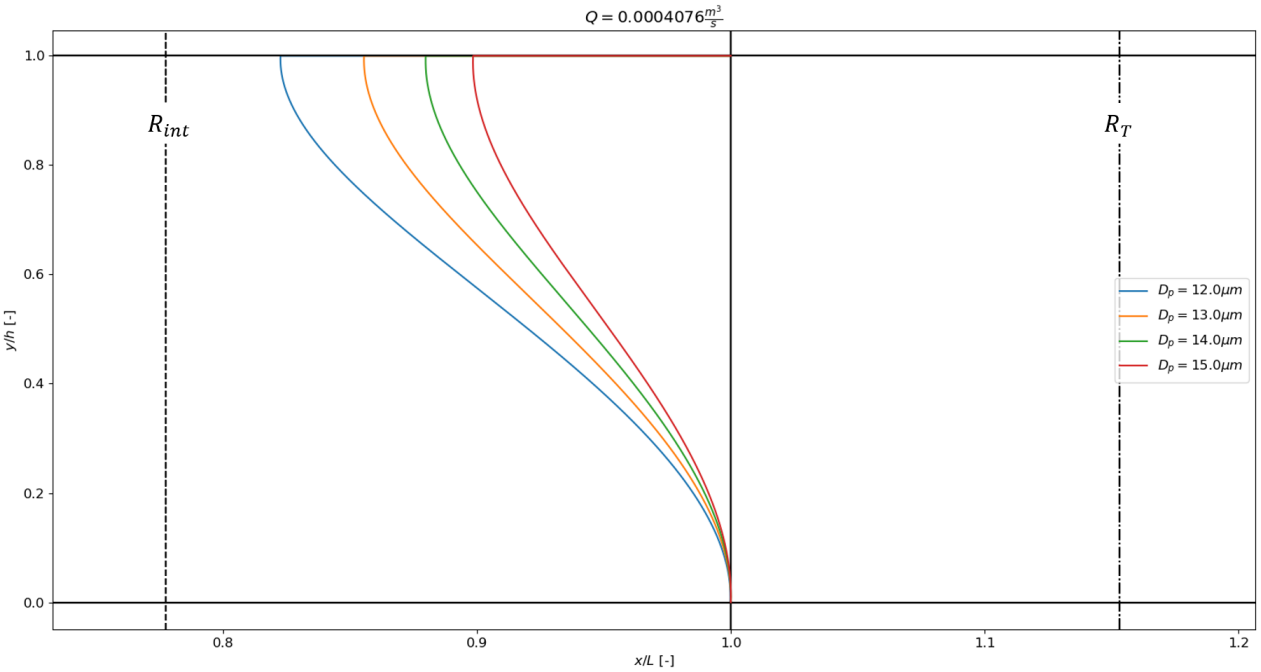

Figure 6.4: Trajectories of medium-sized methanol droplets within a consecutive discs' section (dual-fuel engine mode)

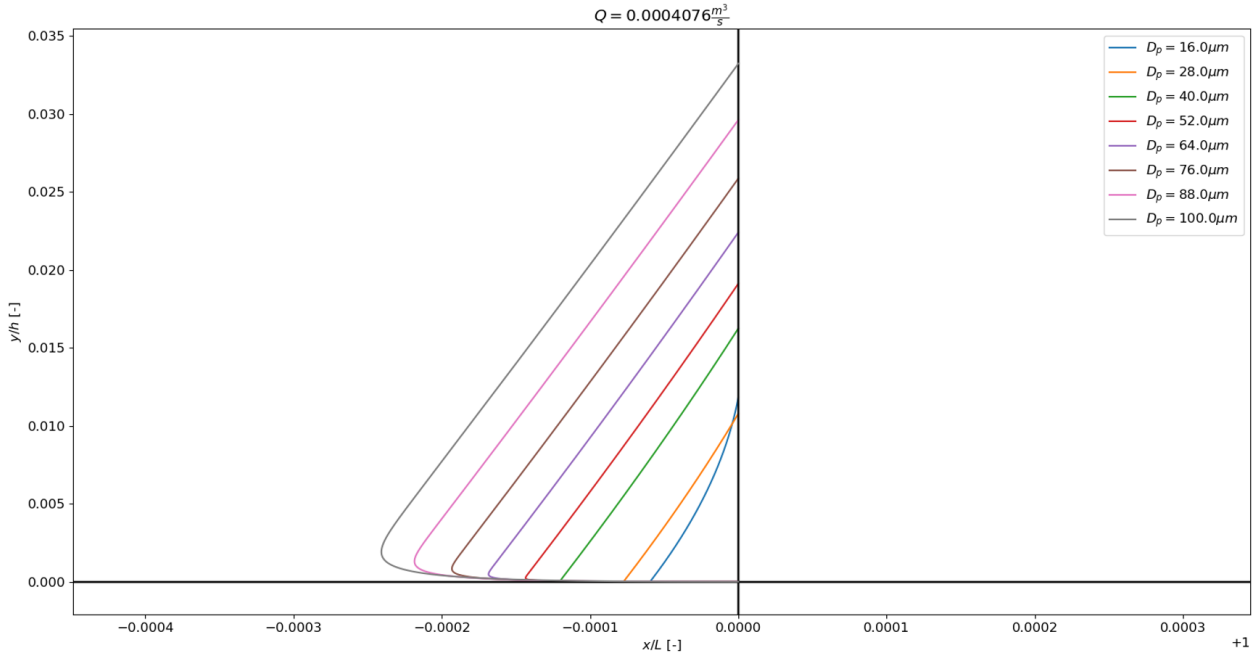

Figure 6.5: Trajectories of big-sized methanol droplets within a consecutive discs' section (dual-fuel engine mode)

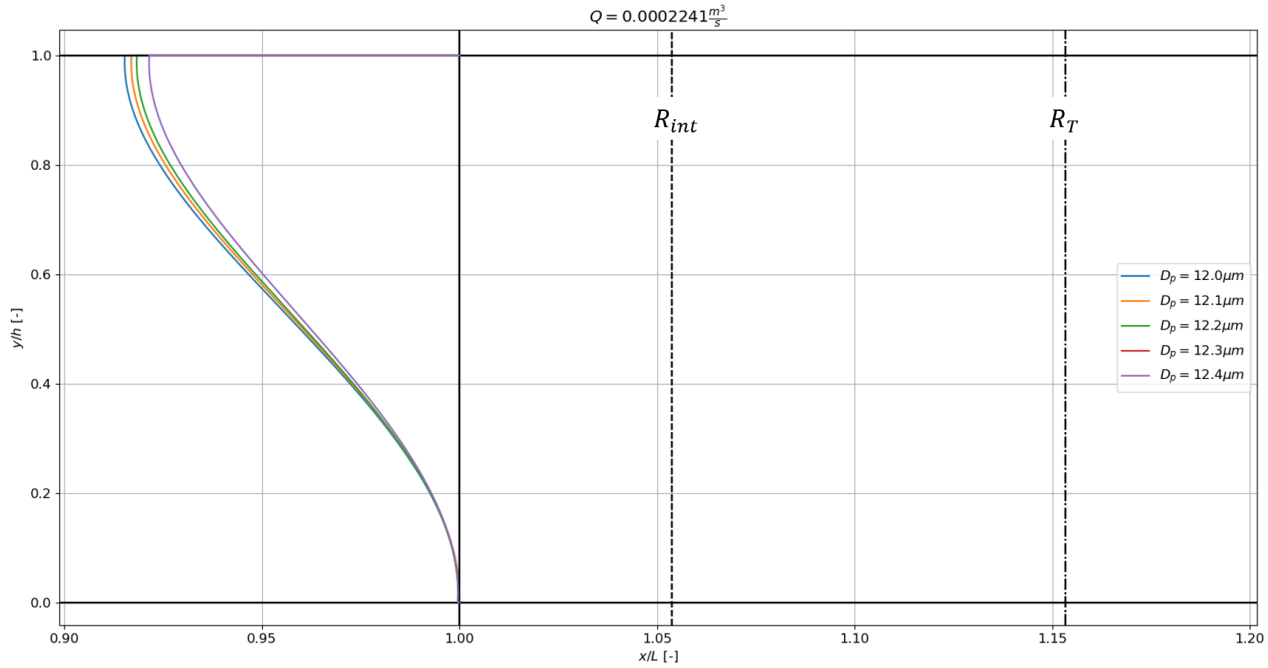

Figure 6.6: Trajectories of medium-sized methanol droplets within a consecutive discs' section (single-fuel engine mode)

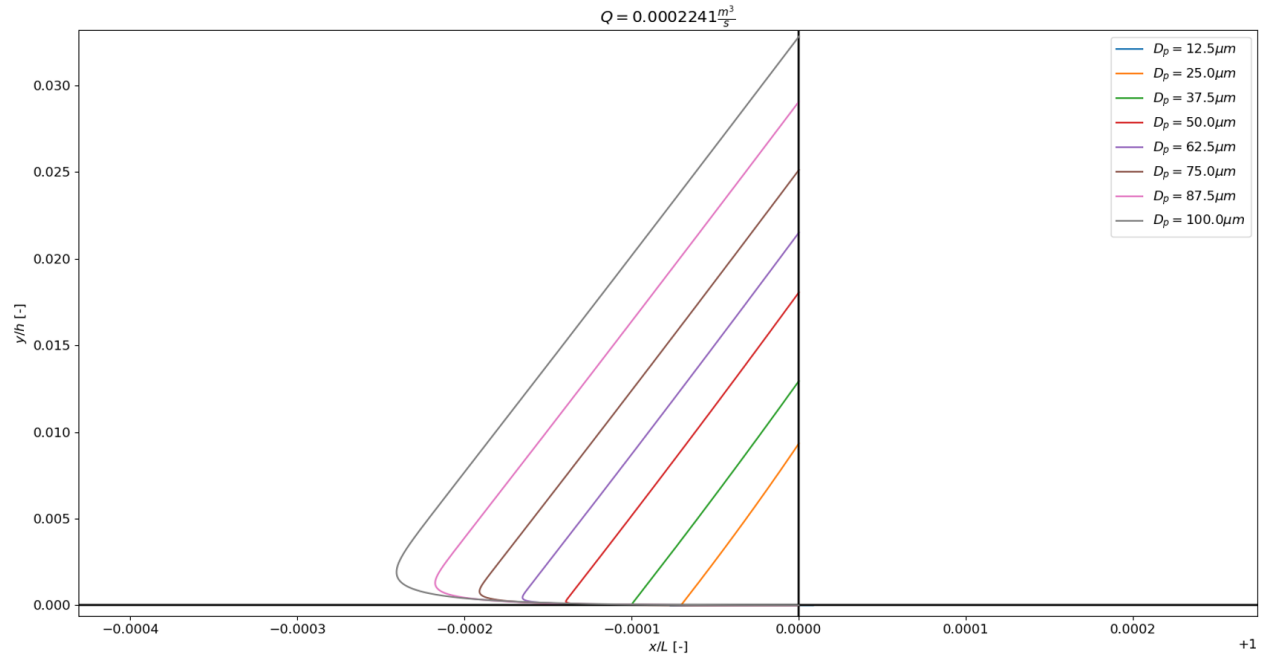

Figure 6.7: Trajectories of big-sized methanol droplets within a consecutive discs' section (single-fuel engine mode)

In all plots, it can be observed that all droplets get collected in the heavy phase outlet section. Thus, with the found design specifications, the modelled separator is capable of achieving full separation. Droplets with diameters smaller than the presented values also get discharged in the methanol outlet section. Their motion is such that they instantaneously change their direction towards the separator wall. However, their trajectories are not shown here for more efficient graph readability and because no major differences were found between the two studied operational modes.

The droplets' behaviour for the other single cases is analysed below.

Figures 6.4 and 6.6 represent the trajectories for the so-called "medium droplets". For a higher volume flow, the travelled distance by the droplets is bigger compared to a lower volume flow. This is due to the greater velocity in both x- and y-directions assumed by the single droplet. Furthermore, the graphs show that the travelled distance increases the smaller the droplet diameter. It might be hypothesised that smaller droplets have less resistance to oppose the fed mixture flow. This trend is less evident for a smaller volume flow because a smaller amount of droplets hits the upper disc. Conversely, diameters outside the depicted range leave the discs' section quickly. This aligns with the resulting interface position which assumes a different value compared to the higher volume flow case. In fact, for the latter, R_{int} falls inside the discs' section, whilst the interface allocates outside the discs 'section in the lower volume flow scenario. As also discussed in the previous section, the higher the mixture flow the higher its velocity. Hence, for higher flows, the dispersed droplets are dragged more towards the discs' section rather than the centrifuge outer wall.

Regarding bigger droplets, results are shown in figures 6.5 and 6.7. No major differences between the two operational cases are found. The results presentation is limited to their observation due to the nonlinearity of the problem. The differential equations of motion found in chapter 4 present a balance between drag and centrifugal forces. Both forces scale with the droplet diameter, the drag pushes the droplet inside the discs' section while the centrifugal gravity outside. Furthermore, the drag is proportional to the flow velocity. Hence, within a non-linear problem, for different combinations of flow velocity and droplet diameter, the relationship between all these parameters is hard to imagine. However, given that the droplets leave the discs' section almost instantaneously it can be assumed that the centrifugal force dominates over the drag. Additionally, it is observed that for higher volume flows the droplets travel a bigger distance compared to lower volume flows. However, this difference is slight compared to the medium-sized droplets case.

Moreover, big droplets in the presented ranges require a few milliseconds to get discharged, with bigger droplets travelling a longer distance. Droplets in the medium-size range, require some minutes to coalesce. More specifically, as the velocity of the droplet can be imagined as being dominated by the entering mixture velocity, the droplets require some seconds in their upward trajectory which leads them to hit the upper disc. However, as kinetic energy is lost by the moment of the contact [79], the droplet needs to win the resistance of the incoming mixture encountered when flowing towards $x/L = 1$, i.e. towards the methanol outlet section. The demanded time increases the lower the droplet diameter. Concerning the droplets having the smallest diameter in figures 6.4 and 6.6, the 12 μm sized droplets need around 10 minutes to get discharged in dual-fuel mode. In single-fuel engine mode, where the separator-fed volume flow is lower, the discharged time is also lower, standing at about 5 minutes. In both single-fuel and dual-fuel operations, the time to fill the separator and discharge the first fuels batch is in the order of a few seconds, as calculated with equations 6.1, 6.2 and 6.3. Hence, the separator starting time, and consequently, the bunkering operations, is dictated by the dispersed droplets' coalescence time inside the discs' section.

The final centrifugal separators' main specifications are listed in table 6.1. To assess the validity of the centrifuge model the results can then be assessed via comparison with the existing centrifugal separators and evaluation of the assumptions behind the developed model.

Table 6.1: Final main specifications of the modelled centrifugal separator

Parameter	Symbol	Unit	Value
Fed mixture volume flow (DF mode)	$Q_{sep,DF}$	[m^3/s]	$4.076 \cdot 10^{-4}$
Fed mixture volume flow (SF mode)	$Q_{sep,SF}$	[m^3/s]	$2.241 \cdot 10^{-4}$
Discs length	L	[m]	0.084
Outer radius	R_T	[m]	0.087
Methanol outlet section diameter	D_h	[m]	0.004
HVO outlet section diameter	D_l	[m]	0.205
Separator total diameter	D_{TOT}	[m]	0.379
Discs inclination angle	φ	[deg]	65
Rotational speed	ω	[rad/s]	50

6.2.3. Results validation and hypotheses evaluation

This subsection discusses the obtained centrifugal separator results and evaluates the hypothesis made for its modelling.

Firstly, the obtained separator design is compared to the existing designs from the literature. A disc-bowl type centrifuge by *Alfa Laval* [101] works at a bowl speed of 71.7 rad/s, a value close to but higher than 50 rad/s obtained in this study. The difference lies in the higher separator capacity. The *Alfa Laval* design is, in fact, a high-capacity centrifuge, working at a volume flow 35 to 64 times higher than the working conditions of this case. The higher volume flow allows for a higher rotational speed to efficiently allocate the interface section between the light and heavy liquids. Furthermore, glycerol and methyl esters are the separated compounds in the *Alfa Laval* separator, whose density difference is 331 kg/m^3 [47], i.e. higher than 30.5 kg/m^3 of the HVO-methanol scenario. It might be assumed that for the same reasons concerning the interface position, the *Alfa Laval* design presents a heavy phase outlet section diameter of 0.05 m, higher than the results derived in this model. The same discussion applies to the tested oil-water separator by J.P. van der Linden at a rotational speed of 91.7 rad/s [95]. Similar conclusions can also be drawn comparing the separator design of this study with the one used by R. Plat [78] in its experiments. Different test conditions were performed with the volume flow falling in the same order of magnitude of the values obtained in this analysis. However, the discs' length and the separator outlet radius are respectively 16.7% and 47.2% smaller than the obtained values in this case. The cause behind this can still be assumed to lie in the higher density difference between the tested oil and water liquids by the author compared to the HVO-methanol scenario. The resulting total centrifuge diameter equals 0.379 m, a value 34.9% bigger than the maximum diameter typical of marine separators installed on Feadships [112]. Here again, the cause might be the lower density difference between the considered fuels compared to the MDO-water case of marine separators. The value of the total centrifuge diameter is, in fact, dominated by the HVO outlet section diameter, as it can be seen in table 6.1, which however aligns with the recommendations from the centrifuge manufacturers [100].

Furthermore, the calculated starting time is in the range of 5-10 minutes depending on the volume flow fed to the separator. This is mainly dictated by the coalescence of 12 μm droplets. The literature is absent regarding this specific aspect of the design. The already mentioned centrifugal separators [100, 101] mention a starting time in the range of 2-4 minutes and 6-8 minutes. Nevertheless, it is not clear whether this time only refers to the coalescence of droplets or it includes other processes. For instance, the fed mixture pump and possible heater starting time, or the time for a gradual rotational speed ramping up to the desired operating level.

Alongside the validation of the results, the hypotheses behind the developed mathematical model of the centrifugal separator discussed in chapter 4 can be checked for a model evaluation.

Firstly, as discussed in the previous subsection and as figures 6.4 to 6.7 show, all the droplets are collected with the developed model. Hence, this verifies the hypothesis of complete fuels separation. Among the hypotheses, some forces were neglected, namely Coriolis and shear forces. This hypothesis holds for the obtained separator design. Both forces assume insignificant values compared to the centrifugal force. Starting with the Coriolis force, its ratio with the centrifugal force can be calculated as [78]:

$$\frac{F_{cor}}{F_{\omega}} = \frac{\rho_l \omega D^2}{9\mu_h} \tag{6.11}$$

With the methanol droplet diameter in the range 5-100 μm, the above ratio stands at 0.00025-0.0921. Regarding the shear force its contribution is dictated by the lift forces caused by the droplets' rotation. The ratio between the lift and the centrifugal force equals [78]:

$$\frac{F_L}{F_{\omega}} = \frac{0.172 G_s^{1/2} \rho_h g D sin\varphi cos\vartheta}{\omega^2 \frac{D_{TOT}}{2} {\mu_h}^{1/2}} \tag{6.12}$$

Where ϑ is the angle between the lift and centrifugal forces, which is an unknown for this problem, while G_S is the shear rate expressing the flow velocity gradient:

$$G_S = \frac{V_F(y = Hsin\varphi - D) - V_F(y = Hsin\varphi)}{D} \tag{6.13}$$

With V_F being the mixture flow velocity as in equation 4.28 and $V_F(y = Hsin\varphi) = 0$, given the mixture flow velocity parabolic profile. Now, it shall be considered that F_L/F_{ω} depends on the droplet diameter and G_S is implicitly a function of the volume flow. Hence, F_L/F_{ω} is calculated for the diameter at the extreme values of the 5-100 μm range and for the inlet volume flow equal to $4.076 \cdot 10^{-4}$ and $2.241 \cdot 10^{-4}$ m^3/s dictated by the yacht's operational modes. It results that F_L/F_{ω} ranges $0.00136 cos\vartheta$- $0.0340 cos\vartheta$. Thus, the droplets break-up and deformation caused by shear forces can be neglected for the droplet diameter values considered and for the resulting separator design.

6.3. Chapter conclusion

This chapter covered the integration of the developed mathematical model of the disk-stack centrifugal separator in the multi-fuel system. The experiments conducted on HVO-methanol mixtures and discussed in chapter 3, evidenced incomplete separation between HVO and methanol within the observation time. Hence, the separator integration in the multi-fuel system sought to evaluate the performance of the centrifuge to overcome this challenge. In the previous chapter, the fed mixture volume flows for the considered yacht's operational modes were calculated. These served as inputs for the mathematical model of the separator. An iterative approach was followed to determine the separator design to enlarge the range of droplet diameter values yielding separation and locate the interface section as close as possible to the discs' end section. The main takeaway is the achievement of full separation with the obtained centrifuge design. For the resulting centrifuge design, small methanol droplets sized 5-12 μm and large droplets with a diameter of 12.5/16-100 μm leave the discs' sections almost instantaneously, as dominated by the centrifugal force. Medium-sized droplets require 5-10 minutes to coalesce due to encountered resistance exerted by the inlet mixture. The coalescence time increases the smaller the droplet. Moreover, results validation via comparison with existing separators showed an overall increase in the separator main dimensions. The cause might lie

in the interface location mainly driven by the small density difference between HVO and methanol. Lastly, the evaluation of the developed mathematical model for the centrifuge was conducted by scrutinizing the separator outcomes to ascertain the validity of the underlying assumptions. The outcome of this assessment revealed that the assumptions employed in the model hold true and can be considered valid.

7

Conclusions

In the introduction of this report, the research questions were listed. This chapter provides answers to them which help to answer the main research question. In chapters 1 and 2 the role of HVO-methanol separation was reviewed to enable built-in flexibility to the yacht. The alternative storage of these fuels in the same tanks onboard yields variations in the bunkered fuel's concentration which can cause undesired effects in DF engines. Thus, the main research question to be answered is:

How can HVO and methanol be fully separated prior to their usage in DF engines?

Gravity and centrifugal separation were investigated for this. The following sub-questions related to these technologies are answered as follows.

What is the time required by HVO-methanol mixtures to fully phase separate by gravity?
Experiments were carried out on HVO-methanol mixtures with methanol at 1, 5 and 10-70% volume concentrations. The tests revealed that after 1 hour, all the mixtures failed to achieve a state of full separation. The incomplete separation status was also observed after 3 days with methanol at 1% and 50% v/v. The reason behind the non-achieved full separation within the observation time-frame might lie in the low-density difference between the fuels, while the fuels partial separation can be associated to the different polarity nature of the tested substances. The behaviour of the tested mixtures aligns with the available literature. Overall, the experiment observations strengthen the selection of investigating centrifuges to separate HVO/methanol from methanol/HVO.

How can a centrifugal separator be modelled and what are the problem boundary conditions?
The scope of this study encompasses the evaluation of a disc-bowl type separator performance and its associated startup time. Hence, the motion equations of the individual heavy fuel droplets within the centrifuge discs interspaces were computed. Within a framework of assumptions, the model was constructed based on the centrifugal force, drag and buoyancy acting on the heavy liquid droplets. This resulted in the coupled second-order differential equations 4.15 and 4.16. The interstitial regions between the discs were designated as the boundaries governing the individual droplet's movement. To solve the differential equations and constrain the droplet's motion within the discs' interspaces, initial conditions on the denser droplets' position and velocity were imposed.

How does the fuels separation impact the multi-fuel system schematic?
Within the fuel system, the separator must provide clean fuel(s) to the engines at the required volume flows for a specific output power. Hence, the centrifugal separator working conditions were determined for single-fuel (HVO) and dual-fuel engine modes. Results show the need for

buffer tanks whose capacity is minimised by analysing the bunkering operations. The usage of buffer tanks stems from maintaining the fuels ratio constant in the storage tanks and at the separator inlet. The residual-bunkered fuels ratio is assumed to be equal to 5-95 v/v in the storage tanks. The HVO-MeOH volume concentration was maintained at 90-10 v/v at the separator inlet. To keep the fuels ratio invariable in the storage tanks, a MeOH buffer tank with around 1/20 of the storage tanks' capacity is needed in HVO mode to strip the methanol off from the recirculating line. An HVO buffer tank with about 1/3 of the storage tanks' capacity is required in dual-fuel mode to compensate for the fuels ratio mismatch in the mixture flowing from the storage tanks outlet to the centrifuge inlet section.

How can complete methanol/HVO removal from HVO/methanol be achieved via centrifugal separation?
Two methods were identified for the separator performance assessment, encompassing the methanol droplets' trajectory observation within the discs' interspace and the location of the interface position. With the methanol being the heavy liquid, a full HVO-methanol centrifugal separation can be achieved when the methanol droplets hit the upper disc or leave the discs' section moving towards the outer wall. Regarding the interface position, due to discrepancies in the literature, it is established that the interface can ideally fall inside or outside the discs' section with a certain margin of exceedance. To achieve the aforementioned conditions, a centrifuge final design capable of achieving full separation in both single- and dual-fuel modes was defined. An overall increase in the separator main dimensions is observed in comparison to existing disc-bowl type designs. More specifically, the final centrifuge design has a diameter 34.9% bigger than the maximum diameter typical of marine separators installed onboard Feadships. This value increases to 89.5% compared to centrifuges used for tests. Discs 20% longer than lab centrifuge designs are needed. This result could be attributed to the interface location, mainly driven by the low-density difference between HVO and methanol.

What is the time required by the centrifugal separator to achieve full separation?
This study focused on a continuously operating disc stack centrifuge. Thus, the separation time is represented by the separator startup time. In this study, the startup time was found to be mainly dictated by the motion of the individual methanol droplets within the discs' section. More specifically, the time is droplet diameter-dependent, the latter selected in the range of 5-100 μm. Medium-sized droplets with a diameter of 12-16 μm require 5-10 minutes to coalesce, with the time increasing the smaller the droplet, due to encountered resistance exerted by the fed mixture. Droplets with a diameter outside the mentioned range leave the discs' section almost instantaneously.

7.1. Conclusion on HVO-methanol separation

The answers to the previously research questions collectively address the main research question:

How can HVO and methanol be fully separated prior to their usage in DF engines?

A full separation of HVO and methanol can be achieved by utilising a disc stack centrifuge. The experiments performed on HVO-methanol mixtures evidenced non-achieved full separation under gravity within the 1 hour-three day observation time. This poses limitations to the usage of gravity settling tanks in those scenarios wherein a specific fuel must be supplied to the engine at a required time. An extended fuels treatment duration might prolong the waiting time to sail after bunkering or fuel switchover during sailing, undermining the built-in flexibility nature of the fuel system design. Conversely, the designed centrifuge does not affect the considered yacht's operations. The conclusion that a full fuel separation can be achieved via a disk-stacked centrifuge has a theoretical nature, and for which experimental validation is needed. This result stems from the developed mathematical model

built within a framework of assumptions and validated with the obtained results. Overall, a larger separator than the centrifuges used nowadays for MDO-water treatment is needed. An outcome that might be attributed to the low-density difference between HVO and methanol. Furthermore, for a continuously operating separator, the separation time is dictated by its starting time. This equals a maximum of 5-10 minutes for the medium-sized methanol droplets. Hence, a substantially smaller time than gravity separation observed with the experiments. Alongside a centrifugal separator, HVO and methanol buffer tanks shall be installed to handle the recirculation of the unused fuel during a specific yacht's operational mode, while matching the desired fuels ratio in the storage tanks and at the separator inlet.

8

Discussion and Recommendations

This segment of the report covers the discussions stemming from the previous chapters conclusion. Associated recommendations are also given for further work. Discussions and recommendations are presented in different sections corresponding to a specific report chapter. Personal reflections are given to highlight the relevancy of this study in a wider context.

8.1. Experimental study on HVO-methanol mixtures

In this section discussions and recommendations are presented relative to the experimental study presented in chapter 3.

First, it is recommended to take more samples of the tested mixtures for the same time step as well as extending the time interval in order to get more diameter values. The droplets' diameter distribution obtained is in fact constrained to a single-sample collection at each time step. The extension of the observation time would also yield a more exhaustive response concerning the duration of the complete separation process.

Second, because theories concerning the influence of external factors on the mixture behaviour are in disagreement [71, 72, 73], it is recommended to carry out some tests varying the stirring time and rotational speed. A lower stirring time and/or rotational speed are suggested to be tested to observe possible droplets' size distribution change and therefore the required time to achieve full separation. In the performed tests, the obtained droplets' size might have been influenced by the stirring time and selected rotational speed. Alongside the low-density difference between the fuels, the stirring time and the maximum rotational speed might have decreased the droplets' diameter, potentially due to inadequate time for inter-droplet film drainage [71]. This likely resulted in the impossibility of bigger droplets formation, extending the time required to achieve full separation.

Furthermore, experiments are needed to accurately determine the fuels' properties under the tested conditions. Validation of the mathematical methods presented by Green and Perry [48] is suggested for the specific HVO-methanol case. During the tests the temperature was kept constant at 20°C, thus overall no variation of density, viscosity and interfacial tension is expected to be encountered [68]. Nevertheless, fuels' properties in a liquid mixture can vary depending on aspects different from the temperature. Green and Perry [48] present different methods utilised to determine the density and viscosity of liquid mixtures. The dependency of these properties on pressure, interaction parameters and molecular size is shown.

Lastly, the experimental results showed the presence of methanol in HVO for all the tested concentrations. The quantification of the methanol traces in HVO was rendered impossible under the examined conditions and methodology. However, this determination at each time step is fundamental following the conservative approach of this project. Within the literature review, in fact, the maximum acceptable methanol/HVO concentration in HVO/methanol by PFI DF engines was studied. It was concluded that with the current technology state-of-the-art, no traces of methanol/HVO in HVO/methanol are accepted. Therefore, further research is needed to study incomplete methanol vaporization, reduced engine efficiency and increased dual-fuel engine emissions. Moreover, the usage of additives can be researched to avoid engine corrosion and wear in case MeOH/HVO cannot be removed from HVO/MeOH. Tests can be extended to other types of dual-fuel engines, different from PFI designs, to assess the sensitivity of a set of DF engine technologies to fuels contamination. The results from engine tests would leave indications on the acceptable concentration of HVO/methanol in methanol/HVO. The addition of emulsifiers in the mixture can help to create a more stable emulsion if small traces of the residual fuel are accepted in the combusted fuel by the engines. Within the phase separation experiments, a refractometer might be used to determine the residual volume concentration of the dispersed droplets in the continuous phase. Additionally, chromatography and distillation can be performed to measure the extracted residual methanol volume from HVO [48].

8.2. Mathematical model

In this part of the report, discussions arising from the developed mathematical model of chapter 4 are covered. Suggestions for future research are given.

First, the inclusion of water and/or solid particles in the binary liquid mixture separation model is suggested. Now, the model does not consider water in the HVO-methanol binary mixture to facilitate the analysis. However, water can stem from its condensation in the storage tanks. Similarly, no solids are included which can be found in the bunkered or residual fuel. Furthermore, a study on conventional EN 590 diesel mixed with methanol or HVO is suggested. Moreover, this work considered the mixture of the alternative fuels only, however, EN 590 is currently used while HVO and methanol become increasingly available. Furthermore, fatty acid methyl esters (FAME) are suggested to be investigated in the HVO/EN 590-methanol mixture. FAME can be found in HVO and EN 590 diesel at a maximum of 7% v/v and creates interaction with methanol in the mixture given their polar nature [40, 41]. The assessment of the separator performance can be done by carrying out tests on centrifugal separators with increasing addition of FAME and water content in HVO/EN 590-methanol mixtures.

In addition, a more refined model analysis and experiments are suggested. The developed model assumes no Coriolis effect on the individual denser droplet and no droplets break-up and merge. While these hypotheses were validated with the obtained design in chapter 6, in practice these effects might occur given the nature of the system. In chapter 6, it was seen that medium-sized droplets require more time to coalesce compared to smaller and bigger droplets in the considered diameter range. Hence, small/big-sized droplets can merge with medium droplets or get deformed along their path. The Coriolis effect and droplets' deformation/conjunction can vary the droplets' motion and therefore the separation time. Bigger droplets due to conjunction can yield decreased separation time or obstruction of the mixture's flow given a certain discs' interspace. Hence, validation of the aforementioned hypotheses and results is advised via experiments and computational fluid dynamics (CFD) tools for a more nuanced study. Tests and CFD 3D modelling would also offer

insights into possible effects of the droplets' rotation along the bowl's vertical axis on the separator performance. In fact, in this work, a two-dimensional model was built with the droplet rotation already embedded within the selected reference frame. Moreover, in this work, for a conservative approach, the individual denser droplet is assumed to enter the discs' section at the tip of the lower disc. Nevertheless, the droplets initial position can vary, impacting the discharging time. Tests aiming at determining the concentration of droplets with a certain size moving towards the discs' interspaces would give an indication of the amount of droplets entering at a certain initial vertical position. The definition of the droplets concentration with a certain size within the mixture would allow validation of the hypothesis of ideal separation by applying the formula proposed by R. Plat [78]. Optical or laser-based methods for the determination of the droplets size distribution are suggested [113]. Lastly, identified methods to assess the separator performance encompass the observation of the individual droplet trajectory and the interface position variation. It is recommended to find equations to couple these two methods. In the developed mathematical model, in fact, the interface position and the droplets' trajectories are independent. Additionally, in this study, the interface position formulation used stems from the pressure difference at this location. A more complete formulation could be used as provided by J. P. van der Linden [95] to consider the contribution of various pressure drops. Validation of this formula for the specific case of this study is suggested via experiments to observe the interface position change by varying input parameters.

8.3. Multi-fuel system model

The discussions and recommendations given in this section derive from the multi-fuel system model results discussed in chapter 5.

The results from the fuel-system model evidenced the installation of HVO and methanol buffer tanks to control the mixture composition at the separator inlet and store non-required fuel by the engines. The required space by the buffer tanks can impact the available space onboard. Hence, recommendations are provided to address this potential challenge. First, the buffer tanks might be considered an integral part of the yacht's structure.
Second, for the calculation of the buffer tanks' capacity, service tanks can be considered completely or partially full at the time of bunkering. Data from the existing fleet can be collected to serve this analysis. In this study, a conservative approach was followed. Service tanks were assumed to be empty at the time of bunkering. This situation is likely to occur after the transatlantic trip, wherein the yacht covers its full range, draining the HVO service tank completely. In reality, it can happen that the methanol service tank remains full after this operation mode. Additionally, both HVO and MeOH tanks can remain completely or partially full, especially after a dual-fuel operation. Moreover, a connection can be provided between the methanol buffer and service tanks. Hence, the time to fill the methanol service tank might reduce and thus the HVO buffer tank capacity decreases. Additionally, it can be investigated whether the excess methanol stemming from HVO bunkering can be burned first, leading to a temporary dual-fuel mode prior to the single-fuel (HVO) operations. Furthermore, the obtained results derived from the assumed fixed fuels ratio at the separator inlet. This is an operational restriction stemming from uncertainties related to the available literature on marine centrifuges. In the previous section tests on centrifuges were recommended. It is suggested to test mixtures with denser liquid concentrations different than the assumed 10% v/v. For a given separator design, the tests would help to determine if the discharged light/heavy phase gets contaminated by the heavy/light fuel due to a possible variation of the interface position. Ideal fuels separation for different fuels ratios in the fed mixture would lead to flexibility in operations and reduced fuels re-circulation.

Furthermore, the usage of sensors to determine the residual fuel concentration in the mixture exiting the storage tanks can be investigated. In this work, a mixer is assumed to be installed in each storage tank to create a random dispersion of the residual fuel in the bunkered fuel. Recirculating lines to the storage tanks help to fix the fuels ratio at a steady value in the storage tanks. In this way, it is possible to control the fuels ratio in the mixture flowing from the storage tanks to the centrifuge. However, a mixer installed in the storage tanks can lead to more complex design and refitting. A study on the usage of sensors can help understand whether the mixer installation in the storage tanks can be obviated, while the fuels ratio in the fed mixture entering the separator can be controlled via a feedback loop.

Lastly, in the previous section, the inclusion of EN 590 diesel was suggested to be studied in a mixture with HVO or methanol. EN 590 diesel is the heavy fuel in a mixture with HVO or methanol, while methanol can have a higher density than HVO [35, 41]. Hence, depending on the mixed fuels in the storage tanks, methanol and EN 590 diesel can come out as heavy or light liquids from the centrifugal separator. Thus, it is suggested to research the possibility of manually switching the connections of the separator outlet channels when bunkering. However, a highly sensitive system prone to human errors might restrict the yacht's operation to either EN 590 or HVO. The usage of dedicated separators might overcome this challenge.

8.4. Separator integration in the multi-fuel system

This section covers discussions on conclusions drawn in chapter 6. Related indications for further work are also presented.

The results were generated for a set of variables constituting separator design parameters. Nevertheless, the number of discs and the vertical distance between them were kept constant as they do not impact the interface position with the used formulation. It is recommended to vary the discs' vertical distance to assess its influence on the droplets' coalescence time and thus the separator starting time. A further check can be done on the number of discs, which varies the volume flow of the entering mixture within each discs' section.

Furthermore, given the methanol low flash-point, a centrifuge blanketing system can be considered to mitigate flammability risks. No safety considerations were presented in this study. However, safety is a vital aspect of the design. Similar considerations can be extended to other components of the multi-fuel system, namely tanks and fuel lines.

Lastly, in the previous sections tests on the centrifugal separator and engines were recommended to respectively validate the mathematical model and define acceptable fuel contamination limits in engines. If the tests on the centrifuge reveal traces of HVO/methanol in methanol/HVO in concentration levels non-accepted by engines, a radical change of the fuel separation treatment approach is needed. Bladder tanks installed in conventional storage tanks are recommended to be researched. The storage of one fuel can be done in a flexible container assuming a pre-designed shape while at full capacity. Simultaneously, the remaining space around the bladder tank can be occupied by the other fuel. In this way, the outer layer of the bladder tank serves as a demarcation, preventing the intermixing of the two fuels. Independent fuel lines shall be installed to pump the desired fuel in/out of the storage tanks. Alternatively, a tanks-cleaning system can be investigated. Guidelines to the yacht's operators shall be defined in this respect.

Personal reflections

This work was opened with a quote from Christiana Figueres, Executive Secretary of the United Nations Framework Convention on Climate Change (UNFCCC) from 2010 to 2016, who led the climate change negotiations which yielded the Paris Agreement. In 2014 C. Figueres, speaking to reporters, said :

"We will move to a low-carbon world because nature will force us, or because policy will guide us. If we wait until nature forces us, the cost will be astronomical."

From this statement, the role of politics is evident in tackling climate change. Nevertheless, the word "policy" must not be entirely confined to its conventional political connotation but should be defined within diverse contexts. In the maritime industry, the imperative task of decarbonizing the shipping sector necessitates concerted efforts from various stakeholders. Given the global scope of the maritime domain, it is incumbent upon governments to collaborate harmoniously to ensure the availability of alternative fuels on a large scale. This becomes particularly vital due to the inherent challenges associated with this endeavour, where the implementation of a multi-fuel system has been explored to not undermine the yacht's operations. Nevertheless, the developments of certain technologies and policies constraints the full usage of the studied alternative fuels, in a scenario wherein conceptual research on the impact of alternative fuels usage on the ship design has been extensively performed.

The conclusions and recommendations derived in this work, highlight the role of regulatory bodies and systems manufacturers. The research lacks information on dual-fuel engines for HVO and methanol usage. Notably, there is a gap in the available information concerning dual-fuel engines for the use of hydrotreated vegetable oil (HVO) and methanol. Specifically, the sensitivity of dual-fuel engines to the utilization of non-pure fuels remains poorly understood. This knowledge gap influences the confidence levels in decision-making strategies and engineering design processes. Similar considerations apply to fuel cell technologies, wherein power conversion systems manufacturers are urged to conduct rigorous testing and maintain their technological developments at a brisk pace. The outcomes of these tests assume fundamental importance in facilitating the establishment of standards for alternative fuels' quality. Regulatory bodies should cooperatively work with engineers and manufacturers to release standards on alternative fuels' quality. The standards should refer to both single and multi-fuel blends since a single fuel cannot be identified as the only solution to the decarbonisation of the shipping sector.

The 40% CO_2 reduction target by 2030 set by the IMO is clear. Nevertheless, the absence of the aforementioned critical information presents substantial challenges to the design of new vessels and the retrofitting of existing diesel-powered ships, potentially leading to an undesirable scenario within the decarbonization timeline. However, regulatory bodies and systems manufacturers can overturn this situation by being the "policy" guiding the new generation ship designs towards sustainability.

References

[1] Feadship. *Obsidian: Feadship's first delivery of 2023 raises the bar on carbon reduction*. July 2023. URL: https://www.feadship.nl/press/obsidian-feadships-first-delivery-of-2023-raises-the-bar-on-carbon-reduction (visited on 09/06/2023).

[2] P. Friedlingstein et al. "Global Carbon Budget 2022". In: *EARTH SYSTEM SCIENCE DATA* 14.11 (2022). JRC131176, pp. 4811–4900. ISSN: 1866-3508. DOI: http://dx.doi.org/10.5194/essd-14-4811-2022.

[3] Collins M. et al. "Long-term Climate Change: Projections, Commitments and Irreversibility". In: *Climate Change 2013: The Physical Science Basis. Contribution of Working Group I to the Fifth Assessment Report of the Intergovernmental Panel on Climate Change* (2013). Cambridge University Press, Cambridge, United Kingdom and New York, NY, USA.

[4] *Paris Agreement*. UNFCCC, 2015.

[5] European Commission. *Reducing emissions from the shipping sector*. n.a. URL: https://ec.europa.eu/clima/eu-action/transport-emissions/reducing-emissions-shipping-sector (visited on 04/15/2023).

[6] Kries Maarten J.W. "A Methanol impact tool for yachts, assessing the impact of using methanol as an alternative fuel on the design, emissions and costs of yachts". MA thesis. Delft University of Technology, 2021.

[7] IMO. *Revised GHG reduction strategy for global shipping adopted*. 2023. URL: https://www.imo.org/en/MediaCentre/PressBriefings/Pages/Revised-GHG-reduction-strategy-for-global-shipping-adopted-.aspx (visited on 08/22/2023).

[8] *Report of the Marine Environment Protection Committee on its seventy-eight session*. IMO, June 2022.

[9] Cozijnsen E.J. "The footprint of yacht production: Defining a framework for the Yacht Environmental Transparency Index". MA thesis. Delft University of Technology, 2019.

[10] Siepmann T. "Integrating Large-Scale Hydrogen Storage on Superyachts: A Feasibility Analysis and Concept Study". MA thesis. Chalmers University of Technology, 2019.

[11] Lambregts T.R.L. "Fuel-Flexibility, Fuel-flexible fuel cell systems for super yachts". MA thesis. Delft University of Technology, 2021.

[12] SuperYacht Times. *Feadship announces in-build hydrogen fuel-cell superyacht*. Apr. 2023. URL: https://www.superyachttimes.com/yacht-news/feadship-hydrogen-yacht (visited on 04/14/2023).

[13] van der Vliet N.M. "Green Refits: Reducing yacht operational emissions through refitting". MA thesis. Delft University of Technology, 2021.

[14] Visser B.C.W. "The Plug-in Hybrid Electric Superyacht: An operational data-driven design". MA thesis. Delft University of Technology, 2021.

[15] *green maritime methanol - groene maritieme methanol*. n.a. URL: http://greenmaritimemethanol.nl/ (visited on 08/16/2023).

[16] Methanol Institute. *Ports with Available Methanol Storage Capacity*. n.a. URL: https://www.methanol.org/marine/ (visited on 02/21/2023).

[17] Feadship. *Roadmap to ZERO - Feadship achieves major milestone on roadmap towards carbon neutrality*. 2022. URL: https://www.feadship.nl/press/roadmap-to-zero (visited on 04/15/2023).

[18] ABS. *Marine Fuel Oil Advisory*. American Bureau of Shipping, 2021.

[19] H. David McGeorge. *Marine Auxiliary Machinery*. Oxford: Elsevier, 1998. ISBN: 0 7506 4398 6.

[20] David Albert Taylor. *Introduction to marine engineering*. Oxford: Elsevier, 1996. ISBN: 0 7506 2530 9.

[21] J., Harmsen and P., Hart. *Green Maritime Methanol: Towards A Zero Emission Shipping Industry*. Green Maritime Methanol, 2021.

[22] J. Souza Rosa et al. "Dual fuel ethanol port injection in a compression ignition diesel engine: Technical analysis, environmental behavior, and economic viability". In: *Journal of Cleaner Production* 308.127396 (2021). ISSN: 0959-6526. DOI: https://doi.org/10.1016/j.jclepro.2021.127396.

[23] J. Dierickx et al. "Performance and emissions of a high-speed marine dual-fuel engine operating with methanol-water blends as a fuel". In: *Fuel* 333.1 (2023). ISSN: 0016-2361. DOI: https://doi.org/10.1016/j.fuel.2022.126349.

[24] Tol R.S. "Combustion of methanol/diesel blends in compression ignited engine: Research into the effects of methanol/diesel blends on the performance and emissions of a diesel engine based on experiments and simulations". MA thesis. Delft University of Technology, 2020.

[25] *Methanol fuel and methanol fuel additives*. United States patent. Mar. 1983. URL: https://patents.google.com/patent/US4375360A/en (visited on 04/28/2023).

[26] R.M. Estefan and J.G. Brown. "Evaluation of Possible Methanol Fuel Additives for Reducing Engine Wear and/or Corrosion". In: *Section 4: JOURNAL OF FUELS & LUBRICANTS* 99.4 (1990), pp. 942–964. DOI: https://doi.org/10.4271/902153.

[27] C. S. Cheung et al. "Investigation on the Effect of Port-Injected Methanol on the Performance and Emissions of a Diesel Engine at Different Engine Speeds". In: *Energy Fuels* 23.11 (2009), pp. 5684–5694. DOI: https://doi.org/10.1021/ef9005516.

[28] C.A. Farina, G. Faita, and F. Olivani. "Electrochemical behaviour of iron in methanol and dimethylformamide solutions". In: *Corrosion Science* 18.5 (1978), pp. 465–479. ISSN: 0010-938X. DOI: https://doi.org/10.1016/S0010-938X(78)80040-7.

[29] B. H. West et al. "Federal Methanol Fleet Project Final Report". In: (1993). No. ORNL-TM-12278. Oak Ridge National Lab., TN (United States).

[30] B. West and R. McGill. "Oil Performance in a Methanol-Fueled Vehicle Used in Severe Short-Trip Service". In: (1992). SAE Technical Paper 922298.

[31] K. Otto et al. "Steel Corrosion by Methanol Combustion Products: Enhancement and Inhibition". In: *FUELS AND LUBRICANTS* 95.6 (1986). SAE Technical Paper 861590, pp. 1034–1043. ISSN: 2688-3627. DOI: https://doi.org/10.4271/861590.

[32] A. Datta, S. Dutta, and B.K. Mandal. "Effect of Methanol Addition to Diesel on the Performance and Emission Characteristics of a CI Engine". In: *Journal of Basic and Applied Engineering Research* 1.3 (Oct. 2014), pp. 8–13. ISSN: 2350-0077. URL: http://www.krishisanskriti.org/jbaer.html.

[33] A. Datta and B.K. Mandal. "Effect of alcohol addition to diesel on engine performance, combustion and emission characteristics of a CI engine". In: *2017 International Conference on Advances in Mechanical, Industrial, Automation and Management Systems (AMIAMS), Allahabad, India* (2017), pp. 110–114. DOI: 10.1109/AMIAMS.2017.8069198.

[34] D.S. Shukla, A.K. Gondal, and P.C. Nautiyal. "Effect of methanol fuel contaminants in crankcase oils on wear". In: *Wear* 157.2 (1992), pp. 371–380. ISSN: 0043-1648. DOI: https://doi.org/10.1016/0043-1648(92)90073-H.

[35] J. Ellis and K. Tanneberger. *Study on the use of ethyl and methyl alcohol as alternative fuels in shipping*. EMSA, SSPA, 2015. URL: https://emsa.europa.eu/air-pollution/alternative-fuels/items.html?cid=329&id=2726.

[36] H. Hazar and I. Temizer. "The Engine Performance of a Diesel Engine and the Research of the Effect of Fuel Additives on Engine Oil and Engine Parts". In: *Scientific Bulletin of the "Petru Maior" University of Tîrgu Mureș* 9(XXVI).2 (2012), pp. 50–57. ISSN: 2285-438X. URL: http://scientificbulletin.upm.ro/.

[37] P.C. Nautiyal, A.K. Gondal, and D. Kumar. "Wear and lubrication characteristics of a methanol-fuelled compression ignition engine — A comparison with pure diesel and bifuel operation". In: *Wear* 135.1 (1989), pp. 67–78. ISSN: 0043-1648. URL: https://doi.org/10.1016/0043-1648(89)90096-3.

[38] Alfa Laval. *Fuel handling in Emission Controlled Areas*. Alfa Laval.

[39] LibreTexts Chemistry. *5.3: Polarity and Intermolecular Forces*. 2020. URL: https://chem.libretexts.org/Courses/University_of_Kentucky/UK%5C%3A_CHE_103_-_Chemistry_for_Allied_Health_(Soult)/Chapters/Chapter_5%5C%3A_Properties_of_Compounds/5.3%5C%3A_Polarity_and_Intermolecular_Forces (visited on 02/27/2023).

[40] John D. Roberts, Ross Stewart, and Marjorie C. Caserio. *Organic chemistry: Methane to macromolecules*. New York: W. A. Benjamin, INC., 1971. ISBN: 8053-8332-8.

[41] Neste. *Neste Renewable Diesel Handbook*. Espoo: Neste Proprietary publication, Oct. 2020.

[42] M. Lapuerta et al. "Molecular interactions in blends of alcohols with diesel fuels: Effect on stability and distillation". In: *Fuel* 139 (2015), pp. 171–179. ISSN: 0016-2361. DOI: https://doi.org/10.1016/j.fuel.2014.08.055.

[43] R.W. Kiser, G.D. Johnson, and M.D. Shetlar. "Solubilities of Various Hydrocarbons in Methanol". In: *Journal of Chemical and Engineering Data* 6.3 (1961), pp. 388–341. DOI: https://doi.org/10.1021/je00103a009.

[44] R. Privat, J.-N. Jaubert, and M. Molière. "The thermodynamics of alcohols-hydrocarbons mixtures". In: *MATEC Web of Conferences* 3 (2013), p. 01018. URL: https://doi.org/10.1051/matecconf/20130301018.

[45] L. Sorsamäki and M. Nappa. *Design and selection of separation processes*. VTT Research report. VTT, Dec. 2015.

[46] A. De Haan, H. B. Eral, and B. Schuur. *Industrial Separation Processes: Fundamentals*. Berlin: Boston: De Gruyter, 2020. URL: https://doi.org/10.1515/9783110654806.

[47] ECHA. *Chemicals regulated substances*. n.a. URL: https://www.echa.europa.eu/ (visited on 08/18/2023).

[48] D. W. Green and R. H. Perry. *Perry's Chemical Engineers' Handbook*. 8th ed. McGraw-Hill, 2008.

[49] A. Mersmann, M. Kind, and J. Stichlmair. *Thermal Separation Technology: Principles, Methods, Process Design*. Springer, 2011. ISBN: 978-3-642-12524-9. DOI: 10.1007/978-3-642-12525-6.

[50] N. P. Cheremisinoff. *Industrial Solvents Handbook*. 2nd ed. Marcel Deker, Inc., 2003. ISBN: 0-8247-4033-5.

[51] C.M. Hansen. "The Universality of the Solubility Parameter". In: *Industrial & engineering chemistry product research and development* 8.1 (1969), pp. 2–11. DOI: https://doi.org/10.1021/i360029a002.

[52] n.a. *Surface tension values of some common test liquids for surface energy analysis*. n.a. URL: http://www.surface-tension.de/ (visited on 04/03/2023).

[53] Micro Care. *How Does the Surface Tension of a Solvent Affect My Cleaning Results?* n.a. URL: https://www.microcare.com/en-US/Resources/Resource-Center/FAQs/How-Does-the-Surface-Tension-of-a-Solvent-Affect-M (visited on 04/03/2023).

[54] J. D. Seader, E. J. Henley, and D. K. Roper. *Separation Process Principles: Chemical and Biochemical Operations*. 3rd ed. United States of America: John Wiley & Sons, Inc., 2011. ISBN: 978-0-470-48183-7.

[55] G. Puxty, W. Conway, and P.H.M. Feron. "4 - Liquid absorbent selection criteria and screening procedures". In: *Absorption-Based Post-combustion Capture of Carbon Dioxide* (2016). Ed. by P. H.M. Feron, pp. 69–100. DOI: https://doi.org/10.1016/B978-0-08-100514-9.00004-4.

[56] R. W. Rosseau. *handbook of Separation Process Technology*. New York, Chichester, Brisbane, Toronto, Singapore: John Wiley & Sons, Inc., 1987. ISBN: 0-471-89558-X.

[57] R. Patiño-Camino et al. "Surface tension of diesel-alcohol blends: Selection among fundamental and empirical models". In: *Fluid Phase Equilibria* 555 (2022), p. 113363. ISSN: 0378-3812. DOI: https://doi.org/10.1016/j.fluid.2021.113363.

[58] Engineering ToolBox. *Methanol - Dynamic and Kinematic Viscosity vs. Temperature and Pressure*. 2018. URL: https://www.engineeringtoolbox.com/methanol-dynamic-kinematic-viscosity-temperature-pressure-d_2093.html?vA=40&degree=C# (visited on 04/05/2023).

[59] *Biodiesel Production Techniques*. Food Technology Fact Sheet. FAPC-150. Robert M. Kerr Food & Agricultural Products Center, 2007.

[60] M. Kato et al. "Density behavior of alcohol-diesel fuel mixtures". In: *Journal of The Japan Petroleum Institute* 34.2 (1991), pp. 186–190.

[61] Monique B. Vermeire. *Everything you need to know about marine fuels*. Ghent, Belgium: Chevron Marine Products, 2021.

[62] T. Frising et al. "Contribution of the Sedimentation and Coalescence Mechanisms to the Separation of Concentrated Water-in-Oil Emulsions". In: *Journal of Dispersion Science and Technology* 29 (2008), pp. 827–834. ISSN: 0193-2691. DOI: 10.1080/01932690701781501.

[63] P. Bol et al. "The Kinetics of Droplet Sedimentation in Liquid-Liquid Extraction". In: *Chemie Ingenieur Technik* (2020). DOI: 10.1002/cite.202000126.

[64] M. Ishii and N. Zuber. "Drag coefficient and relative velocity in bubbly, droplet or particulate flows". In: *Aiche Journal* (1979), pp. 843–855. ISSN: 0009-2509. DOI: https://doi.org/10.1016/0009-2509(54)85015-9.

[65] J.F. Richardson and W.N. Zaki. "The sedimentation of a suspension of uniform spheres under conditions of viscous flow". In: *Chemical Engineering Science* 3.2 (1954), pp. 65–73. ISSN: 0009-2509. DOI: https://doi.org/10.1016/0009-2509(54)85015-9.

[66] P. D. Komar and C. E. Reimers. "Grain Shape Effect On Settling Rates". In: *The Journal of Geology* 86.2 (1978), pp. 193–202. DOI: http://www.jstor.org/stable/30060800.

[67] S.Dey, S. Z. Ali, and E. Padhi. "Terminal fall velocity: the legacy of Stokes from the perspective of fluvial hydraulics". In: *Proc. R. Soc. A.* 475 (2019). DOI: http://dx.doi.org/10.1098/rspa.2019.027.

[68] J. Kamp, J. Villwock, and M. Kraume. "Drop coalescence in technical liquid/liquid applications: a review on experimental techniques and modeling approaches". In: *Reviews in Chemical Engineering* (2016). DOI: https://doi.org/10.1515/revce-2015-0071.

[69] G. V. Jeffreys and G. A. Davies. "CHAPTER 14 - Coalescence of Liquid Droplets and Liquid Dispersion". In: *Recent Advances in Liquid–Liquid Extraction* (1971), pp. 495–584. DOI: https://doi.org/10.1016/B978-0-08-015682-8.50018-3.

[70] R. M. Wellek, A. K. Agrawal, and A. H. P. Skelland. "Shape of liquid drops moving in liquid media". In: *Aiche Journal* 12 (1966), pp. 854–862.

[71] C.A. Coulaloglou and L.L. Tavlarides. "Description of interaction processes in agitated liquid-liquid dispersions". In: *Chemical Engineering Science* 32.11 (1977), pp. 1289–1297. ISSN: 0009-250. DOI: https://doi.org/10.1016/0009-2509(77)85023-9.

[72] W.J. Howarth. "Coalescence of drops in a turbulent flow field". In: *Chemical Engineering Science* 19.1 (1964), pp. 33–38. ISSN: 0009-2509. DOI: https://doi.org/10.1016/0009-2509(64)85003-X.

[73] H. Sovová. "Breakage and coalescence of drops in a batch stirred vessel—II comparison of model and experiments". In: *Chemical Engineering Science* 39.9 (1981), pp. 1567–1573. ISSN: 0009-2509. DOI: https://doi.org/10.1016/0009-2509(81)85117-2.

[74] Roland Clift, John R. Grace, and Martin E. Weber. *Bubbles, drops, and particles*. London: Courier Corporation, 2005.

[75] L. A. Girifalco and R. J. Good. "A Theory for the Estimation of Surface and Interfacial Energies. I. Derivation and Application to Interfacial Tension". In: *The Journal of Physical Chemistry* 61.7 (1957), pp. 904–909. DOI: https://doi.org/10.1021/j150553a013.

[76] G. Towler and R. Sinnott. "Chapter 16 - Separation of Fluids". In: *Chemical Engineering Design (Second Edition)* (2013). Ed. by G. Towler and Ray Sinnott, pp. 753–806. ISSN: 0378-3812. DOI: https://doi.org/10.1016/B978-0-08-096659-5.00016-X.

[77] G. Towler and R. Sinnott. "Chapter 18 - Specification and Design of Solids-Handling Equipment". In: *Chemical Engineering Design (Second Edition)* (2013). Ed. by G. Towler and Ray Sinnott, pp. 937–1046. ISSN: 0378-3812. DOI: https://doi.org/10.1016/B978-0-08-096659-5.00018-3.

[78] R. Plat. *Gravitational and centrifugal oil-water separators with plate pack internals*. Delft University of Technology. 1994.

[79] Alessandro Di Pretoro and Flavio Manenti. *Non-conventional Unit Operations: Solving Practical Issues*. Gewerbestrasse 11, 6330 Cham, Switzerland: PoliMI SpringerBriefs, 2020. ISBN: 978-3-030-34571-6. URL: https://doi.org/10.1007/978-3-030-34572-3.

[80] *FLOTTWEG SEPARATION TECHNOLOGY FOR THE PRODUCTION OF BIODIESEL*. 84137 Vilsbiburg - Deutschland (Germany): Flottweg SE.

[81] Dolphin Centrifuge. *Disadvantages of a Disc-Stack Centrifuge | Illustrated Guide*. 2020. URL: https://dolphincentrifuge.com/disadvantages-disc-stack-centrifuge/ (visited on 07/04/2023).

[82] T. Santos, J.F. Gomes, and J. Puna. "Liquid-liquid equilibrium for ternary system containing biodiesel, methanol and water". In: *Journal of Environmental Chemical Engineering* 6.1 (2018), pp. 984–990. DOI: https://doi.org/10.1016/j.jece.2017.12.068.

[83] H. Le Ferrand et al. "Time-Resolved Observations of Liquid–Liquid Phase Separation at the Nanoscale Using in Situ Liquid Transmission Electron Microscopy". In: *Journal Of The American Chemical Society* 141 (2019), pp. 7202–7210. DOI: https://doi.org/10.1021/jacs.9b03083.

[84] H. Le Ferrand et al. "Time-Resolved Observations of Liquid–Liquid Phase Separation at the Nanoscale Using in Situ Liquid Transmission Electron Microscopy". In: *Journal Of The American Chemical Society* 141 (2019), pp. 7202–7210. DOI: https://doi.org/10.1021/jacs.9b03083.

[85] X. Zhang et al. “Study liquid-liquid phase separation with optical microscopy: A methodology review”. In: *APL Bioengineering* 7.2 (2023). DOI: https://doi.org/10.1063\%2F5.0137008.

[86] Doetjes G. *Het bepalen van een geschikte emulgator om F76 en methanol gemengd te houden*. 2020.

[87] M. Fossen, M. A. Pasqualette, and J. N. E. Carneiro. “Phase Transitions and Separation Time Scales of CO_2Crude Oil Fluid Systems: Wheel Flow Loop Experiments and Modeling”. In: *Energy & Fuels* 34.6 (2020), pp. 7340–7352. DOI: 10.1021/acs.energyfuels.0c00818.

[88] H.P. Greenspan. “On centrifugal separation of a mixture”. In: *Journal of Fluid Mechanics* 127 (Feb. 1983), pp. 91–101. DOI: https://doi.org/10.1017/S0022112083002633.

[89] U. Schaflinger and H. Stibi. “On centrifugal separation of suspensions in cylindrical vessels”. In: *Acta Mechanica* 67 (May 1987), pp. 163–181. DOI: https://doi.org/10.1007/BF01182130.

[90] U. Schaflinger, A. Köppl, and G. Filipczak. “Sedimentation in cylindrical centrifuges with compartments”. In: *Ing. arch* 56 (Nov. 1986), pp. 321–331. DOI: https://doi.org/10.1007/BF02570612.

[91] Marius Ungarish. “Side wall effects in centrifugal separation of mixtures”. In: *Physics of Fluids A: Fluid Dynamics* 1 (May 1989), pp. 810–818. URL: https://doi.org/10.1063/1.857378.

[92] F. Perazzolo Disconzi and F. Torres Borghi. “Modeling, simulation, and optimization of the centrifugal separation of a microalgae-culture medium mixture”. In: *Biomass and Bioenergy* 143.105871 (Feb. 2020). ISSN: 0961-9534. DOI: https://doi.org/10.1016/j.biombioe.2020.105871.

[93] Christopher Earls Brennen. *Fundamentals of multiphase flow*. 2005. ISBN: 0521 848040.

[94] GEA Westfalia Separator Group GmbH. *Marine System Technology: Concepts and High Performance Equipment for the Engine Room GEA Westfalia Separator*. n.a. URL: https://www.gea.com/en/binaries/BRO-MA-Marine%5C%20System%5C%20Technology-2012-08-EN_tcm11-23607.pdf (visited on 12/06/2023).

[95] J.P. van der Linden. *Liquid-liquid separation in Disc-Stack Centrifuges*. TR Diss 1525, Delft University of Technology. 1987.

[96] Wärtsilä. *Wärtsilä 34DF - Product Guide*. 2022. URL: https://www.wartsila.com/docs/default-source/product-files/engines/df-engine/w34df-product-guide.pdf?sfvrsn=5116cb45_23 (visited on 01/31/2023).

[97] A. Otsuka et al. “Evaluation of Separation Efficiency of Fuel Oil Treatment Systems for Fluid Catalyst Cracking Particles Onboard Actual Vessels”. In: *Journal of the JIME* 45 (2010), pp. 87–90.

[98] N. Kharoua L., Khezzar, and Z. Nemouchi. “Hydrocyclones for De-oiling Applications—A Review”. In: *Petroleum Science and Technology* 28.7 (2010), pp. 738–755. DOI: https://doi.org/10.1080/10916460902804721.

[99] C. Ambler. “The evaluation of centrifuge performance”. In: *Chemical Engineering Progress* 48 (Feb. 1952), pp. 150–158.

[100] *Westfalia Separator Mineraloil Systems GmbH*. GEA Westfalia.

[101] Alfa Laval. *High-capacity disc stack centrifuge for biodiesel production*. n.a. URL: https://www.alfalaval.com/globalassets/documents/products/separation/centrifugal-separators/disc-stack-separators/bd_95.pdf (visited on 06/12/2023).

[102] Alfa Laval. *Different separation technologies*. n.a. URL: https://www.alfalaval.com/products/separation/centrifugal-separators/separators/innovations/separator-innovator/how-separation-works/different-separation-technologies/ (visited on 06/12/2023).

[103] *MENENS Yacht Future Use Case*. Feadship, De Voogt Naval Architects B.V., Mar. 2023.

[104] *Lloyd's Register Rulefinder 2023*. Lloyd's Register Group Limited, 2023. URL: https://www.lr.org/en/rulefinder/ (visited on 02/24/2023).

[105] *SOLAS 2018 - Consolidated Edition*. London: IMO, 2018.

[106] *C32B Engine Specifications*. Pon Power BV, Mar. 2023.

[107] *C32 Marine Generator Set*. Caterpillar, 2017.

[108] Hans Klein Woud and Douwe Stapersma. *Design of Propulsion and electric generation system*. London: IMarEST - The Institute of Marine Engineering, Science and Technology, 2003. ISBN: 1-902536-47-9.

[109] Jeroen Dierickx et al. "Retrofitting a high-speed marine engine to dual-fuel methanol-diesel operation: A comparison of multiple and single point methanol port injection". In: *Fuel Communications* 7 (2021), p. 100010. ISSN: 2666-0520. DOI: https://doi.org/10.1016/j.jfueco.2021.100010.

[110] M. Balat and H. Balat. "Progress in biodiesel processing". In: *Applied Energy* 87.6 (2010), pp. 1815–1835. ISSN: 0306-2619. DOI: https://doi.org/10.1016/j.apenergy.2010.01.012.

[111] Joshua Wilde. *Constrained Optimization*. Aug. 2013.

[112] *GEA Westfalia Separator OTC 2-02-137/OTC 3-02-137. Technical Data: Continuous treatment of fuel and lube oils, hydraulic, diesel, turbine and waste oils*. GEA Westfalia, n.a.

[113] Jacek Majewski. *Measurement techniques concerning droplet size distribution of electrosprayed water*. Przegld Elektrotechniczny, 2013.

[114] Det Norske Veritas Germanischer Lloyd AS Maritime, Høvik, Norway. *Comparison of Alternative Marine Fuels*. July 2019. URL: https://safety4sea.com/wp-content/uploads/2019/09/SEA-LNG-DNV-GL-%20Comparison-of-Alternative-Marine-Fuels-2019_09.pdf (visited on 01/11/2023).

[115] Karin van Kranenburg et al. "E-fuels: towards a more sustainable future for truck transport, shipping and aviation". In: *Production Engineering* (July 2020). URL: http://resolver.tudelft.nl/uuid:487a6a47-853d-4a1d-bc2e-dbe21d584cca.

[116] S. Barber et al. *Hazard Classification and Labelling of Petroleum Substances in the European Economic Area – 2020*. Report no. 22/20. Brussels: Concawe, Oct. 2020.

[117] European Chemical Agency. *Annex I: Classification and Labelling Requirements for Hazardous Substances and Mixture*. n.a. URL: https://reachonline.eu/clp/en/title-i.html (visited on 01/30/2023).

[118] International Union of Pure and Applied Chemistry. *Compendium of Chemical Terminology - Gold Book*. IUPAC Compendium of Chemical Terminology, Aug. 2012.

[119] Canadian Centre for Occupational Health and Safety. *What is a LD_{50} and LC_{50}?* Nov. 2018. URL: https://www.ccohs.ca/oshanswers/chemicals/ld50.html (visited on 01/30/2023).

[120] Horizon Europe NCP. *TRL Assessment*. n.a. URL: https://horizoneuropencpportal.eu/store/trl-assessment (visited on 02/02/2023).

[121] *Directive (EU) 2918/2001 of the European Parliament and of the Council of 11 December 2018 on the promotion of the use of energy from renewable sources (recast)*. Directive. European Union, Dec. 2018. URL: https://eur-lex.europa.eu/legal-content/EN/TXT/?uri=uriserv:OJ.L_.2018.328.01.0082.01.ENG&toc=OJ:L:2018:328:TOC.

[122] *Adoption of the International Code of Safety for Ships Using Gases or Other Low-Flashpoint Fuels (IGF Code)*. Resolution MSC.391(95). IMO, June 2015.

[123] *MSC.1/Circular.1455 - Guidelines for the Approval of Alternatives and Equivalents as Provided for in Various IMO Instruments*. Satutory Document. IMO, June 2013. URL: https://www.imorules.com/MSCCIRC_1455.html (visited on 02/16/2023).

[124] *Adoption of the International Code for the Construction and Equipment of Ships Carrying Liquefied Gases In Bulk (IGC Code)*. Resolution MSC.5(48). IMO, June 1983.

[125] Dagmar Nelissen et al. *Availability and costs of liquefied bio- and synthetic methane: The maritime shipping perspective*. Delft: CE Delft, Mar. 2020.

[126] George Nikolaou et al. *LPG for Marine Engines: The Marine Alternative Fuel. Commercial, Passenger, Offshore Boats/Ships, Recreational Crafts and Other Boats*. 182 avenue Charles de Gaulle, 92200 Neuilly-sur-seine, France: WLPGA, Feb. 2018.

[127] IEA-AMF. *Dimethyl ether (DME)*. n.a. URL: https://www.iea-amf.org/content/fuel_information/dme (visited on 01/27/2023).

[128] Dräger. *Gas Dispersion*. Technical report. Germany, 2011.

[129] Alfa Laval. *Marine biofuels: what to expect in the 2020s*. Alfa Laval, Apr. 2021. ISBN: 100003528-2-EN 2103.

[130] DNV GL. *Using Biodiesel In Marine Diesel Engines: New Fuels, New Challenges*. Technical Regulatory News No.21/2020 - Statutory. Brooktorkai 18, 20457 Hamburg, Germany: DNV GL, Oct. 2020.

[131] A. Lappas and E. Heracleous. "19 - Production of biofuels via Fischer-Tropsch synthesis: biomass-to-liquids". In: *Woodhead Publishing Series in Energy* (2011). Ed. by R. Luque, J. Campelo, and J. Clark, pp. 493–529. DOI: https://doi.org/10.1533/9780857090492.3.493.

[132] ABS. *ABS Regulatory News: MARPOL Annex VI - Biofuels As Marine Fuels*. No.06/2022. 1701 City Plaza Drive | Spring, TX 77389 USA: American Bureau of Shipping, Oct. 2022.

[133] IRENA. *A pathway to decarbonise the shipping sector by 2050, International Renewable Energy Agency*. Abu Dhabi, 2021. ISBN: 978-92-9260-330-4.

[134] H. Aatola et al. "Hydrotreated Vegetable Oil (HVO) as a Renewable Diesel Fuel: Trade-off between NOx, Particulate Emission, and Fuel Consumption of a Heavy Duty Engine". In: *SAE International* (Jan. 2008).

[135] Greenergy. *Safety Data Sheet: HVO - EC 700-571-2*. Greenergy, July 2021.

[136] *Fact sheet n°6: Drop-in fuels*. Fact sheet. DST - Development Centre for Ship Technology and transport Systems, Oststraße 77, 47057 Duisburg, Germany: Interreg, Jan. 2020.

[137] Yuanrong Zhou et al. *The potential of liquid biofuels in reducing ship emissions*. International Council on Clean Transportation, Sept. 2020.

[138] Statista. *HVO biodiesel production volume worldwide from 2014 to 2021*. 2023. URL: https://www.statista.com/statistics/1297290/hvo-biodiesel-production-worldwide/#:~:text=Global%5C%20production%5C%20of%5C%20HVO%5C%20biodiesel,million%5C%20metric%5C%20tons%5C%20in%5C%202021. (visited on 02/22/2023).

[139] SGS Inspire. *Europe: Pure HVO available in nine European countries*. 2021. URL: https://inspire.sgs.com/news/102941/europe--pure-hvo-available-in-nine-european-countries (visited on 02/22/2023).

[140] OFI. *HVO making it big: Oils & Fats International*. 2018. URL: https://www.ofimagazine.com/content-images/news/HVO2.pdf (visited on 02/22/2023).

[141] ENI. *Circular economy in our high-quality advanced biofuels: The Venice and Gela biorefineries represent Eni's commitment to the path towards decarbonisation*. n.a. URL: https://www.eni.com/en-IT/operations/energy-evolution/biorefineries.html (visited on 02/22/2023).

[142] Total Energies. *La Mède: A Multipurpose Facility for the Energies of Tomorrow*. 2023. URL: https://totalenergies.com/energy-expertise/projects/bioenergies/la-mede-a-forward-looking-facility (visited on 02/22/2023).

[143] Total Energies. *A Renewable Fuel For a Low-Carbon World*. 2021. URL: https://www.diamondgreendiesel.com/ (visited on 02/22/2023).

[144] Neste. *Rotterdam refinery - Neste*. n.a. URL: https://www.neste.com/about-neste/who-we-are/production/rotterdam#db5c381b (visited on 02/22/2023).

[145] Cespa. *Cespa to invest up to 5 billion euros and create 170,000 jobs in Andalusia to lead the energy transition*. 2022. URL: https://www.cepsa.com/en/press/cepsa-will-invest-up-to-5-billion-euros-and-create-17000-jobs (visited on 02/22/2023).

[146] Greenea. *Is HVO the Holy Grail of the world biodiesel market?* 2014. URL: http://www.greenea.com/publication/is-hvo-the-holy-grail-of-the-world-biodiesel-market/ (visited on 02/22/2023).

[147] *Commission delegated regulation (EU) 2019/807*. Regulation. European Union, Mar. 2019. URL: https://eur-lex.europa.eu/legal-content/EN/TXT/?uri=uriserv:OJ.L_.2019.133.01.0001.01.ENG.

[148] L. Marelli et al. "The impact of biofuels on transport and the environment, and their connection with agricultural development in Europe". In: (Feb. 2015). Ed. by Adrienn Borka. DOI: 10.2861/241119.

[149] R. Gonçalves dos Santos W. R. da Silva Trindade. "Review on the characteristics of butanol, its production and use as fuel in internal combustion engines". In: *Renewable and Sustainable Energy Reviews* 69 (2017), pp. 642–651. ISSN: 1364-0321. DOI: https://doi.org/10.1016/j.rser.2016.11.213.

[150] B. Rajesh Kumar and S. Saravanan. "Effect of iso-butanol addition to diesel fuel on performance and emissions of a DI diesel engine with exhaust gas recirculation". In: *Proceedings of the Institution of Mechanical Engineers, Part A: Journal of Power and Energy* 230.1 (Nov. 2015), pp. 112–125. DOI: https://doi.org/10.1177/0957650915617107.

[151] S. Verhelst et al. "Methanol as a fuel for internal combustion engines". In: *Progress in Energy and Combustion Science* 70 (2019), pp. 43–88. DOI: https://doi.org/10.1016/j.pecs.2018.10.001.

[152] MAN. *ME-LGI Engines: Liquid Gas Injection - methanol and LPG*. n.a. URL: https://mandieselturbo.com/docs/default-source/shopwaredocuments/me-lgi-engines.pdf?sfvrsn=2 (visited on 01/27/2023).

[153] Wärtsilä. *Wärtsilä 32 Methanol Engine*. n.a. URL: https://www.wartsila.com/marine/products/engines-and-generating-sets/wartsila-32-methanol-engine (visited on 02/16/2023).

[154] Y. Wang et al. "A review of low and zero carbon fuel technologies: Achieving ship carbon reduction targets". In: *Sustainable Energy Technologies and Assessments* 54.102762 (2022). ISSN: 2213-1388. DOI: https://doi.org/10.1016/j.seta.2022.102762.

[155] SFC Energy AG. *Direct Methanol Fuel Cell (DMFC)*. n.a. URL: https://www.sfc.com/en/technology/direct-methanol/ (visited on 02/16/2023).

[156] L. van Biert and K. Visser. "Chapter 3 - Fuel cells systems for sustainable ships". In: *Sustainable Energy Systems on Ships* (2022). Ed. by F. Baldi, A. Corradu, and M.E. Mondejar, pp. 81–121. DOI: https://doi.org/10.1016/B978-0-12-824471-5.00010-4.

[157] EPEA. *Pa-X-ell: Research on fuel cells*. n.a. URL: https://epea.com/en/refernces/pa-x-ell (visited on 02/16/2023).

[158] EPEA. *Methanol Fuel Cell Powered Passenger Ferry Sets Sail*. Aug. 2017. URL: https://maritime-executive.com/article/methanol-fuel-cell-powered-passenger-ferry-sets-sail (visited on 02/16/2023).

[159] Offshore Energy. *RiverCell consortium: Fuel cell unit passes safety testing*. Dec. 2021. URL: https://www.offshore-energy.biz/rivercell-fuel-cell-unit-passes-safety-testing/ (visited on 02/16/2023).

[160] European Commission. *Validation of renewable Methanol based Auxiliary Power System for commercial Vessels*. May 2022. URL: https://cordis.europa.eu/project/id/31414 (visited on 02/17/2023).

[161] European Commission. *Nautical Integrated Hybrid Energy System for Long-haul Cruise Ships*. Dec. 2022. URL: https://cordis.europa.eu/project/id/861647 (visited on 02/17/2023).

[162] ISO. *ISO/AWI 6583: Specification of methanol as a fuel for marine applications*. 2021. URL: https://www.iso.org/standard/82340.html (visited on 04/14/2023).

[163] ABS. *Methanol As Marine Fuel*. American Bureau of Shipping, 2021.

[164] P.S. van Lieshout et al. *Green Maritime Methanol: WP3 factsheet and comparison with diesel and LNG*. TNO report. Leeghwaterstraat 44, 2628 CA, Delft: TNO, Nov. 2020.

[165] *Methanol & Ethanol Fuelled Ships*. Rule note. 92937 Paris La Défense Cedex, France: Bureau Veritas, Aug. 2022.

[166] S. Brynolf, E. Fridell, and K. Andersson. "Environmental assessment of marine fuels: liquefied natural gas, liquefied biogas, methanol and bio-methanol". In: *Journal of Cleaner Production* 74 (2014), pp. 86–95. ISSN: 0959-6526. DOI: https://doi.org/10.1016/j.jclepro.2014.03.052.

[167] A. Martin. *A Step Forward For "Green" Methanol And Its Potential To Deliver Deep GHG Reductions In Maritime Shipping*. Sept. 2021. URL: https://theicct.org/a-step-forward-for-green-methanol-and-its-potential-to-deliver-deep-ghg-reductions-in-maritime-shipping%5C%E2%5C%80%5C%AF/ (visited on 02/13/2023).

[168] Mærsk Mc-Kinney Møller Center. *Maritime Decarbonization Strategy 2022*. Mærsk Mc-Kinney Møller Center, Dec. 2022. URL: https://www.zerocarbonshipping.com/publications/maritime-decarbonization-strategy/.

[169] DNV. *Maritime Forecast To 2050: Energy Transition Outlook 2022*. Germany, Hamburg: DNV, 2022.

[170] IEA, Paris. *Chemicals*. 2022. URL: https://www.iea.org/reports/chemicals (visited on 02/21/2023).

[171] IRENA AND METHANOL INSTITUTE. *Innovation Outlook : Renewable Methanol*. Abu Dhabi: International Renewable Energy Agency, 2021. ISBN: 978-92-9260-320-5.

[172] J. Harmsen et al. *Green Maritime Methanol: WP2 Initiation and Benchmark analysis*. TNO report. TNO, June 2020.

[173] Global Maritime Forum. *Methanol as a scalable zero emission fuel*. 2022. URL: https://www.globalmaritimeforum.org/news/methanol-as-a-scalable-zero-emission-fuel (visited on 02/21/2023).

[174] *Marine Distillate Fuel (DMA/DFA)*. Safety Data Sheet According to Regulation (EC) No. 1907/2006. visited on 01/30/2023. TOTAL, Dec. 2019. URL: https://marinefuels.totalenergies.com/sites/g/files/wompnd1851/f/atoms/files/marine_distillate_fuel_dma_dfa_mtr_eu_en.pdf.

[175] *Methanol: Properties and Uses*. SGS INSPIRE team, Mar. 2020.

[176] *IMPCA Methanol Reference Specifications*. Version 9. Brussels: IMPCA, June 2021.

[177] Joakim Sundnes. *Solving Ordinary Differential Equations in Python*. 2023.

[178] *Unified interpretations of regulations 1.24, 12, 27, 27 and 28.3.3 of MARPOL Annex I*. IMO, Dec. 2016. URL: https://www.register-iri.com/wp-content/uploads/MEPC.1-Circ.867.pdf (visited on 02/24/2023).

[179] Parker. *Marine Fuel Filter Water Separator – Racor Spin-on Series*. 2023. URL: https://ph.parker.com/nl/en/marine-fuel-filter-spin-on (visited on 04/28/2023).

[180] IndiaMART. *Alfa Laval MMPX 403 Oil Separator*. n.a. URL: https://www.indiamart.com/ops-india-enterprise/oil-separator.html (visited on 04/28/2023).

[181] G. Vittori and P. Blondeaux. *Note di idrodinamica*. Genova University Press, 2017.

A

A criteria-driven selection of alternative fuels

In the Feadship roadmap towards net zero global warming potential by 2030, HVO and methanol were selected. among all possible sustainable fuels. A criteria-driven approach was followed for the selection. In this chapter, the criteria are presented. Next, the main HVO and methanol properties are provided.

A.1. Criteria of selection

In this section, criteria are identified to pave the selection of alternative fuels. These criteria are chosen to consider their impact on the ship's fuel system, as well as their environmental footprint, maritime interest, and their level of the close-to-commercialisation state. The chosen criteria are listed below.

1. **Storage:** the physical properties of the fuel affect its storage. Particularly, the fuel phase influences the storage tank geometry [11, 114]. Cylindrical and insulated tanks are needed for cryogenic and pressurized fuels. On the contrary, non-cylindrical tanks can accommodate liquid fuels [115]. The fuel's tank options need to be evaluated relatively to a diesel storage configuration. Given the non-cylindrical shaped diesel tanks it is important to choose tanks of this type for the alternative fuel too. Considering that diesel will have to be bunkered until the alternative fuel becomes available on a large scale, it is not envisaged to replace prismatic diesel tanks with cylindrical ones. A cylindrical tank would in fact yield to higher unusable space on board. Hence, a non-cylindrical volume suitable for both fuels would enhance built-in flexibility.
2. **Hazards:** the hazards of chemical substances are classified by the CLP EC No 1272/2008 regulation. This is a EU regulation on classification, labelling and packaging of substances and mixtures. The aim of the CLP is to guarantee a high level of safety to the human health and the environment. The CLP has been integrated with the United Nations Globally Harmonized System (GHS) of Classification, Labelling and Packaging of Chemicals. Globally, the GHS provides a common basis for the definition and classification of chemicals based on their hazards. The hazards are communicated making use of labels and safety data sheets. Three different hazard types are recognised: *physical hazards* include aspects like explosiveness, flammability, corrosion to metals; *health hazards* encompass for instance acute toxicity, irritation, sensitisation, carcinogenicity; *environmental hazards* consist of hazardous to the aquatic environment [116, 117]. Different classes/categories are identified for a specific compound based on criteria specified in

the CLP Annex I [117]. All the hazards are labelled with statements identified by a code which consists of a letter followed by three digits. The letter can be either "H" (hazard statement) or "P" (precautionary statement). The H-statement points out what the effects that the substance can have on people or environment, while P-statements indicates suggestions to prevent or minimise these effects. The three digits specify the class of the hazard and its classification (e.g. physical, health, environmental, general, prevention) [116].
Among all the types, the DNV GL identifies flammability and toxicity as the main hazards to be handled on board ships [114]. *Flammable liquids* are defined as liquids having a flash point not greater than 60°C. In addition, categories of flammable liquids are defined based on initial boiling point as it can be observed in table A.1. [117]. Together with flashpoint and flammability limits in the air the DNV suggests to consider the auto-ignition temperature to take into consideration the ignition of the substance in the air when no spark or flame is present [114]. Table A.1 shows the flammability hazard classification as to CLP and the relative statement.

Table A.1: Classification criteria for flammable liquids [116, 117]

Criteria	Unit	Category 1	Category 2	Category 3
Flash point	[°C]	< 23	< 23	≥ 23 and ≤ 60
Initial boiling point	[°C]	≤ 35	> 35	-
Statement	[-]	H224: Extremely flammable liquid and vapour	H225: Highly flammable liquid and vapour	H226: Flammable liquid and vapour

Regarding the toxicity hazard in the EC 1272/2008 regulation toxicity means "those adverse effects occurring following oral or dermal administration of a single dose of a substance or a mixture, or multiple doses given within 24 hours, or an inhalation exposure of 4 hours". The hazard classes are [117]:

(a) Acute oral toxicity: it is measured in LD_{50} [117]. In the IUPAC (International Union of Pure and Applied Chemistry) nomenclature LD_{50} is the unit of the *median lethal dose* defined as the "statistically derived dose of a chemical or physical agent (radiation) expected to kill 50% of organisms in a given population under a defined set of conditions [118]". LD_{50} is expressed in mg/kg_{bw} where the subscript "bw" stands for "body weight". The median latent dose physically means the amount of material which kills 50% of tested animals if given all at once. In fact, toxicologists test the dose on animals (e.g. mice), thus the unit mg/kg_{bw} refers to the milligrams of chemical administrated per kilogram of the body weight of the tested animal [119].
(b) Acute dermal toxicity: as for the oral toxicity, the dermal toxicity is also measured as LD_{50} in mg/kg_{bw} [117].
(c) Acute inhalation toxicity: it is subdivided into gases, vapours and dust/mists exposure types. They have different threshold values in CLP and are all measured in LC_{50} [116]. Within the IUPAC nomenclature, LC_{50} is the *median lethal concentration* and it is defined as the "statistically derived concentration of a substance in an environmental medium expected to kill 50% of organisms in a given population under a defined set of conditions" [118]. For vapours and dust/mists the lethal concentration is given in mg/l, i.e. milligrams of the chemical in liters of air. For gases LC_{50} is measured in mg/ppmV, i.e. milligrams of the chemical in parts per million by volume of air [116, 119].

Table A.2 depicts the cut-off values of the acute toxicity and the category hazard statement relative to each exposure route.

Table A.2: Cut-off values of acute toxicity

Exposure route	Unit	Category 1	Category 2	Category 3	Category 4
Oral	LD_{50} [mg/kg_{bw}]	<5	5-50	50-300	300-2000
Dermal	LD_{50} [mg/kg_{bw}]	<50	50-200	200-1000	1000-2000
Gases	LC_{50} [ppmV]	<100	100-500	500-2500	2500-20000
Vapours	LC_{50} [mg/l]	<0.5	0.5-2	2-10	10-20
Dust and mists	LC50 [mg/l]	<0.05	0.05-0.5	0.5-1	1-5
Exposure route		**Category 1**	**Category 2**	**Category 3**	**Category 4**
Oral		H300: Fatal if swallowed	H300: Fatal if swallowed	H301: Toxic if swallowed	H302: Harmful if swallowed
Dermal		H310: Fatal in contact with skin	H310: Fatal in contact with skin	H311: Toxic in contact with skin	H312: Harmful in contact with skin
Inhalation		H330: Fatal if inhaled	H330: Fatal if inhaled	H331: Toxic if inhaled	H332: Harmful if inhaled

3. **Technology readiness level (TRL):** the type of power conversion systems are researched for each alternative fuel. The related TRL will determine the actual feasibility of the dual-fuel system in the roadmap towards 2030. The TRL determination of power conversion systems will be based on the Horizon Europe National Contact Points (NCP). It provides a guide to define the maturity of a product and its relation to the market on a unit scale from 1 to 9 [120]. The TRL scale is presented in figure A.1 with its basic definitions.

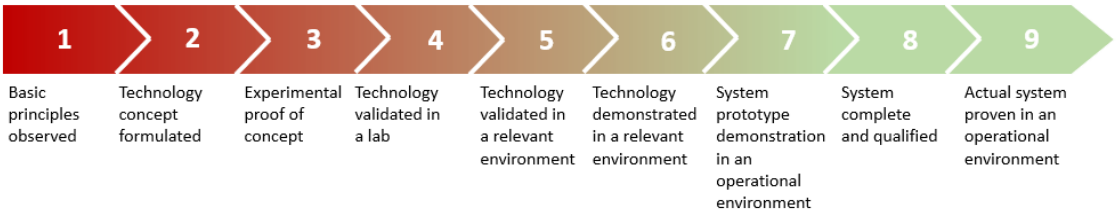

Figure A.1: Technology Readiness Level scale, based on [120]

4. **Emissions:** these are researched to evaluate the environmental impact of the alternative fuel relative to the current fuel of the Feadship's fleet. The global warming potential (GWP) is assessed by investigating WTW GHG emissions. GHG emissions include released CO_2, N_2O and CH_4. They are usually expressed as grams of CO_2 equivalent per MJ of fuel ($CO_{2,e}$/MJ). In December 2018 the European Renewable Energy Directive (RED II) 2018/2001/EU came into force [121]. This promotes the use of renewable sources among European countries and sets targets for GHG emissions savings from different fuels and feedstocks to comply with to get financial support from governments. RED II also provides guidelines to determine GHG emissions. However, since an in-depth calculation of these is not the main purpose of this study, reference will be made to the literature to provide an indication of the reduced emissions. Nevertheless, to provide a first indication for TTW emissions, the RED II directive states that the emissions of the fuel in use shall be equal to zero when performing calculations for all biofuels. This means that for most of the biofuels, the TTW emissions are zero because the CO_2 released during combustion is captured by the plants during their growth.
5. **Regulations:** the availability of regulations and guidelines is fundamental to provide a basis for the fuel system design. In case regulations are not available it is necessary to design the

fuel system such that a level of safety equivalent to existing standards is achieved (*equivalent safety principle*) as regulated by SOLAS Regulation II-1/55 [105]. At the moment, all low flash point fuels different than LNG shall comply with the IGF Code [122] and an alternative design approach shall be followed and approved by the flag administration of the vessel as outlined in the IMO MISC.1/Circ.1455 [123].

6. **Fuel's availability:** it defines to which extend the yachts can bunker a certain alternative fuel in specific territorial waters. The probability of scaling up the alternative fuel's production is qualitatively researched on a large scale.

Selected fuels according to these criteria are non-fossil paraffinic fuels EN 15940 (more specifically HVO) and methanol. These fuels are discussed in the following sections. The following paragraph explains the process behind the exclusion of the researched fuels different than HVO and methanol.

Liquid gaseous fuels were excluded from this study for the following reasons. The shape of the fuel tank already poses limitations on the choice of alternative fuels. Liquid gaseous fuels, namely hydrogen, LNG, pressurized ammonia, liquefied petroleum gas (LPG), liquefied methane and dimethyl ether (DME) are excluded from this research. They would in fact require cylindrical and insulated tanks [11, 114, 124, 125, 126, 127], thus they would not ensure flexibility to the fuel system. It can be argued that ammonia can also be stored in non-cylindrical tanks when it is liquefied cooling it to -33°C [11, 114]. However, a cooled ammonia configuration would require 3.4 times the space of diesel [115]. This would result in loss of luxury space and undermined value of the yacht. Ammonia is also highly toxic [114] and the chemical involved in most explosions and fire accidents [128]. These are non-trivial challenges to address when ensuring safety on board. As a consequence, liquid non-gaseous fuels to be alternatively stored in non-cylindrical tanks better suit for a flexible design. Liquid fuels can also be stored in tanks integrated with the structure of the ship. When compared to small designs, in large yachts a more efficient use of void spaces can be done. That is to say that a percentage of the total fuel can be stored in void spaces within the double hull without compromising the luxury of the yacht [6, 10].

All the studied liquid non-gaseous fuels can be stored in prismatic tanks with little to no extra provisions. All fuels show low to no acute toxicity, while flammability classification varies. TRL, emissions, availability and further aspects can already lead to the exclusion of some fuels. No maritime interest has been observed in sustainable aviation fuel (SAF). Predictions show that its production would not be able to fulfill the aviation industry demand. Hence, the benefits from SAF in the maritime industry are unrealistic on a large scale. Consequently, SAF is left out of this study. Furthermore, SAF competes with the other biofuels regarding feedstocks availability, which is also the reason of uncertain scalability of some fuels. For this reason Fischer-Tropsch (FT)-diesel is excluded. Also, gas-to-liquid (GTL) FT-diesel shows higher WTW emissions, an aspect undermining the zero-carbon targets. Ethanol is left out of this study, since no feedstocks different than biomass are found for its production at the moment. Furthermore, its application is limited to road vehicles and marine experience is absent. The availability of biomass impacts butanol and FAME fuel too. Butanol can be produced from ethanol feedstocks. A production rise is envisaged but its usage as marine fuel is unpredictable due to no highly shared maritime interest. FAME is being used as blending component given microbial contamination and short-term storage issues. Consequently, FAME is not seen as a candidate for a multi-fuel system as a neat product. Regarding propanol and OME, despite their low flammability and non toxicity, their TRL is limited to research stage. This also limits development of marine regulations and quantification of emissions. Propanol remains limited due to its production costs, whilst OME availability cannot be predicted. Consequently, both fuels are excluded.

A.2. Hydrotreated vegetable oil

Hydrotreated vegetable oil (HVO) is a paraffinic fuel belonging to the biofuels category. HVO is also called advanced biodiesel [114] for its similar properties to conventional diesel [129, 130]. In general, the aromatic content is the differentiating factor between paraffinic and conventional diesel fuels. To EN 590:2013 standards the volume of total aromatics is limited to 8% in conventional diesels. In paraffinic fuels the volume of aromatics is below 1.1% in accordance with EN 15940:2016 [41]. As all the paraffinic fuels, HVO does not contain oxygen and therefore it can also be denominated as non-oxygenated compound [41, 131, 132].

HVO is a hydrogenation-derived renewable diesel (HDRD) produced from fats, oils and greases (e.g. used cooking oils, tallow), also referred as FOGs and vegetable oils (e.g. palm oil, soybean oil, rapeseed oil). Additional feedstocks are residual corps and industrial waste (e.g. wood spill) [129, 130]. The HVO obtained from vegetable oils belongs to the *first-generation biofuels*, while HVO made from residual corps and industrial waste is a *second-generation biofuel*. Second-generation biofuels have a smaller well-to-wake (WTW) carbon footprint when compared to MGO [129]. HVO is also known as hydrotreated esters and fatty acids (HEFA) or hydrotreated renewable oil (HRO) [129]. Fats, oils and greases are subjected to hydrotreating [133], more specifically hydrocracking. In this process hydrogen is used to remove oxygen from the vegetable oil [134]. The result is a paraffinic hydrocarbon similar to the ones found in the petroleum-based diesel [129].

Storage

HVO is liquid at 20°C and 1 bar [47], thus storage in prismatic tanks is possible.

Hazards

HVO is a non-toxic colourless, clear and bright fuel [114, 129]. Thus, in terms of acute toxicity, HVO does not pose any issues since it does not meet any of the criteria reported in table A.2. Nevertheless, concerning aspiration hazards it is labelled H304, i.e. it may be fatal if swallowed and enters airways [135]. HVO is a flammable liquid: it belongs to category 3 of flammable fuels classified as H226 as having a minimum flash point of 55.1°C and a boiling point range of 180-320°C. Its explosion limits are ranged 0.6-7.5% [114, 129, 135] and the auto-ignition temperature is equal to 204°C [135].

Technology readiness level

HVO technology readiness level can be assumed to be relatively high. This fuel can be blended in diesel or deployed as a pure fuel. In the first case the amount of HVO in diesel equals tens of percents and the fuel is labelled as *premium* given the increased cetane number and decreased aromatic content [134]. Neat HVO can be used as a drop-in fuel in diesel engines [114, 129, 134]. Some vessels are currently sailing on HVO without reporting any negative effects [114]. This means that the HVO marine systems have a high TRL and here assumed equal to 7.

Regulations

From a regulatory perspective, HVO is defined in the standard for automotive paraffinic diesel fuel, i.e. EN 590 B7 and EN 15940:2016 class A [129, 136]. HVO quality is not specifically specified under any maritime fuel standard. Nevertheless, as for FT-diesel fuels, considering that vessels are sailing on HVO it is expected that the current maritime standards can be fulfilled.

Emissions

Exhaust emissions of pure diesel are reduced if HVO is blended with it [134]. These blends meet the EN590:2004 (maximum sulphur content equals 10mg/kg) and ASTM D 975 standard requirements [130, 134]. H. Aatola et al. found that a mixture of HVO and EN 590 where HVO is blended at 30%

leads to a 5% reduction of emitted NOx in comparison to a pure EN 590 usage. A NOx cut of up to 16% resulted from a pure HVO deployment [134]. HVO is sulphur free and therefore no SOx is emitted. Released PM can be reduced up to 30% [137], although this result is engine load and speed dependent. Regarding WTW emissions, HVO has a slightly lower impact than ultra low sulphur MGO. HVO derived from palm and soy oil respectively shows roughly 5% and 20% GHG reduction. This because of the strong impact of indirect land use change (ILUC), dictated by deployment of oilseeds which induces land conversion to maintain a stable food supply-demand [137].

Availability

Global HVO production tripled from 2014, accounting for 7.4 Mt in 2021. Europe is the largest HVO producer speaking for 45% of the global production [138]. In Europe, from 2021 neat HVO is available in Belgium, Denmark, Finland, Estonia, Latvia, Lithuania, the Netherlands, Norway and Sweden. For vessels it is available in Germany, the UK and Switzerland. The largest HVO plant is located in The Netherlands. A growth in capacities is planned in France, Italy, Sweden and Finland. Hence, the total produced HVO is expected to grow further by 2030. While Europe and USA are projected to remain leaders in the HVO production, Asia is envisaged to enlarge its capacity with main hubs in Singapore and China [139]. Regarding feedstocks, mostly palm oil was used but with the EU regulations setting limits for utilisation of feedstocks with a high risk of indirect land use change (ILUC) [121], the production shifted away from vegetable oils [140, 141]. Mainly food waste (e.g. used cooking and frying oils, animal fats, and vegetable oil processing waste) and agricultural residues are harnessed worldwide nowadays [141, 142, 143]. Some of these plants will be used for the production of HVO for road, maritime, and aviation [140, 144, 145, 146]. Hence, it is fundamental to further research whether the total HVO produced can cover the global maritime demand. Future HVO-plants enlargements show a positive perspective in terms of scalability. The economy of scale is in fact important to overcome higher production costs due to hydrogenation processes when compared to other biodiesels [146]. Furthermore, it has to be considered that HVO will compete with biodiesel for the second-generation feedstock supply. Given in fact the already mentioned restrictions on first-generation feedstocks [121, 147], new raw materials will need to be imported (e.g. from Asia) increasing the final fuel prices [146]. An increase in fuel prices of biodiesels derived from animal fats and used cooking oil is considered in the RED II regulation [121], given the limited availability of these feedstocks [148].

Figure A.2 illustrates the main findings of HVO for the main selected criteria.

Figure A.2: Main findings of HVO fuel

A.3. Methanol

Methanol is an oxygenated compound belonging to the alcohols category where the oxygen is present in the OH-group form as in all the other alcohols. Methanol is the simplest alcohol with a chemical formulation CH_3OH (generally referred as MeOH). It is a primary alcohol according to the IUPAC denomination [40]. It is the compound with the lowest carbon content and highest hydrogen content than any other fuel [35, 114, 133]. Its oxygen content accounts for 49.93 wt% [149, 150].

Methanol production involves CO_2 hydrogenation reaction [6]. Thus, carbon dioxide and hydrogen are needed as reactants. Different methods apply to get these reactants which determine the methanol production sustainability. Methanol can be produced in several ways [6, 35, 133]. First, non-renewable methanol can be formed via the gasification of coal ("brown methanol") or natural gas reforming ("grey methanol"). In the latter scenario, in case carbon capture and storage (CCS) is applied and the captured CO_2 is combined with hydrogen the obtained product is called "blue methanol". This process reduces the footprint of the MeOH production but to drop it further methanol can be formed in a renewable way. Renewable methanol comprises *e-methanol* and *bio-methanol*, also both called *green methanol*. E-methanol is the product of CO_2 hydrogenation where carbon dioxide is obtained from direct air capture (DAC), carbon-intensive industries, or energy transformation processes. Hydrogen stems from renewable-powered water electrolysis. Regarding bio-methanol, renewable electrolysis is combined with biomass gasification/reforming. CO_2 is captured from air while biomass (e.g.agricultural and municipal solid waste) is converted into power and heat in the so-called Bio-Energy with Carbon Capture Storage (BECCS) process [133].

Storage

Methanol is liquid at atmospheric pressure and at a temperature between -93°C and 65°C [114]. Consequently, methanol can be stored in the existing prismatic diesel tanks [21].

Hazards

Regarding hazards methanol belongs to category 3 in terms of acute toxicity. In fact it is labelled H301 with respect to acute oral toxicity, H331 for inhalation and H311 for dermal toxicity [47]. Hence, methanol has a low acute toxicity and it is dangerous for humans if swallowed, in contact with skin and inhaled in high concentrations [35, 6]. For this reason, humans are sensitive to methanol poisoning but the cure is well understood [151]. Methanol is a colourless fuel with a pungent odor [35, 47]. It has a flashpoint in the range 9-12°C [6, 47, 114] and flammability limits of 6-36 volume % in air [35, 114]. The methanol autoignition and boiling temperatures are equal to 440-470°C and 64.7°C respectively [35, 47, 114]. Given these features and with reference to table A.1 methanol is classified as H225 highly flammable liquid (category 2) according to Regulation (EC) No. 1272/2008 [47].

Technology readiness level

For power generation on board methanol can be deployed in ICEs and fuel cells. TRL is ranged 5-7. Regarding engines, methanol can be used as neat fuel or blended with another alcohol (e.g. ethanol) and/or another fuel (e.g. gasoline) [151]. Methanol can be blended with diesel too but an emulsifier is required [21, 151]. Spark ignited engines can run on 100% methanol. Here a partly-evaporated methanol-air mixture enters the cylinder and it is ignited by a spark [21]. Minor modifications might be needed to the fuel injector [6]. Compression ignited engines can also be used. Given the poor methanol auto-ignition capabilities methanol is either mixed with diesel (requiring an emulsifier for a better mix) or a pilot fuel (e.g. diesel) enters the engine separately [6, 21]. This latter approach, called dual-fuel approach, is more common and it comprises direct injection (DI) and port fuel injection (PFI) options. The former consists of a custom cylinder head with separate injectors, one for methanol and one for the pilot fuel. An alternative DI design consists of a custom injector capable of injecting

the pilot fuel and methanol together. The PFI design comprises the introduction of methanol into the engine's intake ports requiring less modifications to the engine in case of refitting. A last option consists of a glow plug ignition. This allows methanol to reform into hydrogen inside the engine. Subsequently, hydrogen is pre-ignited acting as a pilot fuel for the remaining methanol [6]. Currently the MAN ME-LGI two-stroke engine series is commercially available [152] while Wärtsilä dual-fuel four-stroke engines are in operation on board passenger ships [153]. For these reasons the assigned TRL for methanol dual-fuel engines is 7, while it stands at 5-6 for spark ignited and compression ignited pure methanol engines.
Different fuel cell types can be used to convert the methanol stored on board into power. These comprise proton exchange membrane fuel cells (PEM-FC), direct methanol fuel cells (DMFC) and solide oxide fuel cells (SOFC) [6]. Low temperature (LT), high temperature (HT) PEMFC and SOFC can run on hydrogen, thus a reforming system on board is required to convert methanol into hydrogen [11]. Regarding DMFC no reforming is needed. At the moment the technology is still under theoretical research stage [6, 154]. The delivered power is limited and the efficiency is lower compared to other FC types, as well as methanol crossover represents a major challenge [6]. However, DMFCs can be bought as they are [155] but integration on ships needs to be demonstrated. Consequently, the assigned TRL equals 6. PEMFC shows a higher number of demonstration and pilot projects than SOFCs. This reflects the fact that PEMFC is a more mature technology than SOFC, given the low power density and high capital cost of SOFCs [156]. Projects are on going with HT-PEMFC with integrated methanol reformer on board to demonstrate integration of the technology in the ship environment [157, 158, 159]. The assigned TRL to HT-PEMFC is 7. SOFC state-of-the-art include the Wärtsilä coordinated METHAPU project ended in 2010 and aimed at validating SOFC on board cargo vessel [160]. Similarly, the ongoing Nautilus project focuses on validating a digital design and a physical demonstrator of SOFCs on board cruise ships to comply with safety regulations [161]. The assumed TRL of SOFCs is 5.

Regulations

Nowadays the methanol's quality is regulated through the ASTM D-1152/97 and/or the International Methanol Consumers and Producers Association (IMPCA) specifications. The IMPCA standards regulate the methanol's quality in the chemical industry [35]. At the moment the ISO/AWI 6583 international standards are under development in order to extend regulations for the methanol's quality to the marine industry [162]. In terms of fuel storage on board safety requirements need to be met in compliance to the IMO Maritime Safety Committee (MSC) MSC.1/Circ.1621. This is entitled "Interim Guidelines for the Safety of Ships using Methyl/Ethyl Alcohol as fuel" and it will become part of the IGF Code [21, 163, 164]. Additional safety measures are regulated by the IMO SOLAS Chapter II Part B Reg. 4.2 and Part F Reg. 4.2 addressing protection from fire. Further reference is made in SOLAS Chapter II for other safety provisions [105]. In particular, IMO CCC6 2019 comprises specifications for the cofferdam, i.e. a structural space surrounding the tank to prevent spilling and protect from hazards such as fire [6, 35]. Lastly, the IBC Code - International Code for the Construction and Equipment of Ships Carrying Dangerous Chemicals in Bulk, Amended by Resolution MEPC.225(64) can be applied. Although this does not regulate combustion of low flash point liquid fuels the location of tanks is addressed [21, 35]. On top of international standards classification societies namely Lloyd's Register, DNV and Bureau Veritas have been developing design regulatory and requirements for methyl/ethyl alcohol fuels [35, 114, 165]. Overall, considering that vessels are sailing on methanol and with reference to the alternative design approach specified under the IMO MISC.1/Circ.1455 [123] it can be considered that the fuel can be compliant with the IGF code [122].

Emissions

In a well-to-wake scenario (WTW) methanol does not emit SOx since it is sulphur free. Furthermore, the reduction of released PM from methanol combustion is ranged 60-100%. Regarding well-to-wake impact, bio-methanol derived from miscanthus and corn stover can cut WTW emissions between 74 and 82% [137]. 92.3% and 98% emissions reductions are observed for farmed wood- and black liquor-derived methanol respectively [35]. S. Brynol calculated the WTW GHG emissions for a ro-ro vessel fuelled with methanol produced from willow or forest residues [166]. The results integrated by TNO in a comparative analysis with MGO depict a reduction of 92.6-97.5% emitted GHGs [164]. Grey methanol from LNG has a higher impact than MGO. LNG-derived methanol accounts for higher WTW emitted GHGs than MGO of 5-10% [137, 167]. Lastly, e-Methanol produced from renewable electricity and captured CO_2 shows 3 $gCO_{2,e}$/MJ which represents about 96% GHG emissions reduction compared to conventional MGO [167, 168].

Availability

Nowadays 98 Mt of methanol are produced from fossil sources [35, 169]. The fossil-based production is explained by its low costs [35]. China is the major producer accounting for 57% of the methanol global production [35, 170]. In China, methanol is coal-derived [35, 170] while gas-based plants are located in America and Europe for instance [35]. e-Methanol and bio-methanol yearly production is expected to rise to 250 Mt and 135 Mt respectively by 2050. [171]. Current plants for bio-methanol synthesis are present in Sweden and Canada, where MeOH is derived from black liquor and wood waste respectively. Renewable methanol from geothermal energy is produced in Iceland, which represents the major exporter of methanol used in Europe [35]. In Norway a project is expected to be commissioned in 2024 for the production of methanol from renewable electrolysis and CO_2 capture [170]. Methanol is used for the chemical production of formaldehyde, acetic acid, and other chemical and construction applications which account for nearly 60% of the market. Methanol is also used as a blend for ethanol, and feedstock for FAME and DME production. Hence, estimations show that the use of methanol as a direct fuel is limited to 1.5 Mt [172]. At the moment, methanol is already used as shipping fuel with more than 100 ports providing its availability [16]. However, it is not entirely clear whether in the available ports methanol is sold as marine fuel or chemical compound to be shipped for the chemical industry. However, its availability means that a certain experience regarding fuel handling and safety is in place [173]. Nevertheless, the production of methanol remains limited on a large scale. As indicated by IRENA [171] and the Global Maritime Forum [173] the challenges of e-methanol scalability are economic rather than technological. That is to say that technology for CO_2 capture and H_2 is at a sufficient level but capital investments are needed to build the plants. On the other side, bio-methanol from crops can undermine the food chain for indirect usage of land. Furthermore, compliance with some criteria is necessary to assess the impact on soil quality and erosion, water and fertilizers consumption, biodiversity concerns, and seasonal availability. The availability of feedstocks such as forestry and agricultural waste has to be considered relative to other advanced biofuels production. Lastly, the Global Maritime Forum underlines that the methanol demand from non-maritime industries should be considered [173].

Figure A.3 illustrates the main findings of methanol for the main selected criteria.

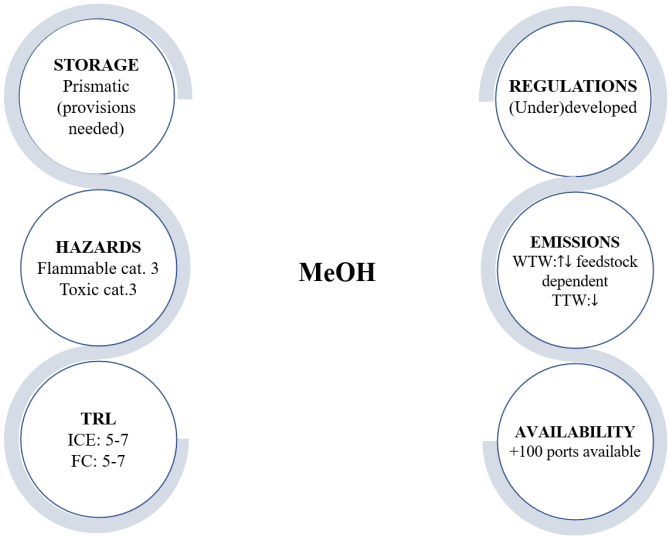

Figure A.3: Main findings of methanol fuel

A summary of the prioritized fuels is reported in table A.3, while their properties are shown in table A.3. The properties of DMA/DFA diesel are also depicted to observe the main differences with the selected fuels. Properties of these fuels refer to ISO standards [41, 61] and data collected from literature [6, 174]. Properties of HVO refer to EN 15940 standards [41] and literature [41, 47, 114, 129, 134, 135]. Regarding methanol, considering that ISO marine standards are still under development, data are merely gathered from available literature [6, 35, 47, 114, 150, 151, 175] and IMPCA methanol standards [176].

Table A.3: Pros and cons of prioritized fuels

Fuel	Pros	Cons
EN 15940 (HVO)	- Prismatic tanks usage. - Non toxic. - High TRL for ICEs. - Regulations developed for FT-diesel.	- Current limitations on large scale. - Biomass competition. - Regulations under development for HVO.
Methanol	- Prismatic tanks usage. - Relatively high TRL. - Availability on large scale. - e-MeOH overcomes biomass challenges.	- Low toxicity. - Marine regulations under development.

Table A.4: Main properties of DMA/DFA, HVO and methanol

Property	Unit	DMA/DFA	HVO	MeOH
Chemical formula	[-]	$C_{12}H_{26}$-$C_{14}H_{30}$	-	CH_3OH
Physical state at 20°C, 1 bar	[-]	Liquid	Liquid	Liquid
Density at 15°C	[kg/m^3]	≤ 890	765-800	795.5
Gravimetric LHV	[MJ/kg]	43	44	19.9
Volumetric LHV	[MJ/l]	36-38	34	15.8
Kinematic viscosity at 40°C	[cSt]	2-6	2.5-3.5	0.58
Cetane number	[-]	≥ 51	80-99	2
Octane number	[-]	-	-	111
Flash point	[°C]	≥ 60	≥ 55	9-12
Auto-ignition temperature	[°C]	> 250	204	440-470
Flammability limits in air	[%]	0.5-5	0.6-7.5	6-36
Boiling point	[°C]	150-380	120-320	64.7
Cloud point	[°C]	≤ −10...≤ −34	≤ −34 ... ≤ −10	-
Ash content	[% m/m]	≤ 0.01	≤ 0.01	-
Carbon residue	[% m/m]	≤ 0.30	≤ 0.30	-
Sulfur	[% m/m]	≤ 1.00	≤ 1.00	≤ 0.05
Water	[% m/m]	≤ 0.020	≤ 0.020	≤ 0.100
Oxidation stability	[g/m^3]	≤ 25	≤ 25	-

B

Visual analysis of HVO-methanol phase separation

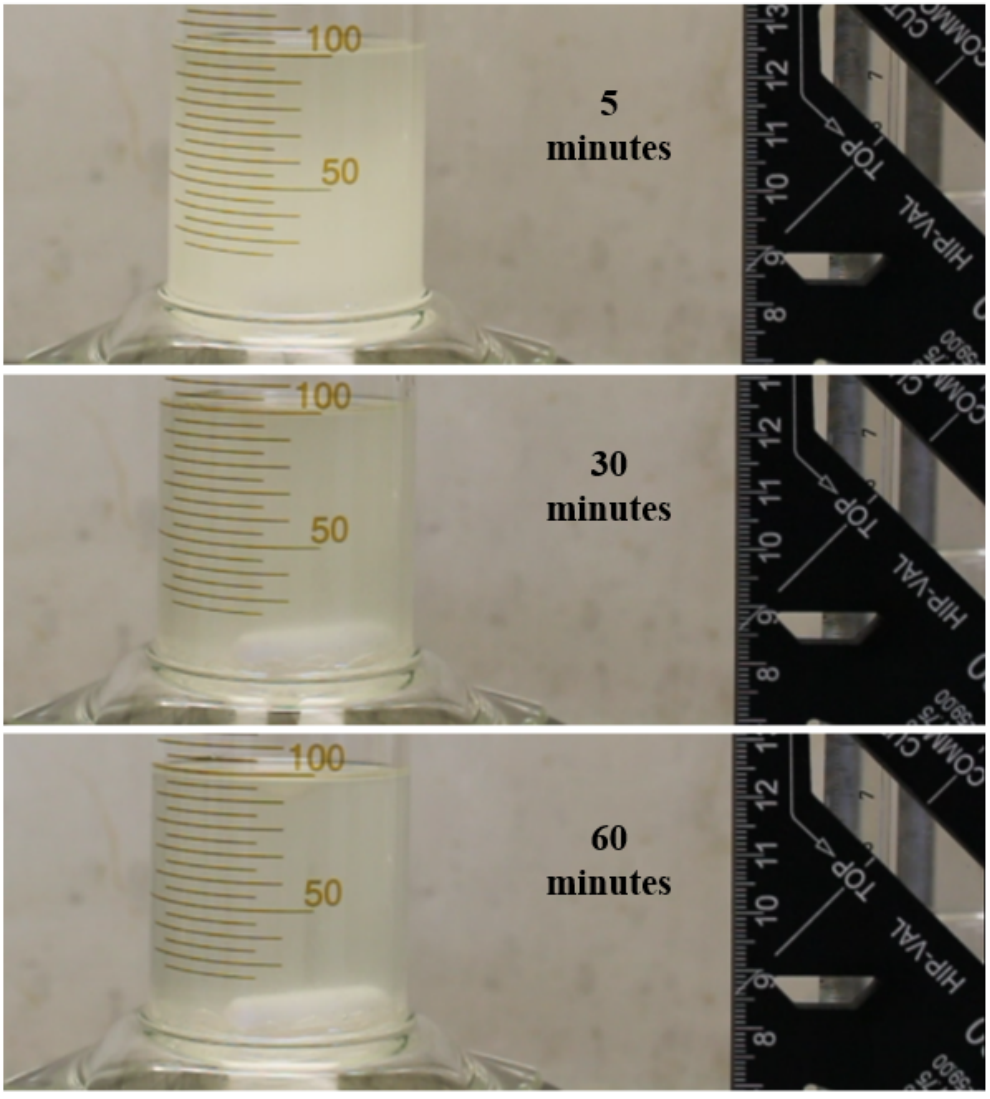

Figure B.1: Visualisation of phase separation (5% v/v MeOH)

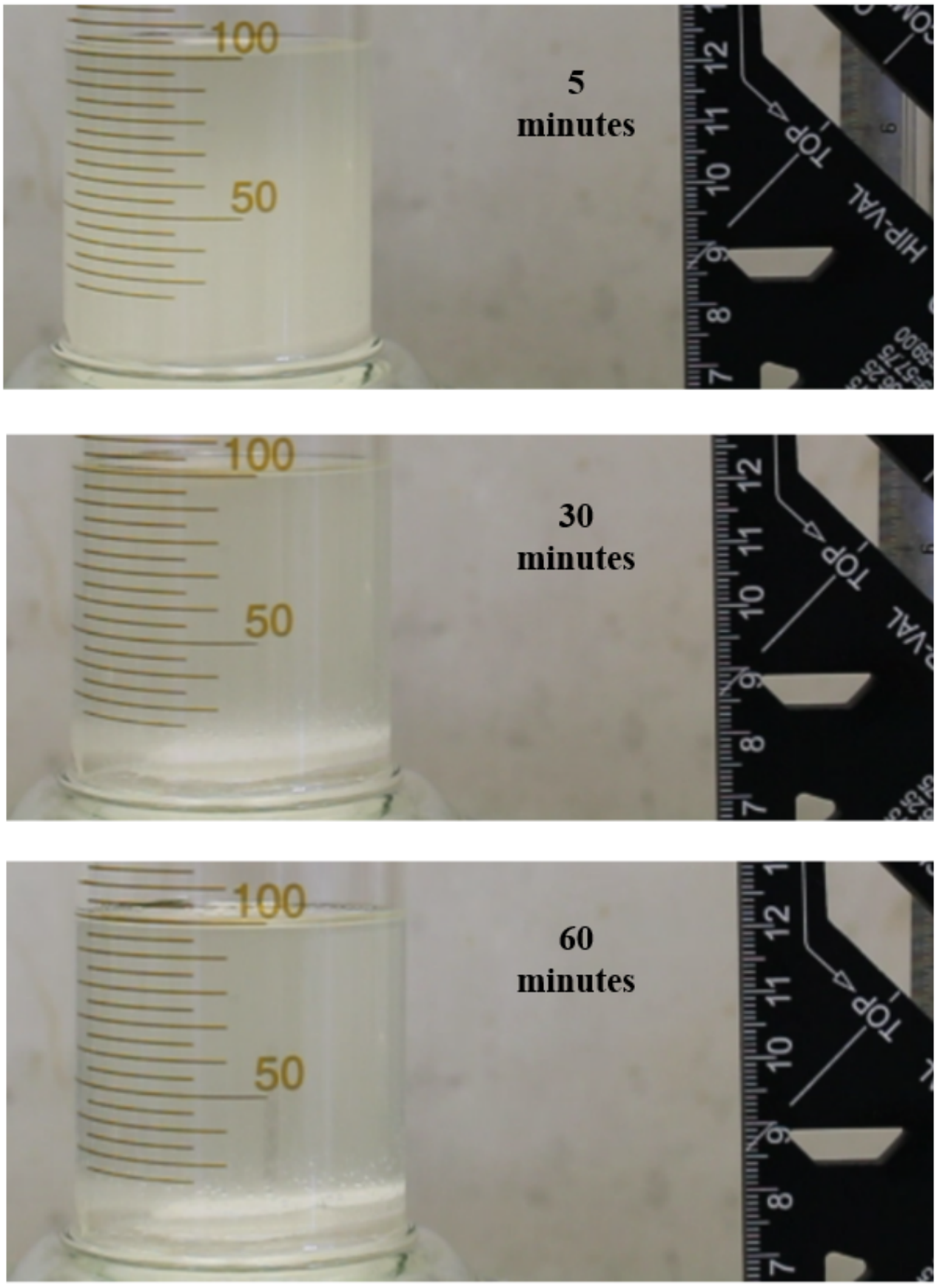

Figure B.2: Visualisation of phase separation (10% v/v MeOH)

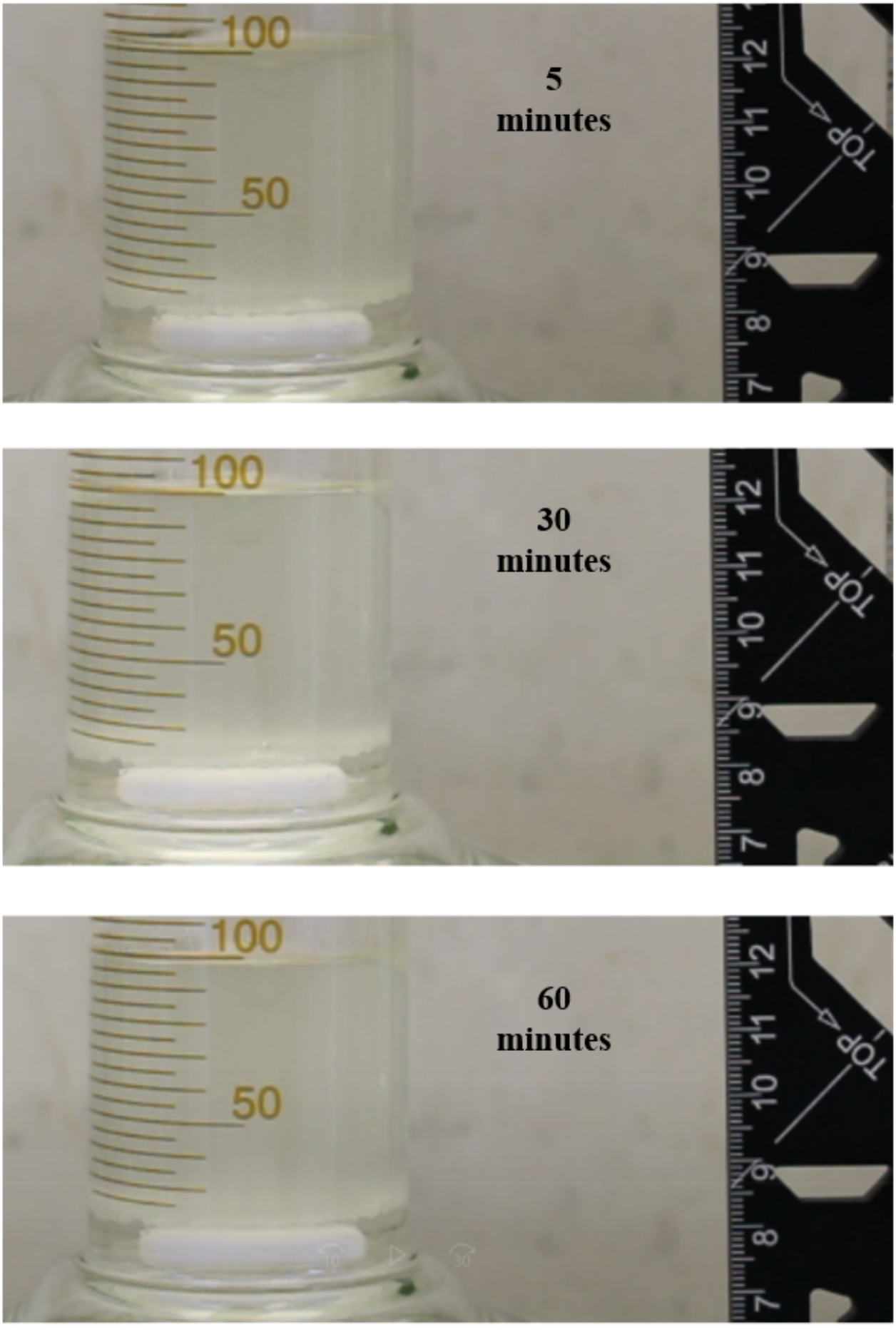

Figure B.3: Visualisation of phase separation (20% v/v MeOH)

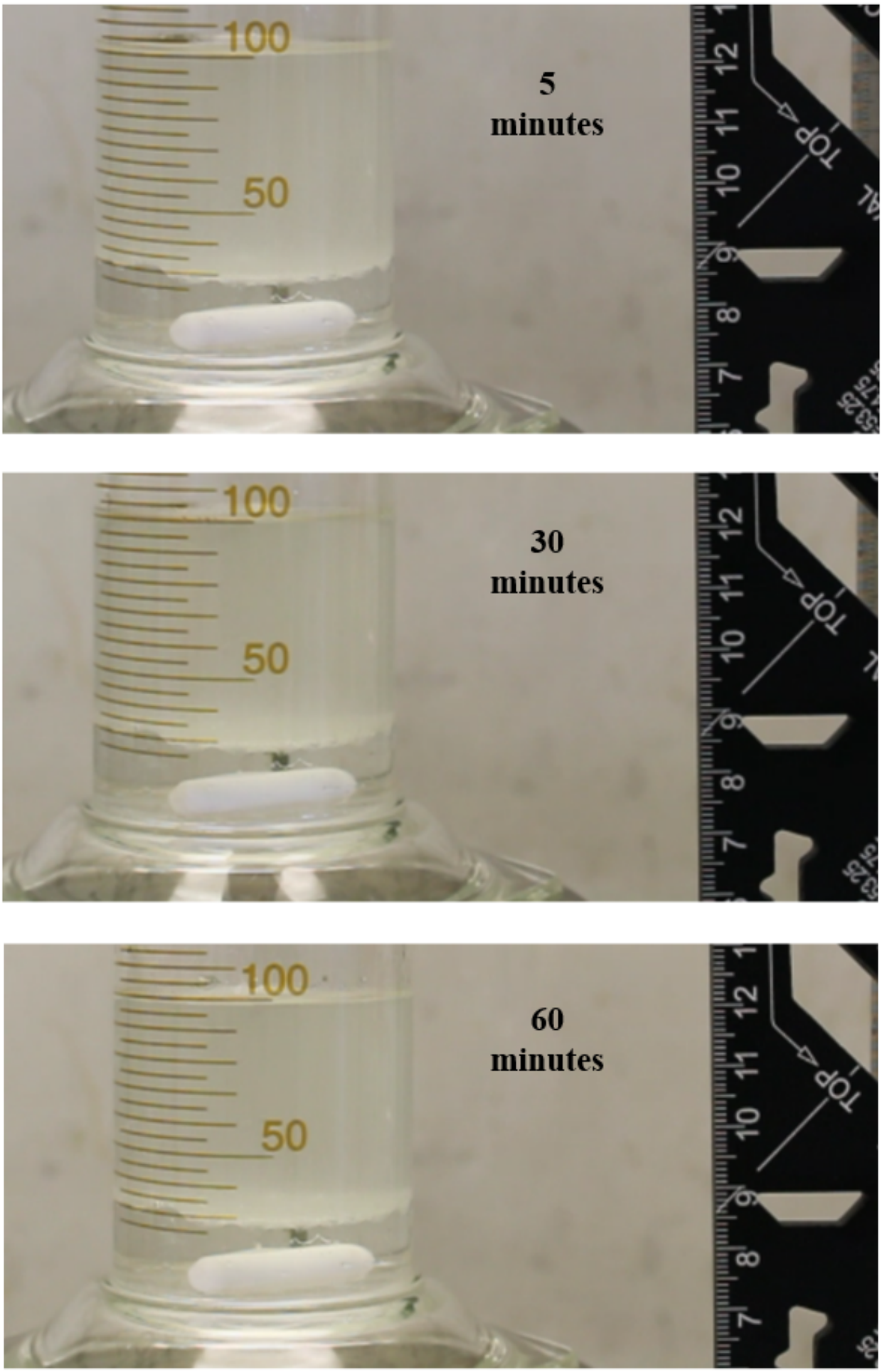

Figure B.4: Visualisation of phase separation (30% v/v MeOH)

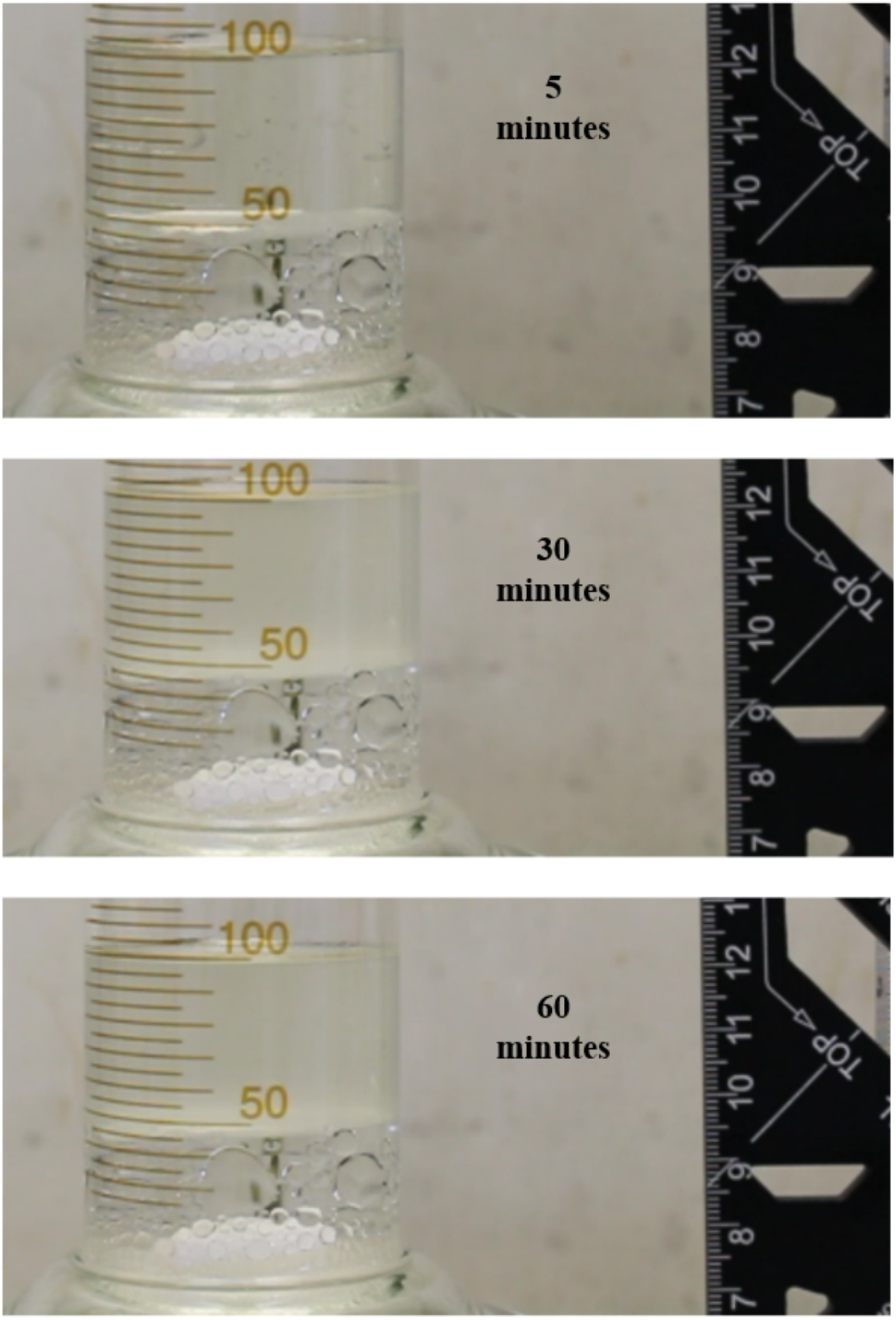

Figure B.5: Visualisation of phase separation (40% v/v MeOH)

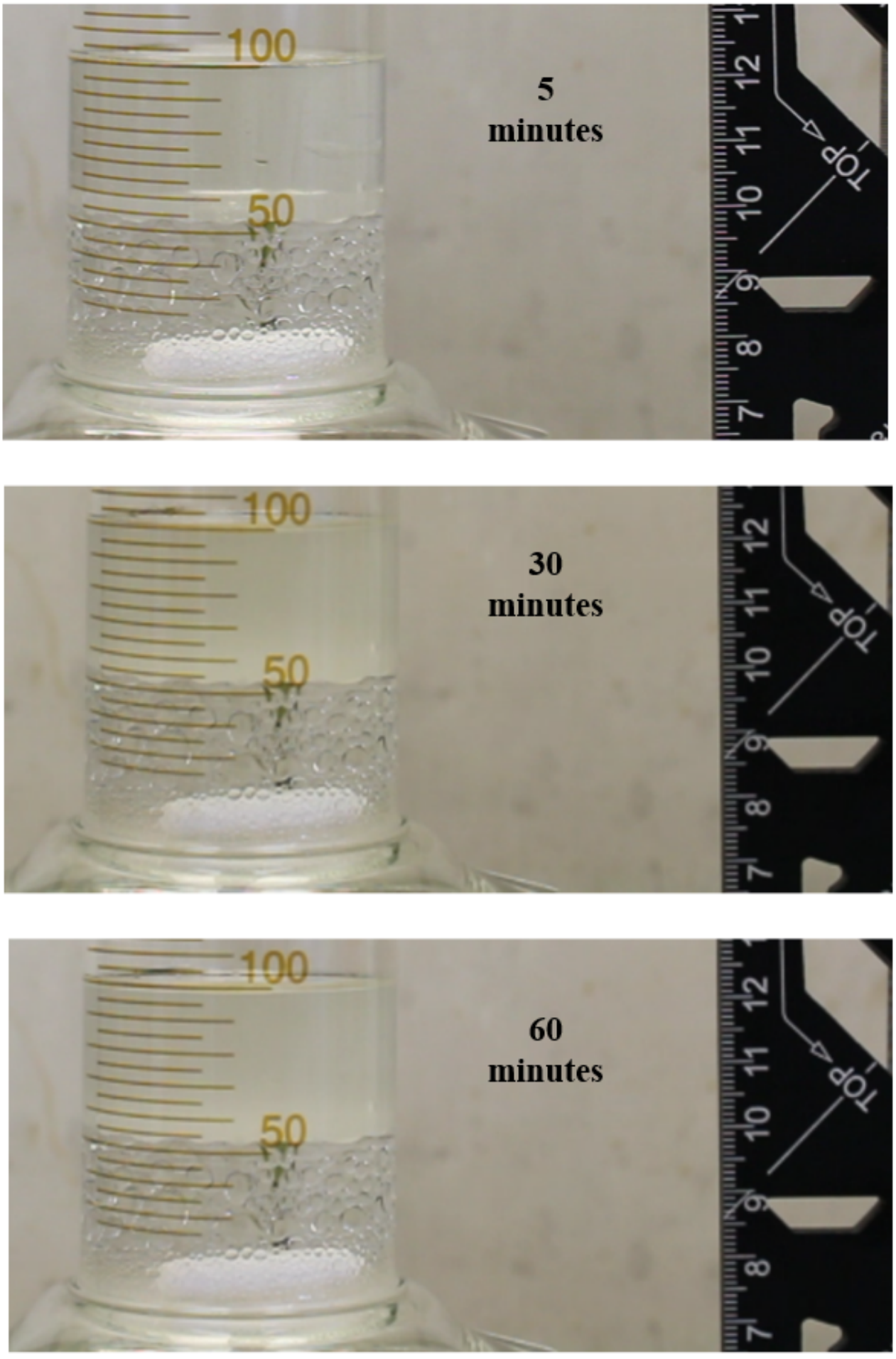

Figure B.6: Visualisation of phase separation (50% v/v MeOH)

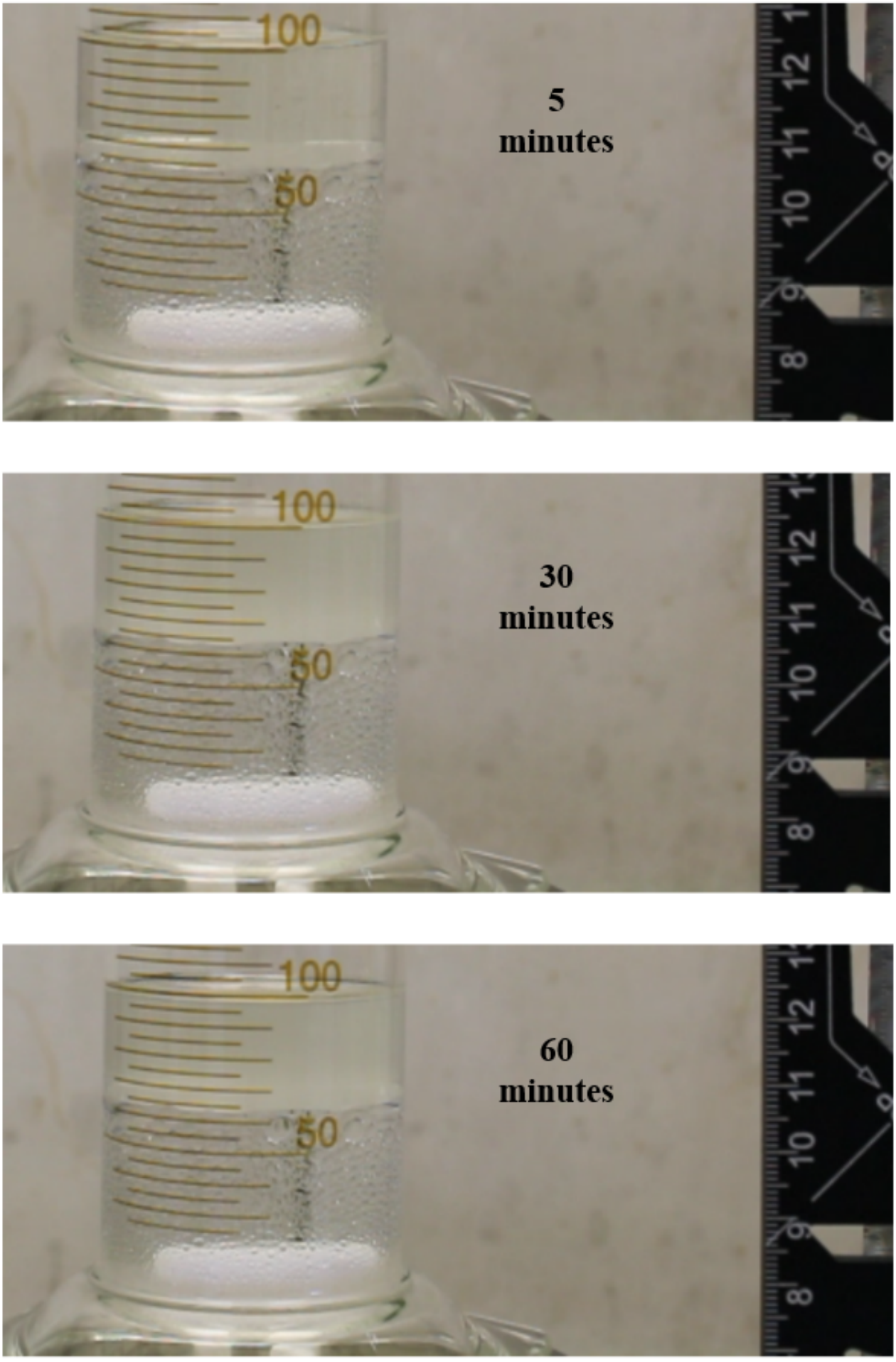

Figure B.7: Visualisation of phase separation (60% v/v MeOH)

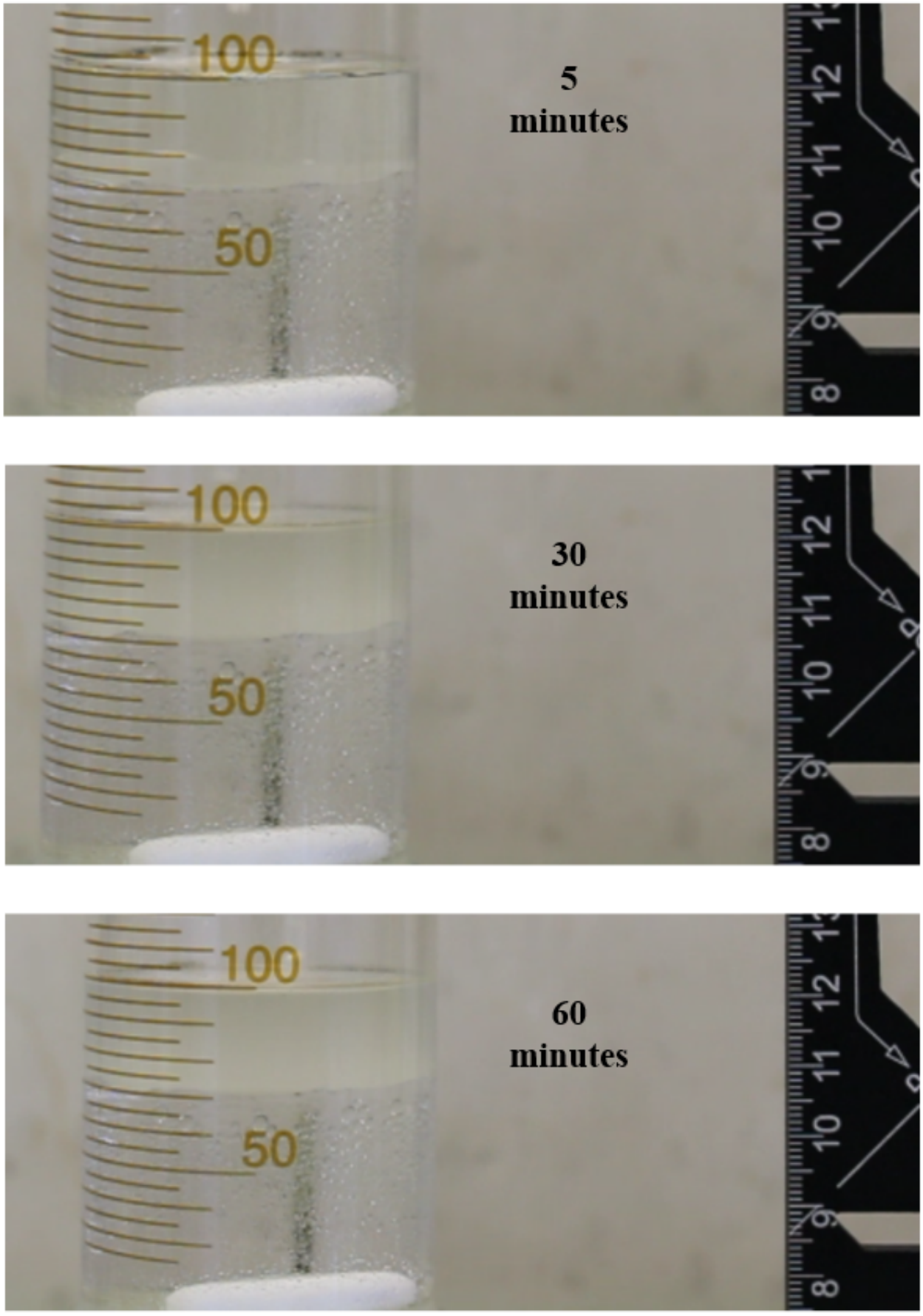

Figure B.8: Visualisation of phase separation (70% v/v MeOH)

C

Derivation of the Reynolds-based term in the equations of motion

In chapter 4 the derivation of the equations of motion is described. In the equations of motion the N term appears. This parameter is function of the Reynolds number and therefore it has different expressions. The derivation of these expressions is presented in the following sections.
The general formulas for the drag coefficient and Reynolds number are reported in [46]. The Reynolds number and the drag force are written below and are valid for all the cases studied:

$$Re = \frac{\rho_h D}{\mu_h}(\dot{x} + V_F) \tag{C.1}$$

$$\vec{F_D} = -\frac{1}{2}\rho_l C_D \frac{\pi}{4} D^2 |\vec{V_d} - \vec{V_F}|(\vec{V_d} - \vec{V_F}) \tag{C.2}$$

Where:

$$\vec{V_c} - \vec{V_F} = \dot{x}\vec{x} + \dot{y}\vec{y} + V_F\vec{x} \tag{C.3}$$

Re < 1
For $Re < 1$ the the drag coefficient equals:

$$C_D = \frac{24}{Re} \tag{C.4}$$

And substituting the Reynolds number in the equation above:

$$C_D = \frac{24\rho_h D}{\mu_h(\dot{x} + V_F)}) \tag{C.5}$$

This expression together with equation C.3 can now be substituted in equation C.2, obtaining:

$$\vec{F_D} = \frac{-3\pi\mu D}{m_d}(\dot{x}\vec{x} + \dot{y}\vec{y} + V_F\vec{x}) \tag{C.6}$$

Hence:

$$N = -3\pi\mu D \tag{C.7}$$

1 < Re < 5

For Re ranged in the range 1-5 the expression for C_D becomes:

$$C_D = \frac{24}{Re}(1 + \frac{3}{16}Re) \tag{C.8}$$

And substituting Re from equation C.1:

$$C_D = \frac{24}{\rho_l D(\dot{x} + V_F)} + \frac{9}{2} \tag{C.9}$$

Substituting the above expression in equation C.2 the drag force equals:

$$\vec{F_D} = -\frac{\pi}{8}\rho_l D^2 \left(\frac{24\mu_h}{\rho_l D(\dot{x} + V_F)} + \frac{9}{2}\right) |\vec{V_d} - \vec{V_F}|(\vec{V_d} - \vec{V_F}) \tag{C.10}$$

$$\vec{F_D} = -\left(\frac{-3\pi\mu_h}{\dot{x} + V_F} + \frac{9}{16}\pi\rho_l D^2\right)\left(\sqrt{(\dot{x} + V_F)^2 + \dot{y}^2}\right)(\dot{x}\vec{x} + \dot{y}\vec{y} + V_F\vec{x}) \tag{C.11}$$

Thus:

$$N = \left(\frac{-3\pi\mu_h}{\dot{x} + V_F} + \frac{9}{16}\pi\rho_l D^2\right)\left(\sqrt{(\dot{x} + V_F)^2 + \dot{y}^2}\right) \tag{C.12}$$

5 < Re < 5000

The formula for the drag coefficient for $5 \leq Re < 5000$ is:

$$C_D = 1.85Re^{-0.6} \tag{C.13}$$

Substituting this expression in equation C.2 the drag force equals:

$$\vec{F_D} = -\frac{\pi}{8}\rho_l D^2 \cdot 1.85\left(\frac{\rho_l D}{\mu_l}(\dot{x} + V_F)\right)^{-0.6}(\dot{x}\vec{x} + \dot{y}\vec{y} + V_F\vec{x}) \tag{C.14}$$

Hence:

$$N = \frac{\pi}{8}\rho_l D^2 \cdot 1.85\left(\frac{\rho_l D}{\mu_l}(\dot{x} + V_F)\right)^{-0.6} \tag{C.15}$$

D

The Runge-Kutta (RK4) numerical method

The RK4 method is described in this section as a tool used for the solution of the denser droplet motion equations in the centrifuge. For this appendix reference is made to [177]. The motion equations found are coupled second order differential equations. Considering a general formulation for ordinary differential equations (ODEs):

$$\begin{cases} u' = f(t,u) \\ u(t_0) = u_0 \end{cases} \tag{D.1}$$

Assuming the solution at time t_n to be known, the solution at time t_{n+1} can be found as:

$$\int_{t_n}^{t_{n+1}} \frac{du}{dt}\, dt = \int_{t_n}^{t_{n+1}} f(t,u(t))\, dt \tag{D.2}$$

Which leads to:

$$u(t_{n+1}) = u(t_n) + \int_{t_n}^{t_{n+1}} f(t,u(t))\, dt \tag{D.3}$$

Given that f is non-linear and u is unknown it is not possible to solve the integral on the right-side of the equation above. For this reason, the explicit Runge-Kutta method can be used. It computes the integral as a weighted sum of u_*, i.e. via a number of intermediate approximations of $f(t_*, u_*)$ for $t_n \leq t_* \leq t_{n+1}$. The Runge-Kutta 4^{th}-order method (RK4) formulation becomes:

$$u_{n+1} = u_n + \frac{\Delta t}{6}(k_1 + 2k_2 + 2k_3 + k_4) \tag{D.4}$$

Where k_i terms are called stage derivatives and they shall be computed sequentially. Their expressions are:

$$k_1 = f(t_n, u_n) \tag{D.5}$$

$$k_2 = f(t_n + \frac{\Delta t}{2}, u_n + \frac{\Delta t}{2} k_1) \tag{D.6}$$

$$k_3 = f(t_n + \frac{\Delta t}{2}, u_n + \frac{\Delta t}{2} k_2) \tag{D.7}$$

$$k_4 = f(t_n + \frac{\Delta t}{2}, u_n + \frac{\Delta t}{2} k_3) \tag{D.8}$$

Hence, the equations above are applied to solve the equations of motion for trajectory 1. And, if the conditions for which the droplet hits the upper disc are met, the equations of motions are also solved for trajectory 2 with initial conditions as in equation 4.22. Moreover, it is worth considering that the Runge-Kutta method introduces an error [177] which depends on the size of the time step. A time discretisation analysis was carried out to remove the dependency of the model on the time step size Δt. It was found out that the solutions of the motion equations converge from a minimum time step $\Delta t = 10^{-5}$ to smaller values. This means that from $\Delta t = 10^{-5}$ the resulting error from consecutive time step simulations becomes negligible. Consequently, 10^{-5} was set as fixed time step for the Runge-Kutta method.

E

Diesel fuel system

This annex describes the main aspects of a fuel oil system. Given that Fadships sail on DMA/DFA, the fuel system described in this section covers a diesel oil system. Its main steps and components are investigated.
Figure E.1 depicts the main steps required to supply fuel to main users on board. First, the fuel is bunkered from receiving stations. Next, diesel is stored in storage tanks and transferred to the purifying system to remove impurities. Lastly, the purified fuel flows to the service tanks where it is stored prior to its usage in power conversion systems.

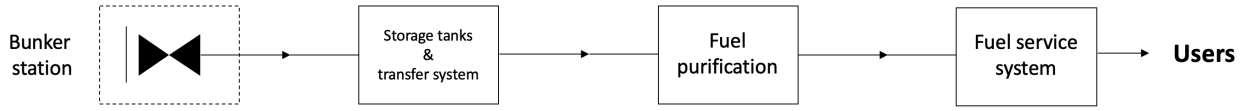

Figure E.1: Main fuel system steps

The main steps are here described with reference to their principle operations and components.

E.1. Fuel bunkering

Transfer pumps are used to move the fuel from on-shore bunker stations to storage tanks. Usually, the ship receives the fuels from the upper deck level, port and starboard. A filter downside the pipes removes the first large impurities [19].

E.2. Transfer system

The fuel is stored in the *storage tanks*. These are designed to accommodate a fuel volume to guarantee the ship's range [104]. Employing transfer pumps, the fuel can flow from one storage tank to another, flowing between starboard and portside, forward and aft for stability reasons [19]. From the storage tanks, the fuel is pumped to the settling tanks and to the separator subsequently.

E.2.1. Storage tanks

There are different types of tanks. *Integral tanks* form a structural part of the hull and are affected by the loads that stress the adjacent hull structure. *(Semi-) membrane tanks* are non-self-supporting

tanks and consist of a layer parts of which are supported through thermal insulation by the adjacent hull structure. *Independent tanks:* are of type A, B, and C and designed using ship structural design procedure, model tests, and pressure vessel criteria. The mentioned tanks are usually for cargo which have boiling points between -55°C and -10°C and therefore requires low temperatures at storage to be liquefied, as indicated in the IGF code [122]. In the case of diesel *free standing tanks* can be used [104]. Generally, they are of prismatic shapes. It is worth pointing out that some of the Feadship's yachts sail in cold regions like the north of Canada and Antarctica. *Alfa laval* suggests to store diesel oil at 30°C, to prevent wax formation, especially during winter conditions [38]. For yachts with lengths equal to or greater than 24m and in accordance with the HSC Code the storage tanks are to be located outside machinery spaces and other areas of major fire hazard. However, free-standing tanks can be located in the main machinery space and they have to be made of steel or equivalent material and be protected from corrosion [104]. In compliance with the safety requirements of SOLAS Regulation II [105] fuel oil tanks need to be ventilated to avoid overpressure. This also applies to any other part of the fuel system "including the filling pipes served by pumps on board". Air and overflow pipes and relief valves are necessary. Self-closing valves and cocks are needed to remove water from the bottom of the tank. A cock or a valve directly positioned on the tank is needed to prevent oil spillage. Oil fuel pipes and their valves and fittings shall be of steel or other approved material. Valves fitted to oil fuel tanks and under static pressure can be made of steel or spheroidal-graphite cast iron. However, the latter material is accepted for pressure below 7 bar and temperatures lower than 60°C. Copper alloy can be another material for valves.

E.2.2. Settling tanks

In the settling tanks diesel is separated from residues by gravity, given the fact that they have different densities. Residues are drained from the bottom of the tanks and stored in the *sludge tank*. As to MARPOL Annex I Regulation 17, sludge tanks shall be installed to accommodate oil residues that cannot be treated with the purification systems on board. The sludge tanks capacity is calculated based on the ship's daily fuel consumption and maximum period of voyage between ports where sludge can be discharged ashore [178]. From the settling tanks, the fuel is pumped to the separators. Usually, two settling tanks are used, each with a 24-hour fuel capacity [19].

E.3. Fuel purification

Fuel purification is performed via filters or separators. Separators are needed in case there is water in the fuel and residuals removal from diesel after settling is not sufficient [108]. Generally, separators are *centrifugal separators*, arranged as *purifiers* or *clarifiers* [19, 20]. The purifier removes water and solids, while the clarifier removes the finer solids remaining. Sludge and water are discharged from the top of the separator and sent to the sludge tanks, while the fuel oil inlet is closed. The purified diesel oil is also discharged from the top of the assembly. Its water content is tested by a transducer and eventually the fuel is conveyed to service tanks. Filters for diesel-water separation can be made of aluminum or plastics [179], while separators are usually made of stainless steel [180].

E.4. Fuel service system

The last block depicted in figure E.1 is the fuel service system. In this schematic, a diesel engine is indicated to provide the simplest example of fuel users. A representation of its main components is given in figure E.2. After purification, the fuel is stored in *service tanks*. For yachts of 500 GT or more, each service tank is designed for at least 8-hour capacity at the maximum continuous rating of the propulsion plant, as indicated in SOLAS Regulation II-1/26.11 [104, 105]. Two service tanks

are required such that one can keep supplying to the users while the other is being cleaned or repaired. The fuel is heated to be injected and burned in power conversion systems [19]. Hence, its viscosity changes and viscosimeters are provided to measure the fuel's viscosity. Given the different temperature between the service tanks and the fuel temperature prior to its combustion, buffer tanks are installed such that the returning fuel from users is temporarily stored there. Given that users require different utilised fuel parameters, different flow meters and viscosimeters are installed before the fuel reaches the specific power conversion system.

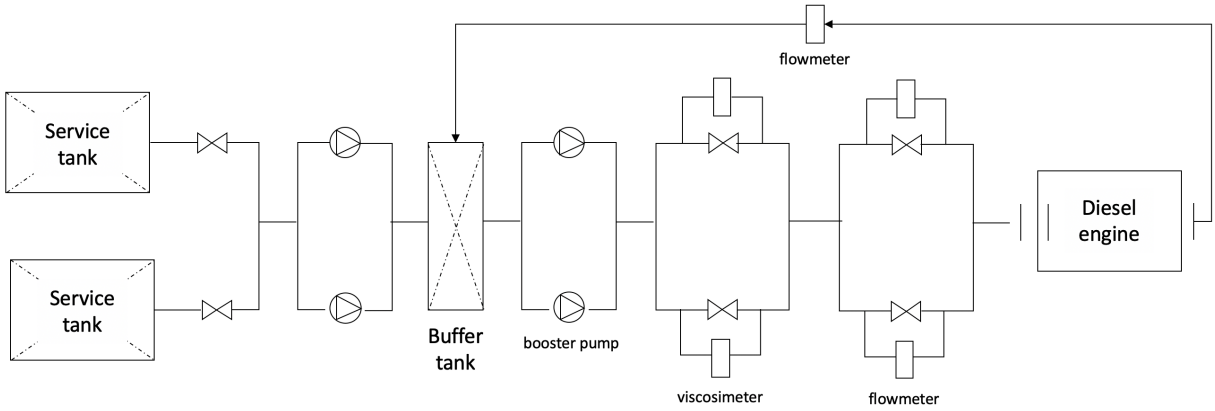

Figure E.2: Fuel service system, based on [19]

F

Mass conservation principle

The principle of mass conservation is used to balance the fuel(s) volume flows at each system section. Its application is used for the multi-fuel system modelling as described in chapter 5. In this appendix chapter reference is made to Vittori and Blondeaux [181].

At each section of the fuel system, the fuel can be though as flowing through an infinitesimal control volume V_0, associated to a surface S_0 at a fixed time t_0. Figure F.1 reports the notation used for the mass balance principle definition.

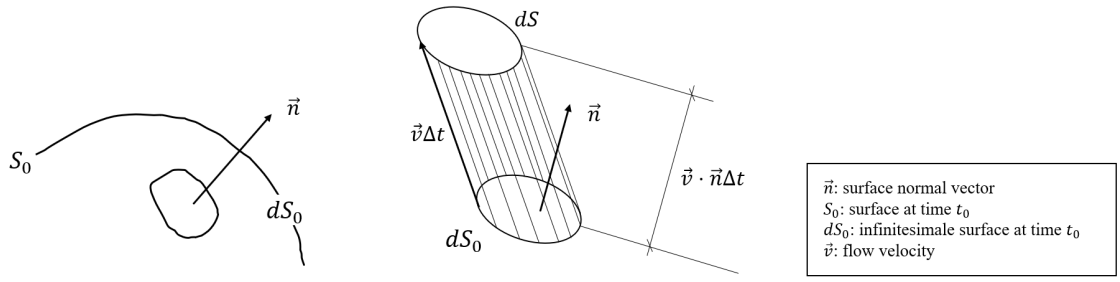

Figure F.1: Infinitesimal surface (left) and mass flowing through an infinitesimal volume (right), adapted from [181]

The mass conservation principle imposes that the mass through the surface S is constant. Hence, with reference to figure F.1, this leads to:

$$\int_{S_0} \rho(\vec{v} \cdot \vec{n})\, dS_0 = -\int_{V_0} \frac{\partial \rho}{\partial t}\, dV_0 \tag{F.1}$$

Within a specific section considered the volume V_0 can be assumed constant. Furthermore, in the hypothesis of incompressible flows, the density of the flow remains constant over time. Thus, equation F.1 becomes:

$$\int_{S_0} \rho(\vec{v} \cdot \vec{n})\, dS_0 = 0 \tag{F.2}$$

Thus, for a certain time t_0 the mass entering the volume V_0 must be equal to the one which flows out. Hence, expressing this in terms of volume flow Q in m^3/s:

$$\sum Q_{in} = \sum Q_{out} \tag{F.3}$$